Experimental Investigations on Water Droplets on Polymeric Insulating Surfaces under the Impact of High Electric Fields

Vom Fachbereich 18
- Elektrotechnik und Informationstechnik -
der Technischen Universität Darmstadt

zur Erlangung des akademischen Grades eines
Doktor-Ingenieurs (Dr.-Ing.)

genehmigte

Dissertation

von

Mohammad Hossein Nazemi, M.Sc.
geboren am 21. September 1979 in Darab (Iran)

Referent:	Prof. Dr.-Ing. Volker Hinrichsen
Korreferent:	Prof. Dr. Christian M. Franck
Tag der Einreichung:	15. September 2015
Tag der mündlichen Prüfung:	18. December 2015

D17

Darmstadt 2016

Acknowledgments

This Thesis is the result of my work as a scientific researcher at the department of High Voltage Laboratories of the Technische Universität Darmstadt. I am pleased to acknowledge those who gave me the possibility to complete this research.
First of all, I would like to express my special deepest appreciation and thanks to my adviser Prof. Dr.-Ing. Volker Hinrichsen, for his patience, encouragement, guidance and support of my research and for allowing me to grow as a research scientist. His advice on both research as well as on my career have been priceless. My special thanks also to Prof. Dr. Christian Franck from ETH-Zürich for accepting and serving to be my co-referee. His excellent comments and discussions made this dissertation more understandable.
This work has been carried out with financial supports of the DFG (Deutsche Forschungsgemeinschaft) within the framework of the Collaboration Research Center Transregio 75 "SFB-TRR75". Special thanks to them without their financial support this project would not have been possible. I would also like to express my gratitude to the workshop of our department for the excellent ideas, preparing all test setups.
This dissertation would not have been appeared in its current form without the help of several students, who contributed the valuable thesis at the department of high voltages laboratories of the TU Darmstadt. Many thanks to all participating students for their contributions.
Special thanks to all of my colleges in the faculty of Electrical Engineering and Information Technology of TU Darmstadt for their friendship and permanent technical support. Particularity, I would like to thank Dr.-Ing. Thomas Wietoska for his brilliant ideas solving my technical problems in the lab. Many thanks to Dr.-Ing. Michael Tenzer, Dr.-Ing. Sébastien Blatt and Dipl.-Ing. Karsten Golde for helping me to solve a lot of administrative tasks at the beginning of my stay in Germany and for translating a lot of Deutsch letters during my work in our department. Thanks to the colleges in the institute of Computational Electromagnetics Laboratory (TEMF), specially to Dr. Erion Gjonaj and Dr. Harald Songoro for their cooperation and support providing simulation results of the dynamic simulation package. My gratitude should also go to my office colleges Constantin Balzer and Henning Janssen for helping me to translate some technical text to German. A warm thank also to my friends Dr. Majid Esmi and Dr. Ehsan Abbasi for proofreading my dissertation and for their comments and argumentation.
Last but not least, none of this would have been possible without the assistance and love of my family. Words cannot express how grateful I am to my beloved wife, Maryam, who spent sleepless nights with me and was always my support in the moments when there was nobody beside me. Thanks to my cute daughter, Negin, who sacrificed a lot of her beautiful times since I was too tired to play with her.

Contents

List of Figures

List of Tables

Abbreviations

AC	**A**lternating **C**urrent
AVI	**A**udio **V**ideo **I**nterleave
BMP	**B**it **M**ap **P**icture
CCD	**C**harged **C**oupled **D**evice
CIGRÉ	**C**onseil **I**nternational des **G**rands **R**éseaux **É**lectriques
DC	**D**irect **C**urrent
DDT	**D**ynamic **D**rop **T**est
EAP	**E**arly **A**ging **P**rocess
EQS	**E**lectro **Q**uasi **S**tatic
ER	**E**poxy **R**esin
FEM	**F**inite **E**lement **M**ethod
fps	**f**rames **p**er **s**econd
FRP	**F**iberglass **R**einforced **P**lastics
HPV	**H**yp**e**r **V**ision
HV	**H**igh **V**oltage
HVDC	**H**igh **V**oltage **D**irect **C**urrent
IEC	**I**nternational **E**lectrotechnical **C**ommission
IEEE	**I**nstitute of **E**lectrical and **E**lectronics **E**ngineering
JPEG	**J**oints **P**hotographic **E**xperts **G**roup
LAP	**L**ate **A**ging **P**rocess
LCC	**L**ine **C**ommutated **C**onverter
LED	**L**ight **E**mitting **D**iode
LMW	**L**ow **M**olecular **W**eight
MPD	High-end **M**easurement and analysis system for **P**artial **D**ischarges
NaCl	**Na**trium **Cl**oride

NCI	**N**on-**C**eramic **I**nsulator
NS	**N**avier-**S**tokes
PD	**P**artial **D**ischarge
PVC	**P**oly **V**inyl **C**hloride
r.m.s	**r**oot **m**ean **s**quare
RRT	**R**ound **R**obin **T**est
RTV	**R**oom **T**emperature **V**ulcanized
SiR	**Si**licone **R**ubber
TB	**T**echnical **B**rochure
TEMF	**T**heorie **E**lektro**m**agnetischer **F**elder
TIFF	**T**agged **I**mage **F**ile **F**ormat
TP	**T**eil-**P**rojekt (German word for Sub-Project)
TR	**T**echnical **R**eport
UHF	**U**ltra **H**igh **F**requency
UV	**U**ltra **V**iolet
VLC	**V**oltage **S**ourced **C**onverter
VOF	**V**olume **O**f **F**luid
WC	**W**ettability **C**lass
WG	**W**orking **G**roup

Symbols

γ	N/m	Surface tension
γ_{LG}	N/m	Surface tension liquid-gaseous
γ_{SG}	N/m	Surface tension solid-gaseous
γ_{SL}	N/m	Surface tension solid-liquid
ϵ_{G}		Relative permittivity of gas medium
ϵ_{L}		Relative permittivity of liquid medium
ϵ_{ra}		Relative permittivity of air
ϵ_{rs}		Relative permittivity of silicone rubber
θ	$^\circ$	Contact angle
θ_{a}	$^\circ$	Advancing contact angle
θ_{r}	$^\circ$	Receding contact angle
θ_{s}	$^\circ$	Static contact angle
μ	mPa $\cdot$ s	Fluid dynamic viscosity
ν	m^2/s	Fluid kinematic viscosity
ρ	kg/m^3	Mass density
ϱ	C/m^2	Surface charge density
σ	µS/cm	Conductivity
τ	s	Time constant
φ_i	$^\circ$	Phase angle
ω_n	rad/s	Angular frequency
Δt_i	s	Time difference between discharges
a	m	Major radius of a deformed water droplet
a_0	m	Initial radius of a water droplet
A_{d}		The ratio of “Length/Height” of the water droplet
A_{dn}		Normalized A_{d} factor

b	m	Minor radius of a water droplet
B	kV/mm · bar	Streamer model coefficient
C_1	F	Capacitance attributed to the gas gap
C_3	F	Parallel capacitor
C_a	F	Capacitance of the test object
C_b	F	Capacitance of a part of dielectric
C_c	F	Capacitance of the gap or cavity
C_d	F	Capacitance of the whole dielectric
C_k	F	Coupling capacitor
d	m	Diameter of the water droplet
d_0	m	Diameter of the water droplet at time t_0
d_i	m	Diameter of the water droplet at time t_i
d_a	cm	Thickness of the air layer
d_s	cm	Thickness of the silicone rubber layer
D	kg/s	Damping constant
D_x	C/m^2	Displacement field density in x-direction
D_y	C/m^2	Displacement field density in y-direction
D_z	C/m^2	Displacement field density in z-direction
E	kV/cm	Electric field strength
E_0	kV/cm	Reference E-field strength without water droplet
E_Gn	kV/cm	Normal component of the E-field strength in gas medium
E_Gt	kV/cm	Tangential component of the E-field strength in gas medium
E_a	kV/cm	E-field strength in air
E_dc	kV/cm	DC E-field strength
$\hat{E}_\mathrm{i}$	kV/cm	Inception E-field strength (maximum value)
$\hat{E}_\mathrm{i,ac}$	kV/cm	AC Inception E-field strength (maximum value)
E_m	kV/cm	Maximum E-field strength
E_s	kV/cm	E-field strength in silicone rubber
f	Hz	Frequency
f_e	N/m^3	Volume force density
f_s	N/m^2	Surface tension tensor
F	N	Force
$\vec{F}_\gamma$	N/m^2	Stress due to interfacial tension

$\vec{F}_\mathrm{E}$	$\mathrm{N/m^2}$	Force density due to E-field stress
$\vec{F}_\mathrm{g}$	$\mathrm{N/m^2}$	Force density due to gravity
$\vec{F}_\mathrm{p}$	$\mathrm{N/m^2}$	Stress due to pressure difference
g	$\mathrm{m/s^2}$	Gravity of earth
$H(q)$	1/pC	Density function of charge magnitudes
$i(t)$	A	Current as a function of time
k		E-field enhancement factor
K	N/m	Spring constant
M	kg	Mass constant
n		Mode number
$n(U)$	1/min	Repetition rate of partial discharges as a function of test voltage
p	Pa	Pressure
q	pC	Apparent charge
q_i	pC	Charge magnitude
$q(t)$	pC	Partial discharge as a function of time
$q(U)$	pC	Discharge magnitude as a function of test voltage
r_0	m	Radius of the water droplet before deformation
R_2	Ohm	Resistance due to conductivity
R_a	µm	Average surface roughness
R_b	Ohm	Resistance of a part of the dielectric
R_c	Ohm	Resistance of the gap or cavity
R_d	Ohm	Resistance of the whole dielectric
R_z	µm	Maximum roughness height
t	s	Time
t_i	s	Time occurrence of the charge
$\vec{T}_\mathrm{e}$	$\mathrm{N/m^2}$	Maxwell stress tensor
u	$\mathrm{m/s^2}$	Fluid velocity
$u(t)$	V	Voltage as a function of time
U	kV	Voltage
U_a	kV	Voltage across the air layer
U_con	kV	Limit value of the voltage across the cavity
U_i	kV	Partial discharge inception voltage
U_s	kV	Voltage across the silicone rubber layer

U_z	kV	Breakdown voltage of the gap
$U_\mathrm{c}(t)$	kV	Voltage across the cavity as a function of time
V	µl	Volume of the water droplet

Abstract

Non-Ceramic Insulators, NCIs, are widely replacing traditional porcelain or glass insulators, due to their low weight, high contamination resistance and hydrophobic surfaces. However, aging of the NCI's surface can gradually decrease the surface hydrophobicity, which leads to corona and even surface flashovers. Deformation of a water droplet affects the E-field distribution present on the insulating surface, making it difficult to estimate the droplet induced electric field enhancement on the insulator surface or to predict the partial discharge inception electric field strength.

PD inception E-field strength of water droplets on hydrophobic surfaces under variation of a large set of parameters is measured, analyzed and discussed in this study. A systematic investigation on the behavior of water droplets at AC, DC and combined AC-DC stress is analyzed and compared, particularly in deformations and PD characteristics point of views.

The major parts of these investigations have also been used to validate the dynamic E-field simulation package recently developed by the Computational Electromagnetics Laboratory (TEMF) of TU Darmstadt. A preliminary good agreement between simulations and experiments has been obtained. However, further cooperation is still needed to complete the validation of new software package.

The maximum allowable E-field strength along a polymeric insulating surface of wettability class WC 1 for a single water droplet on a flat surface has been estimated experimentally to be between 6 and 7.5 kV/cm (peak). The PD inception E-field strength was reduced to about 4.5 kV/cm (peak) for more water droplets on the surface like random spray and dew droplets.

In spite of the benefits of polymeric insulators rather traditional glass and porcelain insulators, they are still in practice a relative new technology. The behavior of water droplets on the surface of polymeric insulators have been shown to be a key parameter to facilitate understandings of long-term and aging behavior of this type of insulators.

Kurzfassung

Aufgrund des geringen Gewichtes, der hohen Fremdsichtwiederstände und der Hydrophobie der Oberfläche werden Polymerisolatoren als Ersatz für die traditionellen Porzellan- oder Glas-Isolatoren zunehmend angewandt. Allerdings kann die Alterung der Oberflächen einen allmählichen Hydrophobieverlust verursachen, welcher zu Korona- und sogar Oberflächenüberschlagen führt. Die Verformung eines Wassertropfens durch die elektrische Feldbeanspruchung ändert die Feldverteilung auf der Oberfläche, wodurch das Vorhersagen von Teilentladungen auf der Oberfläche schwer abzuschätzen ist.

In dieser Arbeit wurden die Teilentladungseinsetzfeldstärken von Wassertropfen auf der Oberfläche von Polymerisolatoren unter Berücksichtigung der Variation verschiedener Parameter gemessen, analysiert und vertiefend diskutiert. Eine systematische Untersuchung des Verhaltens von Wassertropfen unter Gleich- und Wechselspannung sowie kombinierter Beanspruchung wurde durchgeführt.

Die wesentlichen Teile dieser Untersuchungen werden auch zur Validierung des entwickelten dynamischen Feldsimulationspakets beim Institut für Theorie Elektromagnetischer Felder (TEMF) der TU Darmstadt verwendet. Eine vorläufige gute Übereinstimmung zwischen Simulation und Experiment wurde erreicht. Allerdings ist die weitere Zusammenarbeit nach wie vor notwendig, um die Validierung des entwickelten Feldsimulationspakets abzuschließen.

Die maximale zulässige Feldstärke auf der Oberfläche von Polymerisolatoren mit Oberflächenbenetzbarkeitsklasse 1 (WC1) für einen einzelnen Wassertropfen auf einer flachen Oberfläche wurde experimentell zwischen 6 und 7,5 kV/cm (Peak) ermittelt. Jedoch wurde die Teilentladungseinsetzfeldstärke für mehrere Wassertröpfchen, wie sie bei zufälligen Sprüh- und Betauungströpfchen auftreten, auf etwa 4,5 kV/cm (Peak) reduziert.

Trotz aller Vorteile von Polymerisolatoren im Vergleich zu den traditionellen Glas- und Porzellanisolatoren, sind sie noch in der Praxis eine relativ neue Technologie. Das Verhalten von Wassertropfen auf der Oberfläche wurde als ein Schlüsselparameter zum Verständnis des Langzeit- und Alterungsverhaltens diesen Typs von Isolatoren beurteilt.

Chapter 1

Introduction

1.1 Overview

Reliability and power supply continuity of the network is always the major priority of network utilities. To maintain an effective and high quality performance of the power network from both technical and economical points of view, high voltage transmission overhead lines have been widely adopted and customized. High voltage insulators are the key devices, which play important roles in the performance improvement of transmission lines. They are required to withstand the normal operating voltage as well as overvoltages under various environmental conditions such as rain, fog, snow and pollution. Traditional porcelain and glass insulators are extensively being replaced by polymeric or Non-Ceramic Insulators (NCIs) not only in AC transmission systems but also in HVDC as well as in combined AC-DC systems. Integration of an HVDC system to an existing AC transmission line has recently been considered as an attractive method, which can significantly reduce the erection cost of new HVDC towers and avoid the sometimes long lasting discussion about public acceptance of new transmission line corridors [San14, Kna14]. The polymer and composite construction is also used for hollow-core post insulators, for bushings and for housings of surge arresters [Far09]. Main advantages of NCIs are their favorable properties with respect to weight, contamination resistance and surface hydrophobicity [Hac99, Kei03b, Fei09]. However, the aging behavior of polymeric materials at different voltage stresses has become one of the main interesting challenges and an important issue for designers, manufacturers and users of

NCIs. In case of hydrophobic surfaces, no continuous conductive layer of water films can be formed on the surface, and the risk of flashover is reduced; however, corona discharge can occur even on the surface of well-designed polymeric insulators. Water droplets forming on the hydrophobic surface give rise to significant electric field enhancement, especially in close vicinity to the contact line between surrounding air, water droplet and insulator surface [Kei03b, Fei09, Phi99a, Phi99b], which may lead to partial discharges and even flashover. Indoor insulators made of epoxy resins are also subjected to the large variation of temperature and humidity, causing the Early Aging Process (EAP) of an insulator, which leads also to partial discharges [Kei03b, Mbo08]. Deformation of a water droplet due to E-field stress affects the E-field distribution present on the insulating surface resulting in complex phenomena. These deformations of a water droplet make it also difficult to estimate the droplet induced electric field enhancement on the insulator surface or to predict the partial discharge inception electric field strength. This problem has motivated researchers to investigate this phenomenon, and numerous studies have been carried out over a long time, but there is still a lack of understanding about the discharge mechanism of a water droplet on NCI's hydrophobic surfaces.

1.2 Research Objective

Up to now, research in this area has not still convinced manufacturers and users completely being sure about the long-term performance of non-ceramic insulators. In order to improve understanding of the water droplet partial discharges on polymeric insulating surfaces, a systematic experimental investigation about the behavior of water droplets on the surface of polymeric insulating materials, mainly concentrating on PD inception E-field strength under variation of a large set of parameters, is carried out in this study. The research is motivated by the need to understand the discharge mechanism of the polymeric insulating surfaces in the presence of water droplets and is carried out in the frame of the DFG (Deutsche Forschungsgemeinschaft) Collaboration Research Center Transregio 75 (SFB-TRR75) "Droplet Dynamics Under Extreme Ambient Conditions". About 50 scientists from 14 institutes in Stuttgart and Darmstadt in frame of 17 sub-projects, belonging to three different parts of the SFB-TRR75, are working together. The goal of this research center is to gain a better physical understanding of the essential processes as a basis for new analytical and numerical descriptions,

thereby leading to an improved prediction of large systems in nature or in technical applications [Son13a, Wei14]. Figure 1.1 introduces the interactions between investigating focuses and methods used in SFB-TRR75 [Son13b].

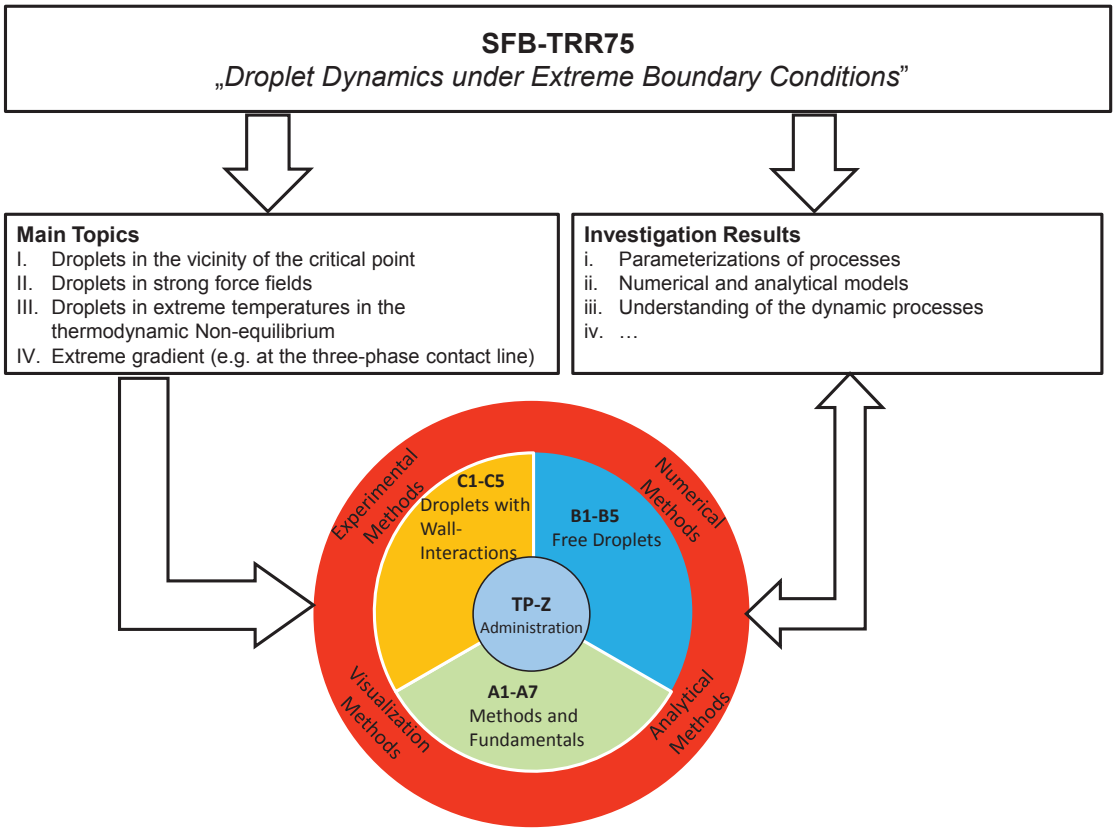

FIGURE 1.1: Interactions between investigating focuses and methods used in SFB-TRR75 [Son13b]

In research area A (TP-A1 to TP-A7), the necessary fundamentals of numerical and analytical methods for all other subprojects are developed. Droplets free of solid boundaries are investigated in research area B (TP-B1 to TP-B5). This extends from deeply supercooled droplets in clouds over drop in cryogenic rocket combustion chambers up to droplet's evaporation near the critical point. In research area C (TP-C1 to TP-C5), droplet-wall interactions are investigated numerically and experimentally. An overview of some of the results obtained by research areas is found in the appearing since 2010 Annual reports of SFB-TRR 75 [Son10, Son11a, Son12a, Son13a, Son14]. The major parts of this study is performed in frame of the TP-C5. In TP-A5 simulations of the mechanical deformation of the water droplet on an insulating surface under the impact of a strong electric field are investigated. A close cooperation between TP-A5 and TP-C5 is established with the goal to develop a simulation tool for droplets deforming under

the impact of an applied external E-field and the consequences with regard to partial discharge inception E-field strengths.

A large set of parameters, which can affect the PD inception E-field strength of water droplets on the surface is analyzed experimentally in this study. The partial discharge of water droplets is also localized in different cases, to find a correlation between calculated E-field strengths and observed partial discharges. Furthermore, and since considering the maximum E-field strength value at triple lines as a threshold of streamer criterion has an uncertainty, it is tried to define a better definition of the E-field enhancement factor based on the integration of the ionization coefficient along a line on the insulating surface. The feasibility of prediction of water droplet's PD inception E-field strength using a developed simple corona discharge model is discussed.

1.3 Structure of the Dissertation

The details of this investigation will be addressed in the following chapters: Chapter 2 introduces a background of non-ceramic insulators and their electrical performance in polluted conditions as well as the theory of partial discharges at AC (alternating voltage) and DC (direct voltage)[1]. Chapter 3 reviews the behavior of water droplets under electric field stress. Deformation of water droplets under the impact of high electric field stress, simulations or calculations of the E-field across an insulator in presence of the water droplet on the surface, discharge activities and surface degradations are briefly reviewed in this chapter. Chapter 5 describes the experimental setup and procedures used in this work, consisting of the test object, the high speed video system and the partial discharge measuring setup. The method of variation of a large set of parameters is also explained in this chapter. Chapter 6 provides the results of experimental investigations in detail with interpretations and discussions. Chapter 7 deals with the simulation results of the non-deformed as well as the deformed shape of the water droplets under different tangential and normal components of E-field stresses. Lastly, the conclusion is drawn and some recommendations are proposed for future research in chapter 8.

[1]The terms "AC" and "DC" stand for "Alternating Current" and "Direct Current", respectively. Combination of theses terms with the word "Voltage", e.g. "AC Voltage" or "DC Voltage" are wrong terminologies, which are used oftentimes in the literature. In this work, the terms "Alternating Voltage" as well as "Direct Voltage" are used often because of their better terminology definitions.

Chapter 2

Theory and Background

2.1 Non-Ceramic Insulators

Polymeric (or non-ceramic) insulators are widely replacing ceramic and glass insulators in transmission and distribution systems. The first polymeric insulators were developed in the early 1970s. They are increasingly used so far as they represent approximately 60-70% of newly installed high voltage insulators in 2000 only in North America [Hac99]. Insulators made of polymeric materials are also often called composite or Non-Ceramic Insulators (NCIs). Composite polymer insulators offer many advantages over traditional ceramic or glass insulators. Low weight, resistance to vandalism, high contamination resistance and excellent hydrophobic surface properties under wet conditions have made polymeric insulators distinctive from porcelain or glass type insulators [Hac99, Kei03b, Fei09]. Figure 2.1 shows the modular design of one polymeric line insulator. The use of polymer as an outdoor weather-shed to protect a central fiberglass (FRP) core from the environment conditions provides a successful alternative to glass and porcelain insulators. Besides the advantages, surface degradation of non-ceramic insulators due to partial discharges as well as their aging process are amongst the most challenging questions for researchers nowadays. Aging of the polymeric insulator surface can gradually decrease hydrophobicity of the surface, which leads to corona and even surface flashovers.

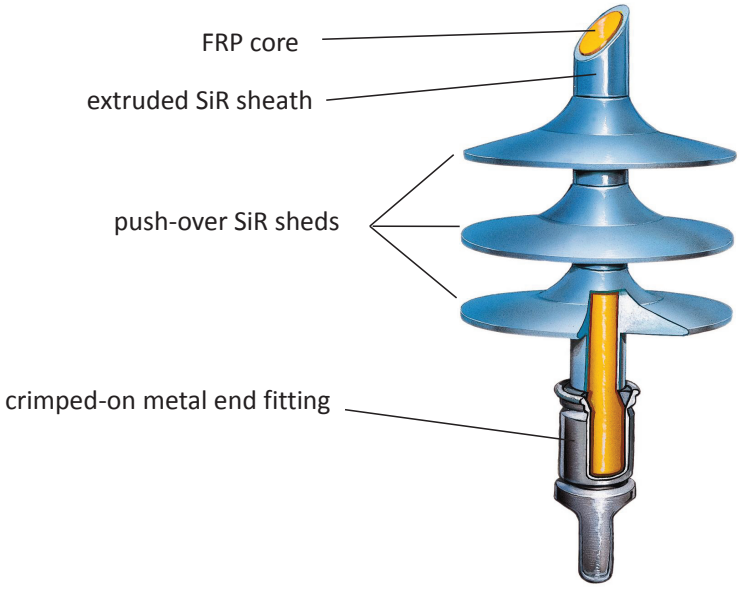

FIGURE 2.1: Cross-sectional view of a non-ceramic line insulator with silicone rubber sheds (Lapp Insulator) [Fei09]

2.2 Wet Conditions

Non-ceramic insulators have a better electrical performance under wet conditions than ceramic or glass insulators. The hydrophobic surface of polymeric insulators, particularly with SiR sheds, provide significantly higher flashover voltages in comparison with the same insulation with hydrophilic surfaces [Bae93]. Under wet conditions, water droplets form on the surface of polymeric insulators enhancing the E-field especially in close vicinity to the contact line between air, water droplet and insulator surface [Fei09]. Changing the shape of a water droplet due to E-field stress affects the distribution of the E-field present on the insulator surface causing partial discharges in the triple line and, consequently, electro-chemical aging of the insulator surface [Kei03b, Sun99, Ada11, Phi99b, Fei09].

2.2.1 Wetting Theory

Wetting phenomena happen at locations where the three states of "solid", "liquid" and "gaseous" are in contact. The relation between the various surface tensions and the contact angle was given by Young in 1805 [You05] as Equation 2.1:

$$\gamma_{SG} = \gamma_{SL} + \gamma_{LG} \cdot \cos\theta \tag{2.1}$$

where γ is the surface tension in N/m and θ is contact angle. S, G and L indices refer to the substrate's surface, the gas and the liquid, respectively. It is important to mention that Young's equation is only valid for ideal and smooth surfaces [IEC03]. The contact angle θ is defined as the angle formed by the intersection of the liquid-solid interface and the liquid-gaseous interface as shown in Figure 2.2. A contact angle less than 90° indicates that the fluid will spread over a large area on the surface; while contact angles greater than 90° generally mean that the fluid will minimize its contact with the surface and form a compact liquid droplet [Yua13].

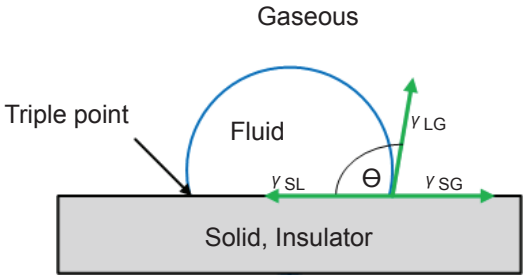

FIGURE 2.2: Fluid drop on a solid surface

2.2.2 Static and Dynamic Contact Angle

The most common quantitative indicator of wettability for polymeric insulators is the contact angle. There exist two different types of contact angles namely static and dynamic contact angles. The so called "static contact angle" θ_s appears on the flat surface of solid materials, while the "dynamic contact angle" i.e. the "advancing angle" θ_a as well as the "receding angle" θ_r can be defined at a drop sliding on an inclined surface of insulators (Figure 2.3). It is also possible to measure the dynamic contact angles on a

horizontal plane by adding and withdrawing water from the droplet by using a syringe with a scale according to [IEC03]. By adding water to the droplet, the advancing contact angle (θ_a) is measured as an angle at the moment when the water droplet front starts to advance on the surface. The receding contact angle (θ_r) is measured in the same way as an angle at the moment when the water droplet front recedes by withdrawing water from the droplet [IEC03]. Usually the static contact angle θ_s is greater than the receding angle, θ_r and less than the advancing angle, θ_a. It has been verified by Hofmann [Hof95] that the receding contact angle correlates best with electrical performance of wetted insulating surfaces. Nowadays with the use of CCD camera and advanced computer software, the measurement of water droplet contact angles at any surfaces has been become an easy task.

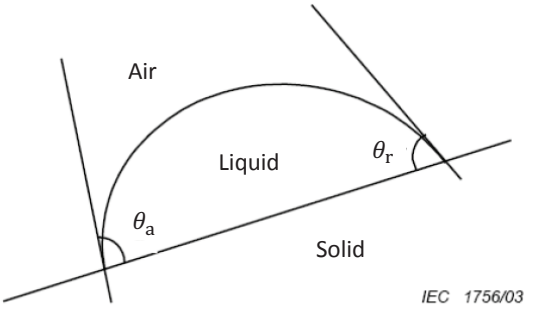

FIGURE 2.3: Contact angle hysteresis [IEC03]

2.2.3 Wettability, Hydrophobicity and Hydrophilicity

Based on the definition in IEC62073 [IEC03], the word "Wettability" refers to a surface ability to be wetted by a liquid. "Hydrophobicity" and "Hydrophilicity" are referred to a low and high level of wettability, respectively. In other words, no water film is formed on a hydrophobic surface, while a hydrophilic surface is wetted by the water in form of a film. A hydrophobic surface has a low surface tension, while a hydrophilic surface has a high surface tension. The wettability of an insulator surface can be measured by three methods [IEC03]:

A. The contact angle method

B. The surface tension method

C. The spray method

The methods differ in accuracy, simplicity, size of measured surface area and applicability [IEC03]. Method A and B are usually applied in laboratories, while method C is suitable for laboratory measurements and on-site measurements on insulations as well [Cig10].

In method A, at least three measurements of the static and dynamic contact angles of a water droplet (usually 50 µl de-ionized water) within a minute after putting the droplet on the surface have to be measured. However, this method requires many measurements if a complete evaluation of the insulator surface is required [IEC03].

In method B, three different mixtures based on tables C.1 to C.3 of IEC 62073 [IEC03] have to be prepared for the measurement of the surface tension in the range of 30 mN/m to 82 mN/m. The liquid will be spread over an area of approximately 5 cm^2 of the insulator surface and the time required for the continuous liquid coverage formed on the surface to break up into droplets will be noted. A time more than two seconds shows that a higher surface tension mixture is needed, while breaking into droplets in less than two seconds proceeds to a lower surface tension mixture. The surface tension of the applied mixture (in mN/m), which remains intact during two seconds as close as possible, is called the surface tension of the measured insulator surface [IEC03].

In method C, the insulator surface is exposed to a fine mist within 20 to 30 seconds. The appearance on the insulator surface after mist exposure will be identified with one of the seven wettability (hydrophobicity) classes (WCs) between 1 and 7. A surface with the WC value 1 is the most hydrophobic surface and a surface with the WC value 7 is the most hydrophilic surface [IEC03]. The disadvantage of this method is that the measurement is dependent on human judgment. Table 2.1 gives a general overview, in which the different wettability classes of polymeric insulator surfaces are classified. Typical photos of surfaces with different WCs are shown in Figure 2.4.

For polymeric insulating materials, not only the degree of hydrophobicity, but also the dynamic properties of hydrophobicity is important. Retention and recovery of hydrophobicity as well as hydrophobicity transfer to pollution layers are the most interesting dynamic properties of hydrophobicity [Lam01]. There is no standardized test procedure for the evaluation of dynamic hydrophobicity properties. However, after a successful identification of material properties of insulation material in CIGRÉ TB No. 255 [Cig04] the CIGRÉ working group D1.14 [Cig10] has offered a report on the test methods and evaluation criteria for the dynamic hydrophobicity properties particularly for retention

and transfer of hydrophobicity. The report summarizes that the retention of hydrophobicity can be measured based on the Dynamic Drop Test (DDT) and will be evaluated as the time elapsed for stressed area of the material sample to change from hydrophobic to hydrophilic state [Cig10]. The hydrophobicity transfer can also be evaluated as the time needed for the changing of hydrophilic state of the sample material surface to the hydrophobic state at a specific applied pollution layer and under given conditions of storage [Cig10].

TABLE 2.1: Criteria for the determination of wettability class (WC) [IEC03]

WC	Description
1	Only discrete droplets are formed. Their shape when viewed perpendicular to the surface is practically circular. This corresponds to $\theta_r = 80°$ or larger for the droplets.
2	Only discrete droplets are formed. The major part of the surface is covered by droplets with a shape, as seen perpendicular to the surface, still regular but deviates from circular form. This corresponds to $50° < \theta_r < 80°$ for the majority of droplets.
3	Only discrete droplets are formed. The major part of the surface is covered by droplets with an irregular shape. This corresponds to $20° < \theta_r < 50°$ for the majority of droplets.
4	Both discrete droplets and wetted traces from the water runnels or water film are observed (i.e. $\theta_r = 0°$ for some of the droplets). Less than 10% of the observed area is covered by water runnels or film.
5	Both discrete droplets and wetted traces from the water runnels or water film are observed (i.e. $\theta_r = 0°$ for some of the droplets). More than 10% but less than 90% of the observed area is covered by water runners or film.
6	More than 90% but less than 100% of the observed area is covered by water runnels or film (i.e. small non-wetted areas/spots/traces are still observed).
7	Continuous water film is formed over the whole-observed area.

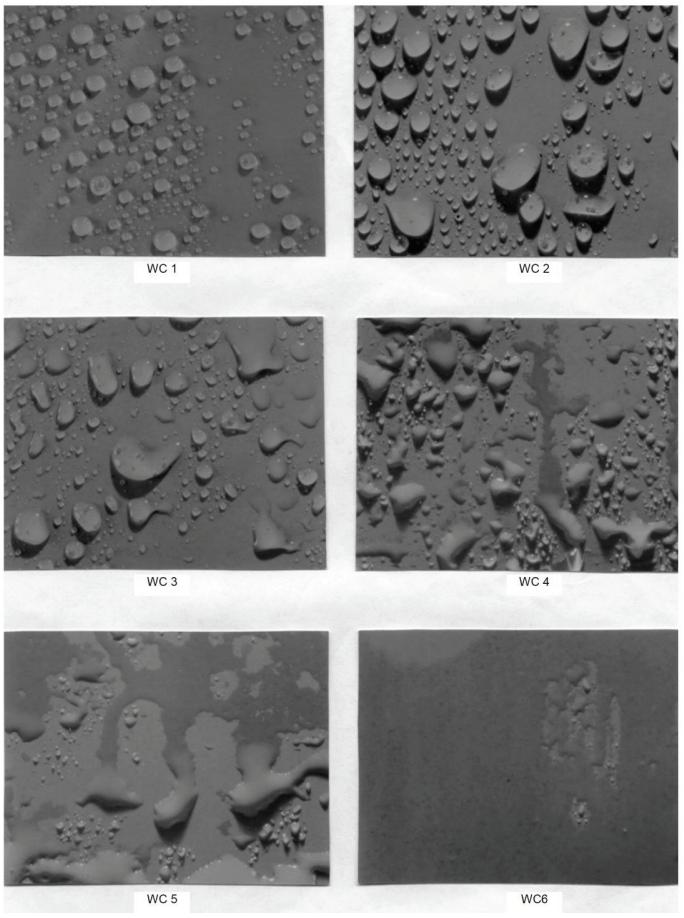

FIGURE 2.4: Typical examples of surfaces with wettability class (WC) from 1 to 6 [IEC03]

2.2.4 Dynamic Drop Test (DDT)

In this test, two electrodes separated by 50 mm are located on 60 degrees tilted material sample as depicted in Figure 2.5 [Cig10]. The electrolyte flows on the surface using an appropriate pump. Depending on the flow rate, drops roll off the surface with a certain frequency. A constant flow rate of about 1.0 ± 0.2 $\frac{\text{ml}}{\text{min}}$ of the conductive electrolyte with conductivity of 1.5 ± 0.2 $\frac{\text{mS}}{\text{cm}}$ at the test voltage of 3 to 6 kV leads to a drop frequency of 12 ± 1 min^{-1} [Cer08]. Due to micro discharges caused by electrolytic flow along the surface and the simultaneous voltage stress, the hydrophobicity will be slowly lost and a continuous path between the electrodes may be formed. The occurrence of a 2 ± 0.5 mA (r.m.s) leakage current for a time of 4 ± 0.5 second is defined as a failure criterion (loss of hydrophobicity) [Cer08]. The question, whether DDT results are reproducible or not, has convinced the CIGRÉ WG D1.14 to perform a round robin test.

The round robin testing has been performed by five participating laboratories. Technische Universität München, University of Applied Science Zittau/Görlitz, Toyohashi University of Technology, University of Miyazaki and Shizuoka University were involved to determine if the proposed method is sufficiently reproducible. A comparative analysis of the results approved the reproducibility of DDT results [Cig10].

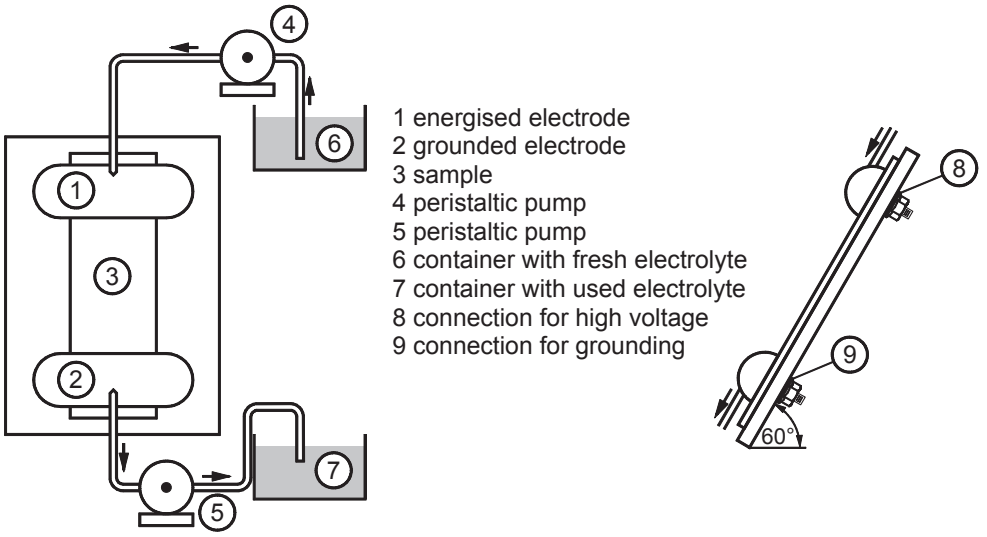

FIGURE 2.5: The schematic test setup for dynamic drop test [Cig10]

2.3 Insulator's Electrical Performance under Wet Conditions

One of the most important parameters related to the electrical performance of an insulator is characterized as its electrical flashover strength under wet and polluted conditions. The flashover voltage of an insulator is extremely reduced by spreading conductive pollution layers along its surface. Such layers are formed on humidification of dust, carbon black, salt or other chemical pollutants on the surface. These deposits in dry state are usually harmless. The most critical situation (time) is during the onset of dew, fog or rain after a long dry period.

2.3.1 Flashover Mechanism on Hydrophilic Surfaces

The mechanism of pollution flashover of traditional porcelain or glass insulators can be explained considering the generated dry band areas over the insulator surface [Far09, Wil99, Chr07, Bo12]. The arc formation process on a polluted hydrophilic surface is

illustrated in Figure 2.6 [Far09]. Normally, a dry pollution layer has high resistivity, and consequently no significant effect on the electrical performance of insulators. But a wet pollution layer with a completely uniform layer of conductivity gives a uniform field distribution due to the electric flow of leakage current flowing on the surface. However, practical inhomogeneities in the external layer always lead to formation of some dry spots, and consequently current displacement on the edges of such areas. The increased current density at the edges causes a further growth of the dry zone across the flow of current due to coalescence of dry points. It may eventually lead to the complete interruption of the current path and result in formation of a dry band with significant voltage drop across the band. When this value is sufficiently large, it results in flashover of the dry band. Thereafter rapid enlargement of the dry band will occur by arc heating.

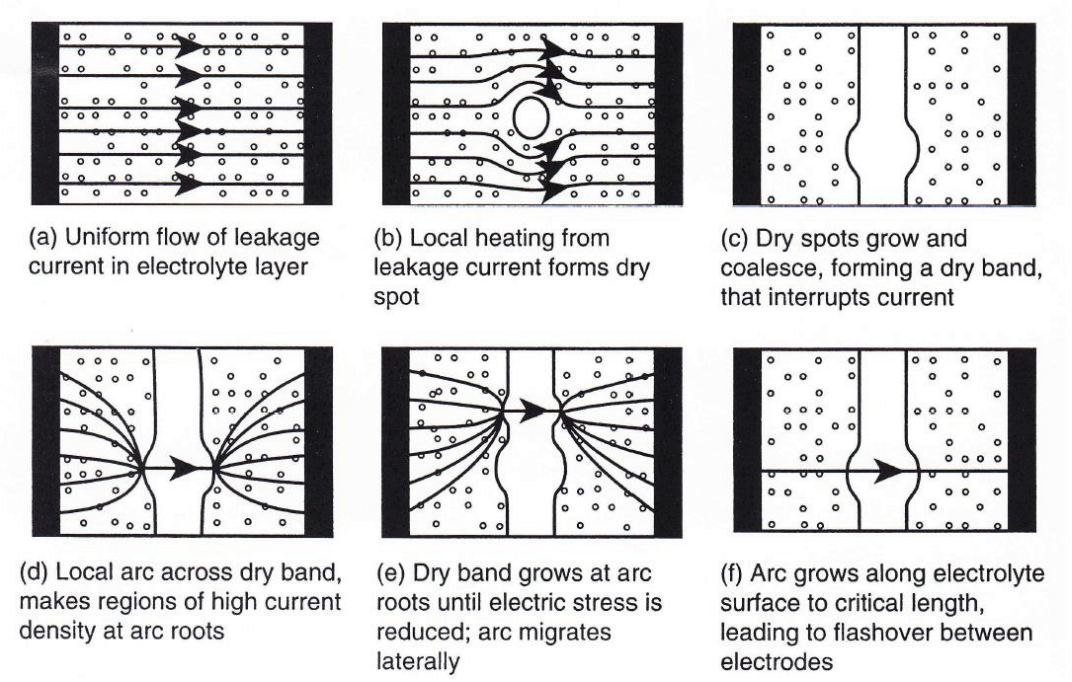

FIGURE 2.6: Flashover mechanism on hydrophilic surfaces [Far09]

2.3.2 Flashover Mechanism on Hydrophobic Surfaces

Since there is no continuous wet layer on the surface of polymeric insulators, the mechanism of pollution flashover in this type of insulators is different from traditional porcelain or glass types. A typical flashover mechanism of a hydrophobic surface is illustrated in

Figure 2.7 [Far09, Kar95]. Water droplets forming on the hydrophobic surface of polymeric insulators absorb pollutants and then become conductive. The wet region around each water droplet grows by diffusion. Significant electric field enhancement, especially in close vicinity to the contact line between surrounding air, water droplet and insulator surface provides the first small amount of leakage currents (the first signal of partial discharges) developing in different paths [Kei03b, Fei09, Phi99b, Phi99a]. Increase in E-field tends to develop a discharge among filament paths on the surface. Generated surface discharges force the surface losing its hydrophobicity, which leads to formation of wet areas on the surface. The wet areas short out the insulator with an electrolyte layer, causing a flashover.

Flashover mechanism for real insulators is much more complicated, as there are usually a large number of dry bands on the surface. However, a lot of comprehensive publications about contamination flashover models can be found in the literature [Far09, Tav04, Gua90, Riz81, Riz97, Far97, Gho95].

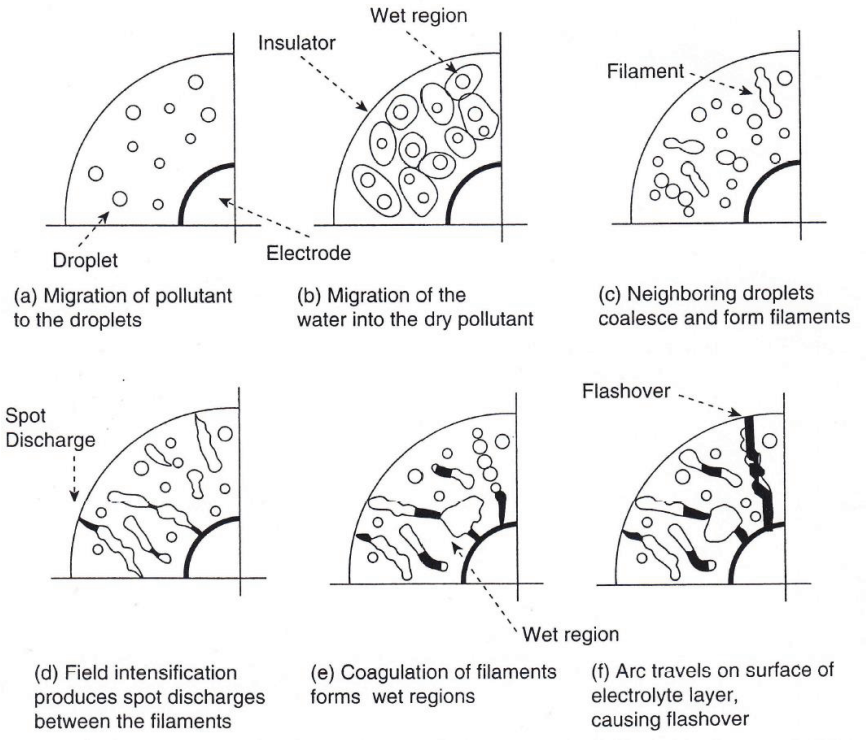

FIGURE 2.7: Flashover mechanism on hydrophobic surfaces [Far09] (quarter section of a top view to the insulator surface)

2.3.3 Aging Phenomena

In contrary to the ceramic and glass insulators, which are not subjected to aging, polymeric insulators in outdoor as well as in indoor applications start to be aged with loss of hydrophobicity due to increase in dry band arcing. Subsequently the polymeric insulating materials degrade in the form of tracking and erosion[1]. Summarizing the hypothesis suggested by Gorur et al. [Gor92], the aging mechanism of SiR polymeric insulators starts with the loss of hydrophobicity due to dry band arcing. The aging process follows with a reduction in the quantity of Low Molecular Weight (LMW) of polymer chains[2] on the surface, resulting in an increased leakage current and surface roughness. In the next step, top surface layers will be de-polymerized and the physical surface structure will be changed due to crystallization and clustering of filler particles on the surface. Ultimately, tracking and/or erosion of the material will appear [Gor92].

For indoor insulation, the large changes in temperature and humidity will lead to condensation on the surface of insulators, and corona effect of water droplets will accelerate the aging process of the surface. For outdoor insulation fog, rain, dew, snow and ice are considered as climatic parameters. Before breakdown, the aging process is described by two main steps. The first one is called the "Early Aging Process" (EAP), during which the leakage current is weak and capacitive, and partial discharges occur occasionally. At the end of the EAP, partial discharge rate increases and makes the surface less hydrophobic. The surface of the insulator becomes wet and the "Late Aging Process" (LAP) sets in, characterized by an increase of the leakage current with a predominantly resistive component [Mue85, Kal02, Kal05, Mbo08].

An early aging model of epoxy insulators has been developed in a series of dissertations at TU Darmstadt supervised by Prof. König [Mue85, Kal05, Kei03a]. In [Mue85] the aging process of insulating materials and the influence of pollution layers from physical and chemical points of view are described. Kaltenborn [Kal05] has pointed out that the aging process can be divided into three periods, namely, early aging, late aging and tracking time. Figure 2.8 shows the developed aging model of polymeric surfaces

[1] Tracking means the progressive degradation of the surface of a solid insulating material by local discharges to form conducting or partially conducting paths, while erosion means the loss of material by leakage current or electrical discharge [IEC07]

[2] Hydrophobicity is defined by LMW components at the outer surface of the material. The loss of hydrophobicity can then be recognized due to the loss of LMW components on the surface, which may be removed either by excessive wetting conditions along with the application of electrical filed, or by dry band arcing [Ami07]. LMW fractions in SiR diffuses from the bulk of the material to the surface and covers the contaminants, so the hydrophobicity will be recovered [Gor92].

under electrical and environmental stress [Fei09]. The EAP occurs due to ignition of partial discharges at triple zones. The discharges dissociate the surrounding air into ozone and nitrogen oxides, forming acids in the presence of water droplets. These aging processes are also known as "electrolytic PD erosion" [Fei09]. Degradations of the surface under partial discharge activity cause the loss of hydrophobicity and the increase in conductivity of pollution layers, developing towards LAP. At a leakage current of several milliamperes the water droplets are evaporated and the dry zones are formed [Fei09]. A thermal surface deterioration will be started due to these high resistive leakage currents, and the chemical erosion on the hydrophilic surface will cause an electrical breakdown.

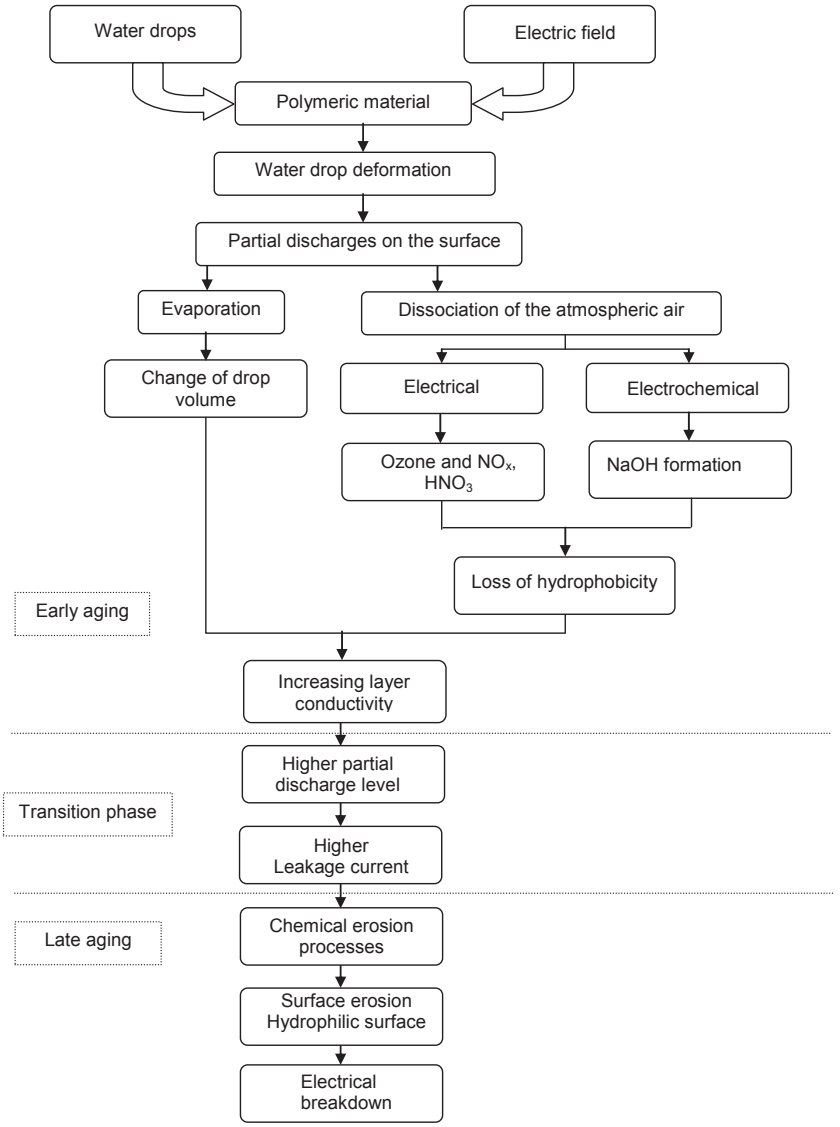

FIGURE 2.8: Aging model of polymeric surfaces under electrical and environmental stress [Fei09]

The developed EAP model of polymer insulators has been upgraded by Feier-Iova [Fei09], considering the water droplet deformation as a major responsible factor for the local electric field intensification (Figure 2.9). However, the deformation of water droplets are considered based on the electro-static simulation results. The developed dynamic simulation package by Songoro [Son15] can be used for the simulation of water droplet deformations in future works.

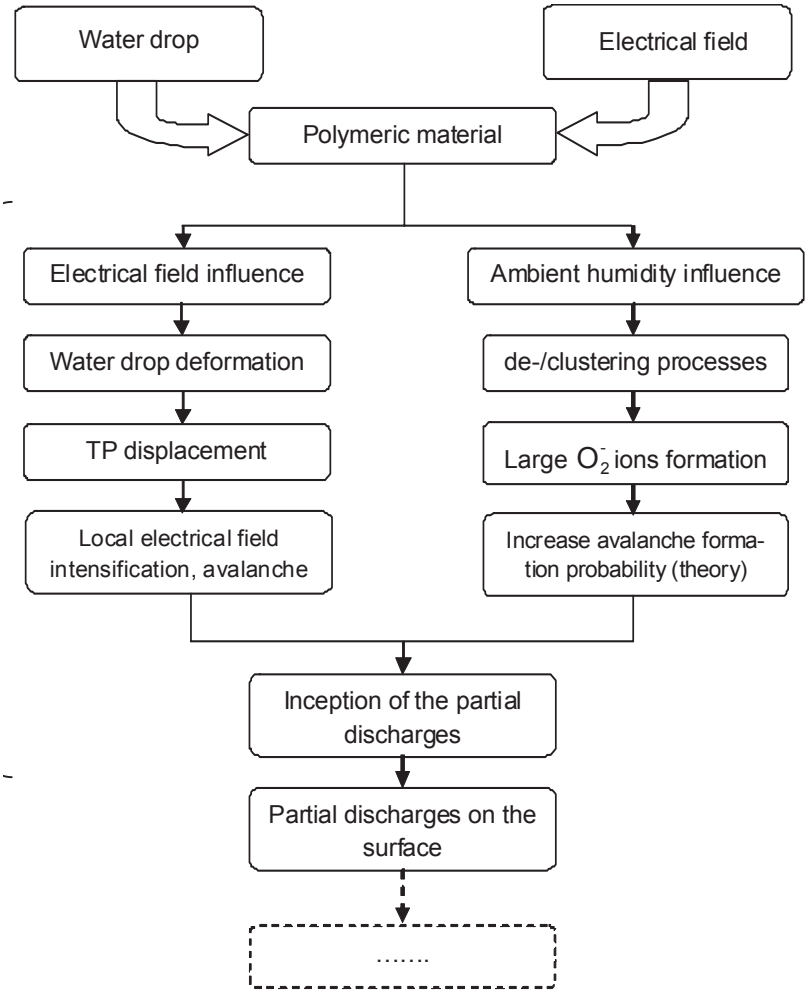

FIGURE 2.9: Update of the aging model [Fei09]

Although the hydrophilic surface recovers back to hydrophobic condition in several hours, due to the high contamination resistance of SiR materials, the question still needs to be answered if non-ceramic insulators after several years in service can offer the same excellent electrical performance compared to new insulators, in which their surface is

undoubtedly hydrophobic. Some utilities are still reluctant to use composite insulators because of the remaining uncertainty of their long-term reliability, the unknown life expectancy and the lack of adequate detection technology of faulty insulators [Hac99]. Theses doubts have been become the main topics of researchers working on polymeric insulators.

2.4 Partial Discharges

In the IEC-Standard 60270, Partial Discharge (PD) is defined as "*localized electrical discharge that only partially bridges the insulation between conductors and which can or cannot occur adjacent to a conductor*" [IEC00]. That means only a part of the insulation fails by partial discharges, and the insulation can still withstand the electric field stress. However, if the partial discharge exists inside the insulation, in course of time the insulation deteriorates and leads to the complete breakdown of the insulation. Partial discharges can be classified into internal and external partial discharges. If the discharge occurs within a solid dielectric such as voids, cracks and inclusions within a solid dielectric, it is referred to as internal partial discharge. If the discharge occurs at the interfaces or along the boundary with different insulation materials, it is referred to as external partial discharge or corona. The behavior of the discharges is different for alternating voltage stress, direct voltage stress and impulse voltage stress. Since the water droplet on an insulating surface provides only external partial discharges, the internal PD is not considered in this work.

2.4.1 PD Characteristics at Alternating Voltages

The PD process requires to be characterized by some parameters. At AC stress, the characteristic parameters are the inception voltage U_i, the apparent sum charge q and the phase angle φ_i [IEC00]. The inception voltage U_i can be defined as the lowest applied voltage at which the magnitude of a PD pulse quantity becomes equal to or exceeds a specified low value. A generic electrode configuration for external partial discharges and its simplified equivalent circuit is given in Figure 2.10 [Koe93], where C_1 represents a capacitance attributed to the gas gap, which discharges completely each time the voltage reaches U_z, the breakdown voltage of the gap F. The charge carriers formed at

the tip of the discharge wander due to E-field resulting in a certain conductivity which is represented by R_2 in the equivalent circuit. C_3 is a parallel capacitance formed by the electrode configuration [Koe93]. Discharge pulses occur as a dense and regular sequence of current pulses at the peak of the test voltage. In a tip-plate configuration, for a high voltage tip the external partial discharge occurs firstly at the peak of the negative half cycle and for an earthed tip the external partial discharge occurs firstly at the peak of positive half cycle, which is illustrated in Figure 2.11 [Kue05].

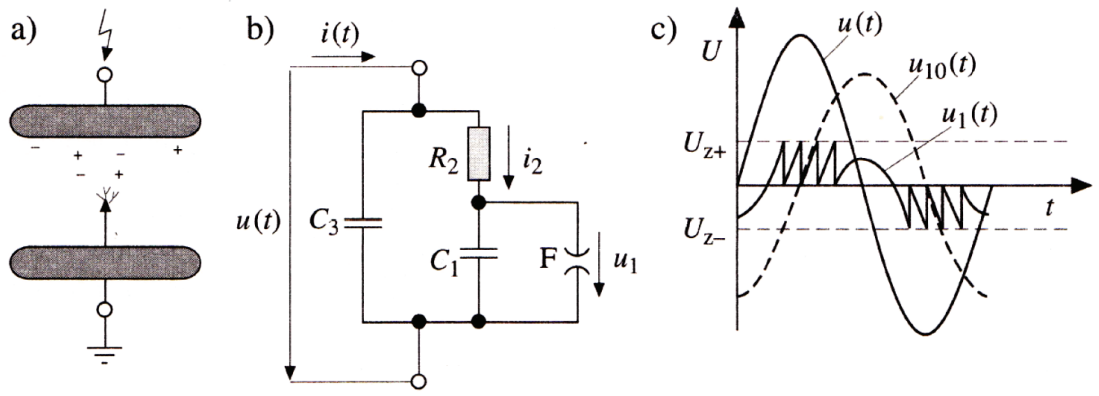

FIGURE 2.10: (a) electrode configuration; (b) simplified equivalent circuit and (c) voltage waveform for external partial discharge [Koe93]

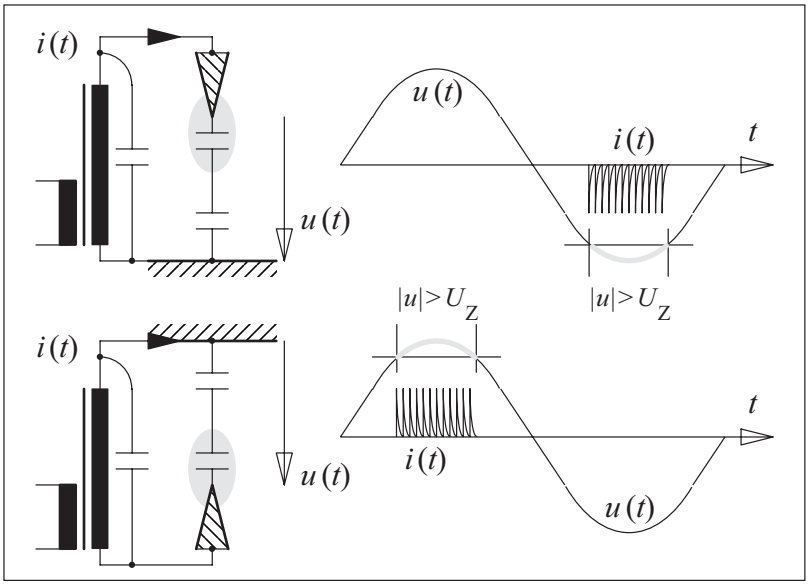

FIGURE 2.11: Tip-plate arrangement as a source of external PD and its characteristics [Kue05]

2.4.2 PD Characteristics at Direct Voltages

Partial discharge characteristics at direct voltage are much more complex than those at alternating voltage. There is no phase resolved information, and the repetition rate of partial discharges is much lower. Also, defining the PD inception voltage as a characteristic parameter at direct voltage is relatively difficult. As successive discharges are time-dependent, the "pre-stress" voltage is an important factor in PD measurements. The partial discharges can continue even after removal of the test voltage, particularly for combinations of solid, liquid and gaseous insulation. It should be considered that single high-magnitude PD pulses can happen during a DC test [IEC00]. Based on the basic interpretation tools for partial discharges at direct voltages proposed by Fromm [Fro95a, Fro95b] and later on by other researchers [Bey02, Mor05, Hoo96, Shu05, Wen08], the mechanism, detection and classification of partial discharges under DC stress are more or less understood. Generally the external and internal partial discharge mechanisms at direct voltages are the same and cannot be separated from each other by external measurements. Figure 2.12 shows an electrode configuration for internal partial discharges and its simplified equivalent circuit suggested by Fromm [Fro95a, Fro95b], where C_d and R_d represent the whole dielectric and R_b and C_b stand for a part of the dielectric in series with the cavity or gap properties (R_c and C_c). Because of the conduction processes at DC, some resistive elements are added to the capacitive equivalent circuit compared to AC, in which the time constant τ (usually 10 to 1000 s) exceeds the duration of a sine wave by several orders. Under DC stress, the voltage $U_\mathrm{c}(t)$ across the void is determined by the test voltage $U(t)$ and by the characteristic time constant τ of the test sample [Fro95a]. The physical mechanism of the partial discharge at direct voltage has been explained by Morshuis [Mor05]. The discharge process is taken into account by a spark gap S. Thus, the time constant for charging the cavity is calculated as [Mor05]:

$$\tau = \frac{R_\mathrm{b} \cdot R_\mathrm{c} \cdot (C_\mathrm{b} + C_\mathrm{c})}{R_\mathrm{b} + R_\mathrm{c}} \tag{2.2}$$

The voltage $U_\mathrm{c}(t)$ across the cavity is given by:

$$U_\mathrm{c}(t) = U_\mathrm{con} - (U_\mathrm{con} - U_\mathrm{r}) \cdot \mathrm{e}^{-t/\tau} \tag{2.3}$$

where U_{con} is the limit value of the voltage across the cavity if no partial discharge occurred (see Figure 2.13 [Mor05, Fro95a]).

$$U_{\mathrm{con}} = U \cdot \frac{R_{\mathrm{c}}}{R_{\mathrm{b}} + R_{\mathrm{c}}} \tag{2.4}$$

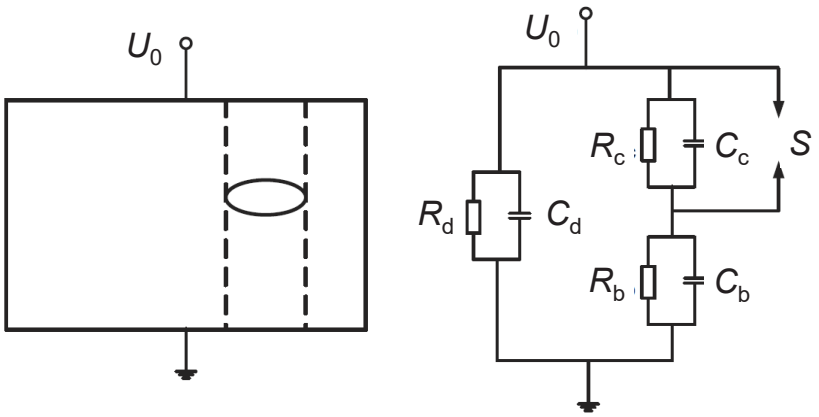

FIGURE 2.12: Electrode configuration for internal partial discharges and its simplified equivalent circuit acc. to [Fro95b]

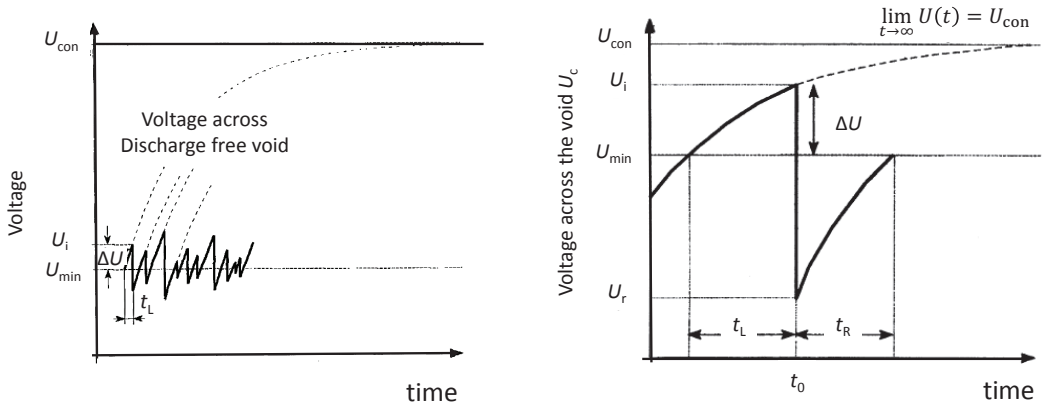

FIGURE 2.13: Recurrence of discharges at direct voltage (left) and voltage across the void (right) acc. to [Fro95b]

Just after corona inception the discharges are less reproducible [Fro95b]. Different ways of PD data representation have been proposed in [Bey02, Mor05]. The basic two available parameters are charge magnitude q_i and time occurrence t_i (or the time difference between discharges Δt_i). A schematic representation of these two parameters at alternating and direct voltages is shown in Figure 2.14.

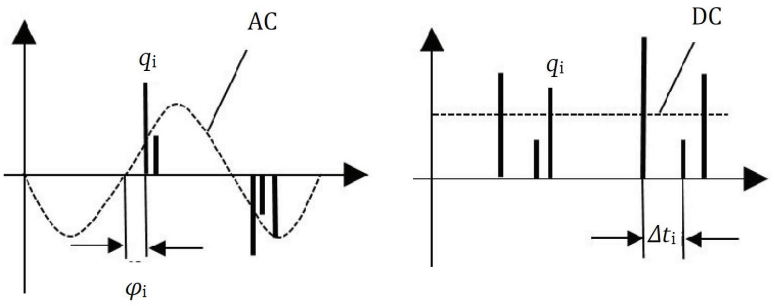

FIGURE 2.14: Basic PD parameters at alternating (left) and direct (right) voltages [Bey02]

From a set of PD data (q_i , Δt_i), various graphical representations may be obtained [Bey02]. Among these additional graphical representations, the PD magnitude as a function of time, $q(t)$, density function of PD magnitudes, $H(q)$, as well as discharge magnitude and repetition rate as a function of test voltage, ($q(U)$ and $n(U)$) are the most attractive options. With their help, external and internal PDs can be distinguished (see Figures 2.15 to 2.17 [Mor05]).

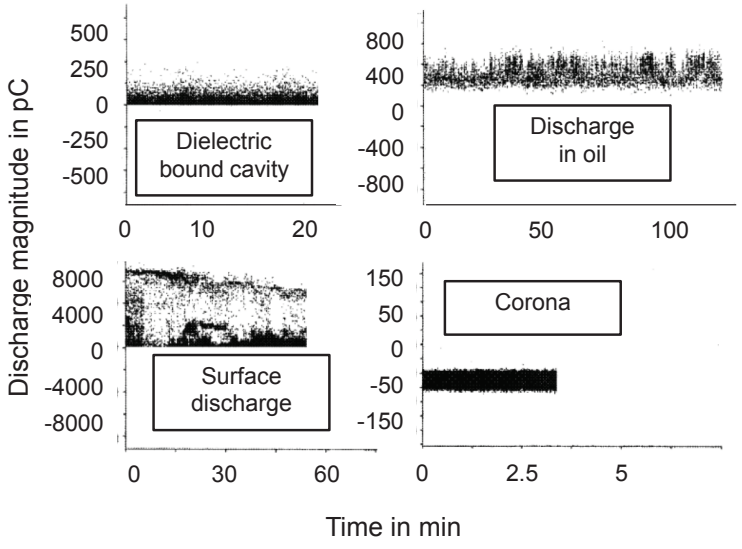

FIGURE 2.15: Examples of PD parameters at direct voltage for different defects [Bey02]; $q(t)$

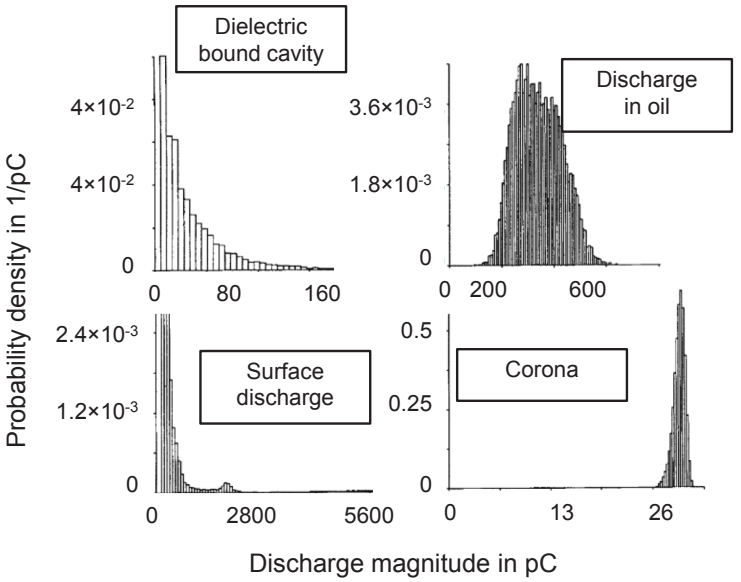

FIGURE 2.16: Examples of PD parameters at direct voltage for different defects [Bey02]; $H(q)$

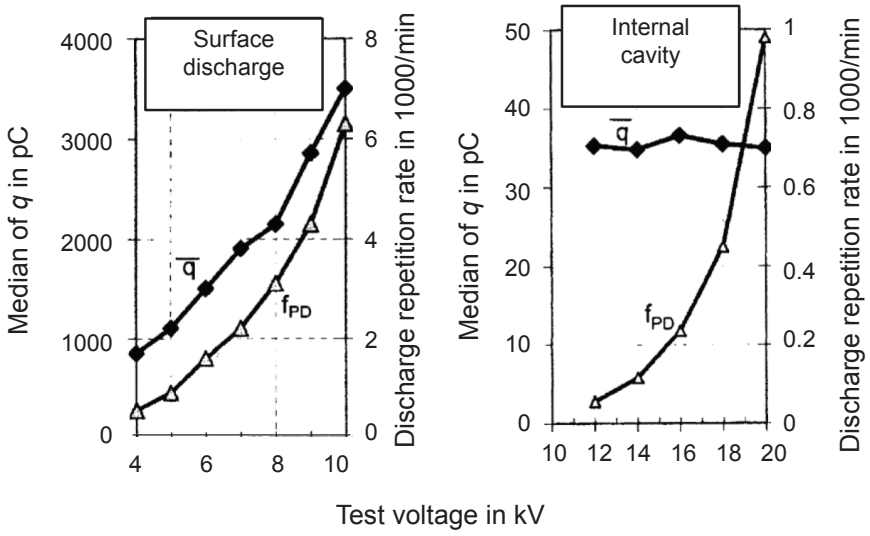

FIGURE 2.17: Examples of PD parameters at direct voltage for different defects [Bey02]; $q(U)$ and $n(U)$

In this work, once a surface discharge is observed, the PD magnitude as a function of time, $q(t)$ is selected as a PD characteristic of the water droplet at DC.

Chapter 3

Water Droplets under Electric Field Stress, Literature Review

Water droplets on polymeric insulating surfaces provide an intensified E-field stress at the common interface between water droplet, insulating surface and surrounding air, which may lead to partial discharges, surface deterioration or even flashover. A changing shape of a water droplet due to E-field stress affects E-field distribution present on the insulating surface resulting to a coupled problem and complex phenomena. Former investigations on water droplets located on the insulating surfaces can be categorized in four dominant aspects:

1. Deformation, break up, resonance and oscillation of water droplets under E-field stress,
2. E-field calculation or simulation on the insulating surface in the presence of water droplets,
3. Partial discharge (corona) from water droplets, discharge and flashover activities and,
4. Surface degradations, aging mechanism and evaluation of material performances.

3.1 Deformation

Deformation of water droplets under high electric field stress has been investigated both theoretically [Fei09, Ima06, Sup08, Bay98, Son15] and experimentally [Kei03b, Fei09, Ima06, Zhu06, Hig07, Yam03, Sch90] earlier. The first theoretical calculation for the oscillations of free water drops with different sizes originates from Rayleigh [Ray79]. Many other researchers have reported later on more calculation methods in the 20^{th} century (e.g. [Oko53, Nix67, BS71, Che84]).
In the equilibrium state the gas/liquid interface is subjected to an interaction of the following external forces per unit area [Ima06]:

- $\vec{F}_\gamma$ due to the interfacial tension;

$$\vec{F}_\gamma = -\vec{n} \cdot \gamma_{\text{GL}} \left(\frac{1}{r_1} + \frac{1}{r_2} \right) \tag{3.1}$$

  where r_1 and r_2 are the principal radii of curvature at any point of gas/liquid interface and $\vec{n}$ is the unit vector normal to the gas/liquid interface.

- $\vec{F}_{\text{p}}$ due to the pressure difference;

$$\vec{F}_{\text{p}} = \vec{n} \cdot \triangle p \tag{3.2}$$

  where $\triangle p$ is the pressure difference between both sides of the gas/liquid interface.

- $\vec{F}_{\text{g}}$ due to the gravity;

$$\vec{F}_{\text{g}} = \vec{n} \cdot g \cdot \triangle \rho \cdot z \tag{3.3}$$

  where g and $\triangle \rho$ are the acceleration of gravity and the density difference across the gas/liquid interface, respectively and z is the vertical coordinate of the corresponding application point.

- $\vec{F}_{\text{E}}$ due to the E-field stress;

$$\vec{F}_{\text{E}} = \vec{n} \cdot \left[\frac{1}{2} \left(\epsilon_{\text{L}} - \epsilon_{\text{G}} \right) \left(E_{\text{Gt}}^2 + \frac{\epsilon_{\text{G}}}{\epsilon_{\text{L}}} \cdot E_{\text{Gn}}^2 \right) \right] \tag{3.4}$$

  where ϵ is the permittivity of the corresponding medium. “L” and “G” indices stand for the liquid and gas, respectively. E_{Gt} and E_{Gn} are the tangential and

normal components of the E-field strength at the gas/liquid interface of the sessile droplet (see Figure 3.1). For the water droplet deformation only the component perpendicular to the surface (E_{Gn}) will influence the force [Son15]. Considering the big difference between the relative permittivity of the gas and the liquid (here $\frac{\epsilon_{\mathrm{L}}}{\epsilon_{\mathrm{G}}} \approx 80$) leads to:

$$\vec{F}_{\mathrm{E}} = \vec{n} \cdot \frac{1}{2} \epsilon_0 E_{\mathrm{Gn}}^2 \tag{3.5}$$

In case of a charged water droplet and considering the Coulomb force the $\vec{F}_{\mathrm{E}}$ due to the E-field stress will be calculated as:

$$\vec{F}_{\mathrm{E}} = \vec{n} \cdot \varrho \cdot E_{\mathrm{Gn}} \tag{3.6}$$

where ϱ is surface charge density.

The interaction of all external forces occurs in the direction normal to the gas/liquid interface, therefore;

$$\vec{n} \cdot \left(\sum F - \gamma_{\mathrm{GL}} \left(\vec{\nabla} \cdot \vec{n} \right) \right) = 0 \tag{3.7}$$

where $\vec{\nabla} \cdot \vec{n}$ is the mean curvature of the gas/liquid interface, which can be re-written as follows according to the Laplace-Young equation of sessile droplet;

$$\vec{\nabla} \cdot \vec{n} = \frac{1}{r_1} + \frac{1}{r_2} \tag{3.8}$$

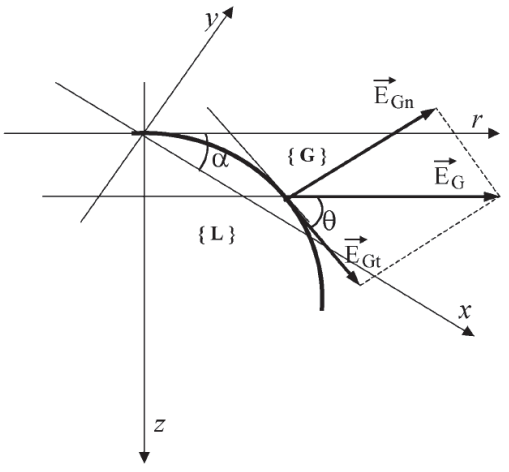

FIGURE 3.1: Normal and tangential components of the E-field strength at the gas/liquid interface of the sessile droplet [Ima06]

The high normal component of the E-field at poles of the water droplet has to be compensated by smaller radii of curvature. Therefore an ellipsoid form of the free water droplet in the direction of E-field lines is expected. Brazier-Smith [BS71] calculated the exact equilibrium shape of isolated droplets and pairs of droplets placed in uniform electric fields of various strengths. This analysis validated the spheroidal approximation for the droplet shape at weak electric fields. If the E-field exceeds the critical value, the equilibrium condition is not fulfilled anymore and the droplet becomes unstable. The instability of the water droplet can be characterized by the formation of conical tips at water droplet poles and/or the development of threads on the droplet surface as well as the splitting into two or more small drops [Fei09]. Cheng et al. [Che84] have pointed out that instability for drops in an E-field occurs when the permittivity and aspect ratio exceed certain critical values. He has confirmed that instability occurs at $a/b = 1.9$ and $\epsilon_0 E^2 r_0/\gamma = 0.24$, where a and b are the major and minor radius of water droplet, respectively. r_0 is the radius before deformation in m and E is critical E-field stress in V/m. $\epsilon_0 = 8.85 \times 10^{-12}$As/Vm is the permittivity of vacuum and γ is the surface tension in N/m. Converting this equation to another form results in:

$$E = \mathrm{c} \cdot \sqrt{\frac{\gamma}{\epsilon_0 \cdot r}} \tag{3.9}$$

Different authors have estimated the constant value c with some small deviations. Feier-Iova [Fei09] has summarized it in Table 3.1.

Studies about oscillation and break up of a water droplet under uniform electric field are also published in [Ada11, Fuj10, She88]. Adamiak et al. [Ada11] proposed a numerical method for prediction of a free droplet distortion in a uniform electric field stress. The mathematical expression of the electric traction acting at every free point on the surface of a droplet immersed in an insulating liquid established by Beroual [Ber92], which has been conducted to the contribution of Imano et al. [Ima06] in 2006. They have developed a mathematical model for prediction of a droplet's deformation on a solid surface in an electric field. Considering a three-dimensional coordinate system (x, y, z), the length, the width and the height of the water droplet plus its contact angle have been formulated in four dependent differential equations by the authors. Dimensions of the water droplet (its length, width and height) as well as its contact angle at any pre-defined E-field stress are used for solving these partial differential equations. Although the obtained results are comparable with the other published papers (e.g [Lan04b]), the proposed

model could compute only static droplets in equilibrium state.

TABLE 3.1: Constant c of equation 3.9 by different authors [Fei09]

Author	Constant c	Method
Kamra [Kam93]	0.273	Experimental, drops suspended by vertical winds in a horizontal electric field
Nolan [Nal26]	0.414	Experimental, free falling water drops in a horizontal field
Macky [Mac31]	0.42	Experimental, free falling water drops in a vertical field
Sherwood [She88]	0.454	Theoretical
Wilson [Wil25]	0.455	Experimental, soap bubble on a wet aluminum plate in a vertical electric field
Taylor [Tay64]	0.461	Theoretical

Resonance frequencies of free water droplets are also investigated and reported in the literature in several publications [Sam70, Fuj10, Yam03, Sch90, Lai09]. According to the basic findings in [Sam70], the resonance frequency of a free water droplet can be calculated in the following form:

$$\omega_n = \left[\frac{\gamma \cdot n(n-1)(n+2)}{a_0^3 \cdot \rho}\right]^{1/2} \quad ; \quad n \geq 2 \tag{3.10}$$

where;

ω_n: Resonance angular frequency of a free water droplet in rad/s; $\omega_n = 2\pi f_n$

γ: Surface tension in N/m

n: Number of peaks on the shape of the water droplet (observed in one oscillation cycle)

a_0: Radius of water droplet in m

ρ: Density in kg/m^3

A similar approach has been proposed by Noblin et al. [Nob04] for a sessile water droplet. In case of ignoring the effects of gravity, which is a valid assumption for droplets with

a radius of curvature less than the capillary length [Nob04, Sha11], the frequency of oscillations is expressed in terms of the droplet's profile length [Nob04]:

$$f = \alpha \cdot \sqrt{\frac{n^3 \pi \gamma}{4 \rho L^3}} \tag{3.11}$$

where L is the droplet's profile length in m and α is the scaling factor. Investigations done by Sharp et al. [Sha11] across the entire range of contact angles have determined a good value of $\alpha \approx 0.81$.

Experimental findings by Fuji et al. [Fuj10] have shown that the vibration frequency of an uncharged water droplet is two times the frequency of the applied voltage, whereas, in the case of an artificially charged droplet, the vibration frequency is the same as that of the applied voltage. It is assumed by the authors that the water droplet can be charged with existing free charge carriers in the lab, however, no quantitative information about the charge magnitudes are reported. Recently Songoro [Son15] has concluded that the vibration frequency of the water droplet as same as the applied voltage frequency is caused by underdamped droplet oscillations which originate in the transient regime.

It has been found by Yamada et al. [Yam03] that the resonance frequency of the vibrating water droplet decreases with increasing volume of the water droplet.

3.2 E-field Simulation

Several electrostatic simulations have been performed to find an enhancement factor of the electric field due to stationary water droplets [Ada11, Fei09, Hig07, FI09, Sar11]. The fundamental issues associated with simulation of shapes of the water droplet in an electric field have been addressed in a series of papers by Langemann and co-workers [Lan03, Lan04a, Lan04b, Lan05, Lan06]. The droplet shape determines the ponderomotoric surface force density caused by the Maxwell stress tensor, and thus the electric field changes the equilibrium of forces at the droplet surface and influences the droplet shape. Therefore, there is a coupled problem between mechanical and electrical sub-problems of the droplet shape, which is decoupled via iteration [Lan06]. Solving the coupled mechanical and electrical sub-problems numerically determines the shape of the droplet in a strong E-field (Figure 3.2), however, the deformation of the water droplet in an iterative proposed model is neglected. The distortion of a free droplet in

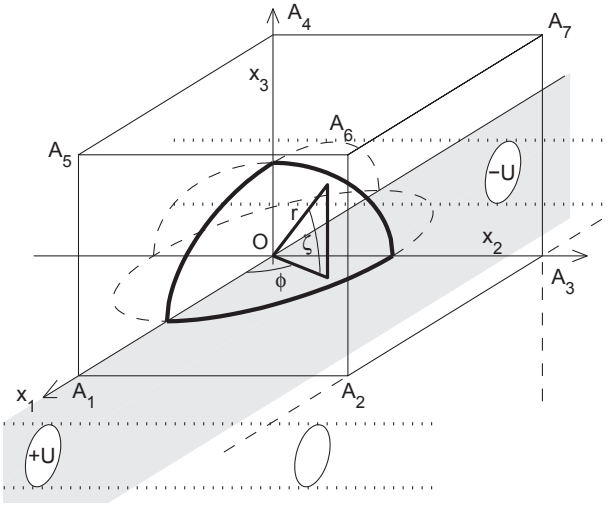

(a) Experimental set-up; the bold lines mark the quarter droplet laying on the surface with the (x_1,x_2)-plane [Lan06]

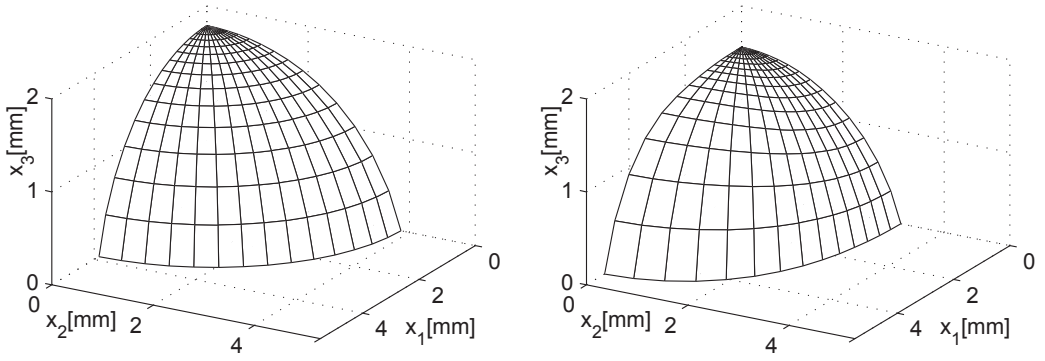

(b) Quarter droplets in the absence of an electric field (left) and in a strong electric field (right), $U = 24$ kV. Plots are not true in scale, height is exaggerated [Lan06]

FIGURE 3.2: Deformation of a water droplet in a strong electric field acc. to [Lan06]

a uniform electric field has also been studied numerically by Adamiak et al. [Ada11] using the Boundary Element Method. The authors have presented a bulking form for the droplet, when it is falling freely. Some analyze of E-field and potential distributions along the surface of polymeric insulators in presence of water droplets are reported in [Jan08, Mar09]. Simulation results of Jang et al. [Jan08] showed that the electric field is concentrated nearby the water droplets and is enhanced with an enhancement factor E/E_0 of about 2.5 at triple zones[1].

[1]It shall be noted that too many different enhancement factors are reported in the literature. Because the value of maximum electric field at the triple line (the common interface between water droplet, insulating surface and surrounding air) reaches to infinity in the ideal case, all simulation packages may have a singularity problem at the triple lines. In other words, by increasing the mesh quality, the value of maximum E-field strength at the triple lines will be increased. Special criteria of convergence have to be fulfilled to be sure that the simulation results are physically correct.

Simulation results of E-field and potential distributions along the surface of silicone rubber polymer insulators under clean and various contamination conditions with/without water droplets in [Mar09] have pointed out that contaminants and water droplets cause highly nonuniform electric field distributions. However, dry contaminants have no effect on electric field distribution when comparing with that of clean conditions [Mar09].
El-Kishky et al. [EK96] found that the maximum E-field intensification of an ellipsoidal water droplet is about 60% higher than that observed with spherical droplets. These investigations have been performed later on by Guan et al. [Gua05] showing only about 25% higher maximum E-field intensification especially for large volumes of water droplets.
A large number of deformed water droplets on an insulating surface stressed by an electric field have been simulated by Feier-Iova [Fei09]. The electric field enhancement is analyzed on the insulator surface along a path 0.1 mm above the insulator surface. To solve the singularity problem, the maximum E-field value at the converge point of 0.1 mm distance from the edge of the water droplet instead of at the triple line has been considered in [Fei09]. Figure 3.3 shows the summarized results of maximum calculated E-field enhancement factors for different shapes of a single water droplet on the surface. It is concluded that the deformed water drops can intensify the electric field at the triple points up to seven times [Fei09]. The simulation results of the initial and elongated water droplets on a SiR surface by Zhu et al. [Zhu03] showed that the maximum E-field of the initial hemispherical and elongated shapes of a water droplet can be four or five times, respectively, higher than that of without water droplet on the surface.
As the water droplets are periodically changing their shape, dynamic simulation tools that take this effect into account are still needed. A dynamic E-field simulation package has been recently developed by Songoro et al. [Son11b, Son12b] as a member of TP-A5 in frame of the SFB-TRR75. The proposed mathematical model of water droplet deformation under the influence of transient high voltage E-fields is derived from Maxwell and Navier-Stokes equations. A novel computational approach based on the finite element method on a moving mesh is used and presented in [Son15]. Figure 3.4 shows a cut plane of the potential distribution with the deformed water droplet overlaid [Son11b].
A close cooperation between TP-A5 and TP-C5 in frame of the SFB-TRR75 has been established with the goal to develop a simulation tool for droplets deforming under the impact of an applied external E-field and the consequences with regard to partial discharge inception E-field strengths. As a result of this cooperation, a contribution of

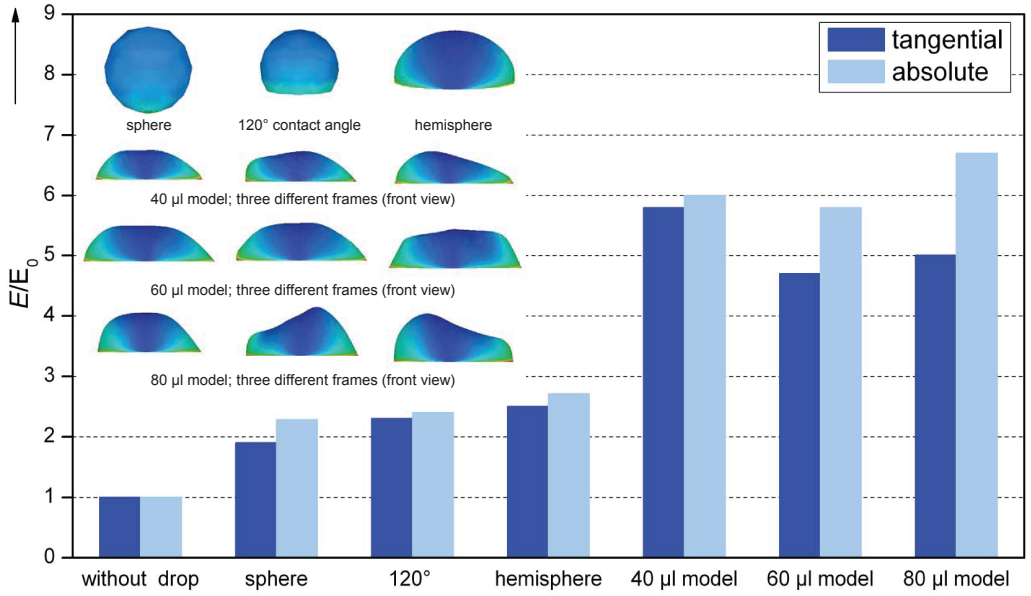

FIGURE 3.3: Maximum electric field intensification at different water drops [Fei09]; for deformed droplets a mean value for $E_{\tan}$ and E_{abs} at three different frames are considered

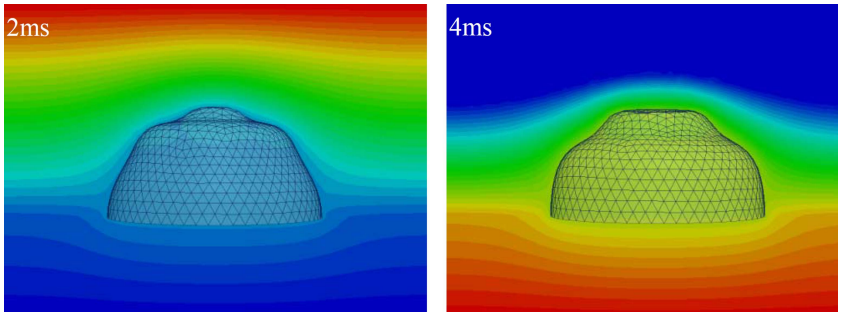

FIGURE 3.4: A cut plane of the potential distribution and water drop shapes at different time instants [Son11b]

water droplet oscillation on the hydrophobic surface of polymeric insulators under AC electric field stress has been published [Son13c]. In this contribution the motion of a single water droplet located on the hydrophobic surface of a silicone rubber sample is simulated numerically by solving the full sets of electro-quasistatics and Navier-Stokes equations. The comparison between simulation and experiment shows a good agreement of the numerically computed droplet motion and the recorded video images for both, horizontal and vertical applied AC electric fields. A typical comparison between simulation and experimental results for a 20 µl water droplet under tangential 50 Hz field stress is illustrated in Figure 3.5. The simulated 3D droplet shape at three different time instants (top) and the corresponding droplet image recorded in the experiment at the

same time instants (bottom) are compared. Obviously, the simulation is able to capture the correct shape deformation in the course of the droplet oscillation.

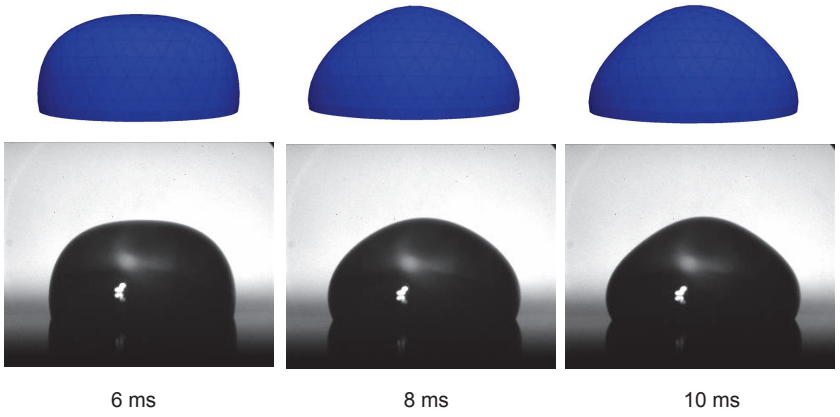

FIGURE 3.5: Simulation and experimental results for the oscillation of 20 µl water droplet under tangential 50 Hz electric field stress; simulation (top) and experimental (bottom) results [more details in [Son13c]].

A useful IEEE task force in 2008 [Phi08] provided some guidelines about the electric field distribution on polymeric insulators. Maximum r.m.s values between 2 and 8.5 kV/cm (preferably 4.5 kV/cm) have been determined for units applied in standard configurations [Phi08]. Considering the E-field enhancement factor at triple lines, the maximum E-field strength value may reach to 25 kV/cm that fulfills the minimum inception E-field strength in air at normal conditions. However, such a generic guideline is almost impossible to develop since it would depend heavily on the insulator manufacturers.

3.3 Discharge Activity

A basic investigation of water droplet corona has been reported in [Eng48], and many contributions continue to investigate corona and partial discharges due to water droplets [Kon53, Sam70, Che77, Phi99a, Kri01a, Kri01b, Lop01, Zhu05, Gao08, Ima09, Zha09, Fei09, Den10]. Main investigations carried out by English [Eng48] and later on by Sugimoto et al. [Sug01] showed that the corona impulse shape initiated from the water surface under strong electric field stress is similar to the well-known "Trichel" pulses that are observed in a tip-plane configuration, however, a large difference in positive and negative corona as well as in time variation of the magnitude and the interval of

the pulses were observed [Eng48, Sug01]. Schütte et al. [Sch90] confirmed that a single droplet placed on a hydrophobic surface behaves (with respect to PD) approximately similar to a free water droplet.

Water drop corona threshold surface E-fields are measured by Philips et al. [Phi99b] and are demonstrated to be between 4.4 and 7.2 kV/cm (r.m.s value) for drops in the 10 to 100 µl range on sheath surfaces (tangential E-field to water droplets) having contact angles between 88 and 115°.

The condensation experiments performed by Lopes et al. [Lop01] at different field levels indicated that there exists a threshold field between 3.0 and 3.5 kV/cm (r.m.s value) above which PD levels increase exponentially.

The nature of discharge phenomena between water drops on polymeric surfaces is investigated by Krivda et al. [Kri01a, Kri01b]. It is pointed out that when several water drops coalesce simultaneously, they bridge a large distance between the electrodes, intensifying the electric field at the ends of water filaments and consequently triggering discharges at the triple points [Kri01a, Kri01b]. Zhu et al. [Zhu05] have shown that due to the deformation of the water droplet a conducting water layer is formed on the surface which develops the dry band arcing. This could also be seen in a large distortion and increasement of the odd harmonic components in the leakage current waveform [Zhu05].

The distortion and movements of single and multiple water droplets on the surface of insulator in AC and DC electric fields are studied by Zixia et al. [Zix03]. It has been pointed out by the authors that the flashover voltage reduces 20% - 30% with increasing the volume of water droplet, but the effect of water droplet conductivity on flashover voltage was small [Zix03].

The flashover voltages for different water droplet arrangements between electrodes are investigated in [Jia06]. The “line” form water droplets arrangement has been found a severe case as it had a lower flashover voltage than that under other arrangement forms like “S”, “V” or “W” forms.

Experimental results of Rowland et al. [Row06] showed that a discharging process on a SiR surface at alternating voltage with a leakage current in the range of 4 mA and below can be divided into six steps: 1) the low-level deformation of drops, 2) initiation of mobile discharges, 3) protrusion appearance, 4) spatial localization of discharges, 5) protrusion extension and 6) the merger of the two drops leading to discharge cessation. These six steps are schematically illustrated in Figure 3.6 [Row06].

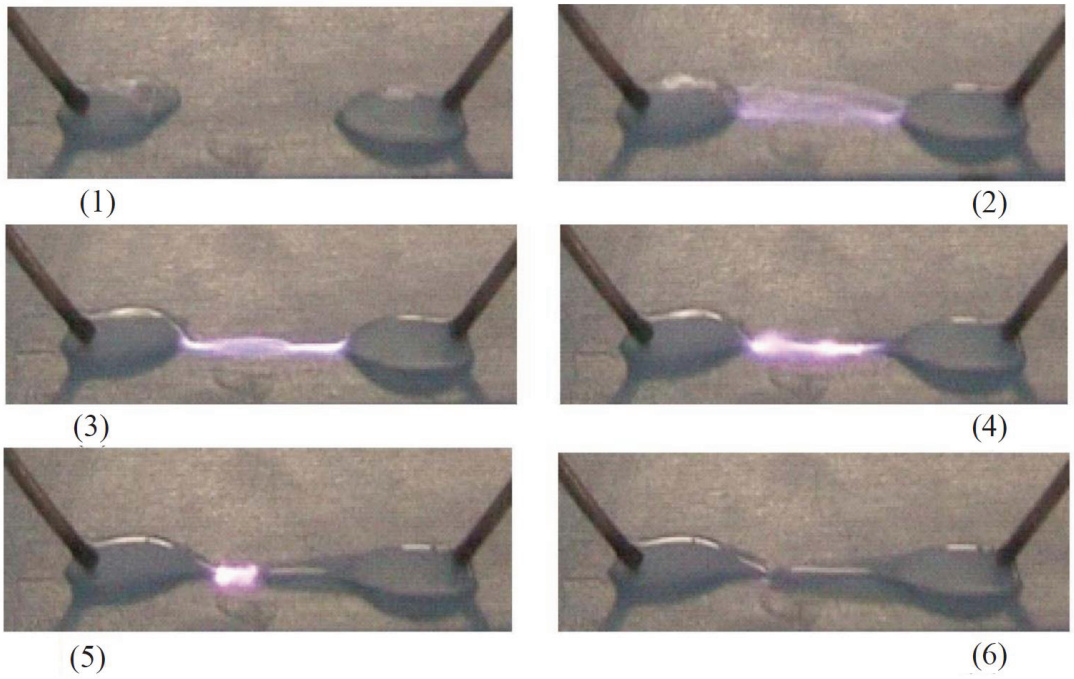

FIGURE 3.6: Six steps of discharge processes on a SiR surface under tangential E-field stress with a current greater than 1 mA acc. to [Row06]

Braunsberger et al. [Bra06] reported the partial discharge inception E-fields of 3.6 kV/cm and 9.8 kV/cm (r.m.s values) respectively for a sessile droplet under tangential and normal E-field stresses. They have also pointed out that simulations using the hemispherical deformation are not sufficient to predict the electrical field intensification which causes partial discharges [Bra06]. This experimental investigation has been approved later on by Feier-Iova [Fei09]. She has concluded that the E-field enhancement factor of deformed water droplet is much higher than that of hemisphere water droplet shape.

The influence of resonance frequency on flashover voltage has been studied in [Hig07]. The results presented by the authors have shown that the corona discharge, disruption of the tip of water channel, emission of fine droplet, and the probably charging of the surface would significantly affect the flashover events rather than resonant vibration [Hig07]. The waveforms of the leakage current on polymeric insulators have been found to be obviously different from those on ceramic insulators with hydrophilic surface. More high frequency components of discharges on a hydrophobic surface are reported in [Gao08]. Interesting investigations by Feier-Iova et al. [FI09] have shown that the PD inception electrical field strength decreases with increasing absolute humidity, although the

breakdown field strength generally increases with increasing humidity. However, no satisfactory explanation could be found.
Using UHF technique by Sarathi et al. [Sar13], the discharge inception voltages initiated by water droplets on epoxy nanocomposites are measured under alternating and direct voltages. It is observed that the discharge inception voltage is higher under a direct voltage compared to that under an alternating voltage, and water droplets under negative polarity of direct voltage had a lower inception value in comparison with those under positive direct voltage. However, no information about "pre-stress" in case of DC inception measurements has been given by the authors.

3.4 Surface Degradation

As explained in section 2.3.3 the loss of hydrophobicity due to increase in dry band arcing will lead to the surface degradation of polymeric insulating materials in the form of tracking and erosion. Some investigations on degradation of polymeric insulators have been carried out in [Sun99, Rey99, Cig10, Kri01a, Kri01b]. Investigations by Phillips et al. [Phi99a] showed that water drop corona can cause cracking of the surface material of SiR non-ceramic insulators in the 500 kV aging chamber. It has been also shown that certain regions of commercially available 500 kV non-ceramic insulators at that time were exposed to surface electric fields that were above the threshold for water drop corona [Phi99a]. Krivda et al. [Kri01b] found that upon removal of the water droplet after being under E-field stress, a faint circular ring of a degraded material (carbon possibly formed from methyl groups in the silicone rubber) can be observed on the surface. Indoor insulators are also subjected to degradation as a result of large changes in temperature and humidity, which lead to the condensation on the surface of insulators. Xu et al. [Xu96] pointed out that the artificial precipitation and high humidity combined with intense UV radiation cause a significant degradation of polymer surfaces. Surface damages are observed to be especially severe for EPDM samples rather than for SiR materials. Figure 3.7 shows typical examples of damage to surfaces of SiR/epoxy resin by corona discharges at alternating voltages.
The literature review by Cigré Working Group D1.27 concluded that the key parameter under DC stresses is not alone to optimize a material for maximal erosion resistance,

but to suppress the resistive leakage currents from reaching values where electrical discharges are initiated [Cig15]. Two typical kinds of tracking and erosion to the surface of SiR/epoxy resin by the salt-fog test at direct voltage are shown in Figure 3.8.

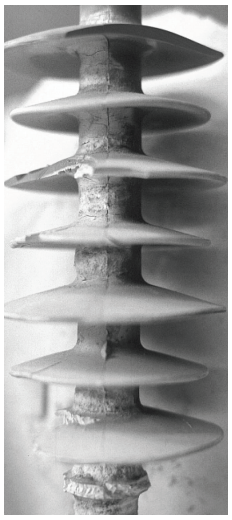

(a) Field degraded HTV silicone rubber insulator [Liu05]

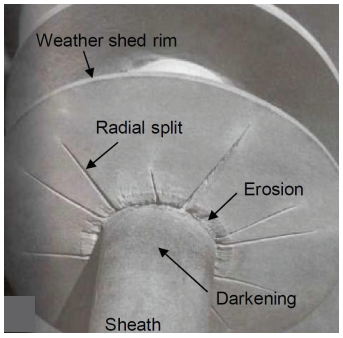

(b) Corona cutting of the housing material of a 230 kV SiR insulator [Pin05]

(c) Tracking and erosion on the surface of one epoxy resin insulator (courtesy of TU Darmstadt)

FIGURE 3.7: Examples of damage to surfaces of SiR/epoxy resin by corona discharges at alternating voltages

(a) Silicone rubber

(b) Epoxy resin

FIGURE 3.8: Tracking and erosion on the surface of SiR/ER insulator under DC stress (courtesy of TU Darmstadt)

Chapter 4

Goals of this study

In spite of the success of non-ceramic insulators in meeting the challenges associated with each of the areas of opportunity, they are still a comparatively new technology. In this regard and although there are a lot of investigations on this topic, there is still a lack of systematic knowledge on failures or unexpected damages. The behavior of the water droplet on insulating surfaces, considering partial discharge activities, is an important key representing the main challenges ahead in order to assure continued and even wider application of NCIs in the future. The aim of this work is to experimentally investigate the behavior of the water droplets on a polymeric insulating surface under the impact of high electric field stress.

An optical diagnostic of single and multiple droplets on epoxy resin surfaces is developed in [Kei03b] to clarify the EAP mechanism of the insulating surface. This aging model has been extended further in [Fei09] on silicone rubber surfaces, considering PD measurements. However, a specific characterization of the movement/oscillation of the water droplets on insulating surfaces under electric field stress and its influence on PD inception E-field strengths is still missing. In this study, a systematic investigation on the oscillation modes of the water droplet as well as its PD inception E-field strength under variation of a large set of parameters will be measured, analyzed and discussed in detail.

Variation of some important parameters, which may have an effect on PD inception E-field strengths, will be experimentally investigated. Three categories of parameters consist of the water droplet, the insulation surface and the E-field stress properties will

be taken into account. PD inception E-field strengths of a single and multiple droplets on the flat and inclined surfaces under tangential and normal E-field stress will be investigated to find extreme severe conditions regarding discharge mechanism of the water droplets.

Using of non-ceramic insulators has been extensively increased recently not only in AC transmission systems but also in HVDC as well as in combined AC-DC systems. HVDC transmission systems are highly recommended for long distances or for off-shore wind parks. Integration of an HVDC system to an existing AC transmission line has also recently been considered as an attractive method, which can significantly reduce the erection cost of the new HVDC towers. This results in mixed AC and DC electric fields on the insulators of both the AC and the DC systems. Therefore, DC and AC/DC insulations shall also be considered and analyzed. The main difference between the behaviour of water droplets (movement analysis and partial discharge characteristics) at AC, DC and combined AC-DC stress will be analyzed and discussed in this work.

In the next step a series of static E-field simulations will be performed to compare the E-field enhancement factor for different configurations, relatively. The partial discharge of water droplets will be localized using a daylight UV-Camera and intensifying lenses to find a correlation between E-field simulation and experimental results as well.

A close cooperation between subprojects TP-A5 and TP-C5 in frame of the SFB-TRR75 is established with the goal to develop a simulation tool for droplets deforming under the impact of an applied external E-field and the consequences with regard to partial discharge inception E-field strengths. The goal is to find enhancement factors of the local E-field in the presence of oscillating water droplets on insulating surfaces. The major parts of this study, performed in subproject TP-C5 in frame of the SFB-TRR75 will be used to validate the dynamic E-field simulation package developed in TP-A5.

In summary, the following scientific remark points have to be discussed in detail:

- Systematic characterization of water droplet oscillation modes under the impact of electric field stress
- Critical parameters, having an influence on the PD inception E-field strength of water droplets on polymeric insulating surfaces

- The main difference between the behavior of water droplets on the hydrophobic insulating surface, consist of movement analysis and PD characteristics at AC, DC and combined AC-DC stress
- Validation of the dynamic simulation package developed in TP-A5

Chapter 5

Experimental Setup and Procedures

5.1 Test Object

To investigate the behavior of an individual water droplet on an insulating surface under *horizontal* (tangential) and *vertical* (normal) E-field stresses, a setup with embedded electrodes according to Figure 5.1 has been developed. Da Silva et al. [Sil09] has pointed out that in case of using electrodes placed on the insulating material, the E-field enhancement factor at electrode edges is higher than at water droplet triple lines. Therefore, for the *horizontal* configuration (Figure 5.1 (a)) the setup developed in former works [Kei03b, Fei09] is used. The advantage of this arrangement is that the necessary voltage to obtain the required electric field is low. Since two electrodes are embedded in insulating plates at opposite sides, no flashover between them may occur. Applying the high voltage between the electrodes generates a virtually homogenous tangential electric field on the surface. Any discharges will then develop between the electrodes, and the electric field is concentrated only in the region between the electrodes.

To generate an exclusively *normal* component of the electric field, two circular electrodes are embedded in insulating materials and arranged in a certain distance from each other, providing a small air gap (Figure 5.1 (b)). Embedding the electrodes in the insulating material avoids any partial discharges at the edges or flashovers between electrodes.

By placing the water droplet on the surface between the electrodes, the behavior of the water droplet under tangential and normal E-field stresses can be investigated.

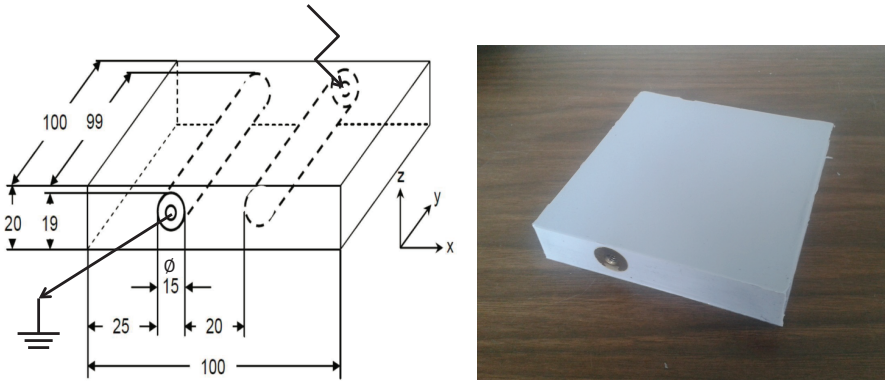

(a) Horizontal (tangential) E-field configuration

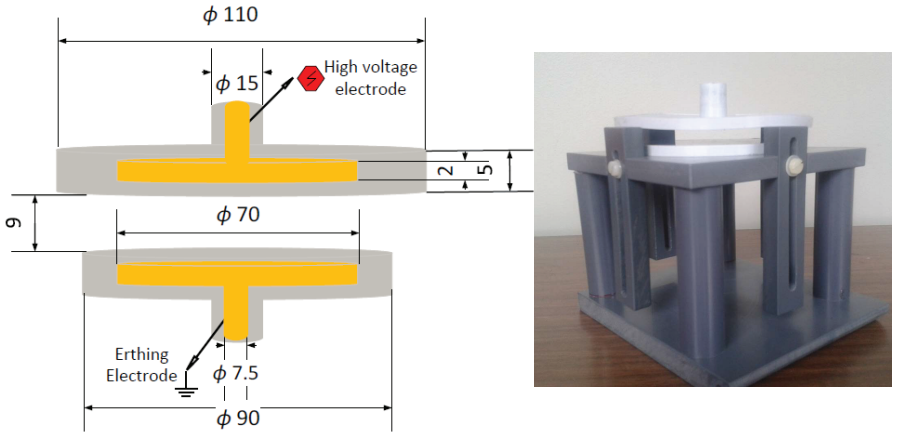

(b) Vertical (normal) E-field configuration

FIGURE 5.1: Configuration of the test specimens (Dimensions in mm)

Silicone rubber (SiR) and epoxy resin (ER) are used as two insulating materials with different degrees of hydrophobicity (wettability classes, WC, acc. to [IEC03]). This is illustrated in Figure 5.2 by two identical water droplets on the surfaces with no electric field, corresponding to WC 1 (contact angle $\geq 80°$) in case of SiR and approximately WC 3 (contact angle $\approx 45°$) in case of ER. To get a quantitative information about the hydrophobicity (wettability) of two insulating materials, the average surface roughness "R_a" as well as the maximum roughness height "R_z" of three new specimens made of ER and SiR are measured using a HOMMELWERKE TURBO WAVE V7.20 surface roughness profilometer[1]. The average surface roughness of SiR specimens lied between 0.084 to 0.101 µm, which was obviously lower than that of 0.155 to 0.196 µm of ER

[1]Many thanks to the State Materials Testing Institute (MPA), TU Darmstadt for surface roughness measurements.

specimens. The maximum roughness height of ER specimens, varying in the range of 1.66 to 3.47 µm has also been observed to be higher than that of SiR specimens, which lied between 0.469 to 0.617 µm. Figure 5.3 shows the measured average surface roughness results of three specimens made of SiR and ER. The used silicone rubber and epoxy resin materials have relative permittivities of 2.9 and 4.1 at 20 °C, respectively. The material used for the production of RTV-Silicone rubber is provided by the chemical company "Wacker" and is called "POWERSIL 600", an elastomer formula, having high tracking and arc resistance. The used epoxy resin material is provided by the "Ciba AG" company and has a lower surface hydrophobicity but is mechanically more robust. The pure resin is mixed with quartz powder in a ratio of 1:2 (pure resin:quartz powder). The "W12 EST" quartz powder is a mineral filler, consisting of 98.5% silicon dioxide.

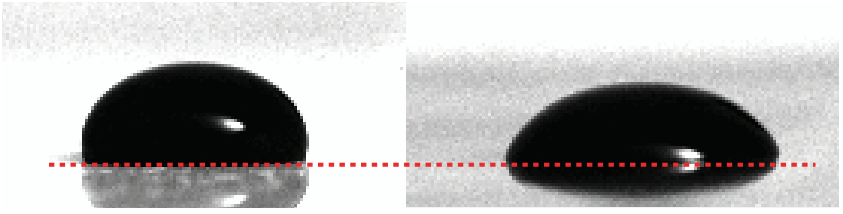

FIGURE 5.2: Degree of surface hydrophobicity of silicone rubber (SiR) (left) and epoxy resin (ER) (right) without E-field (WC1 and WC3, respectively)
(The red dotted line marks the insulator surface. Every things below this line are reflections on the surface)

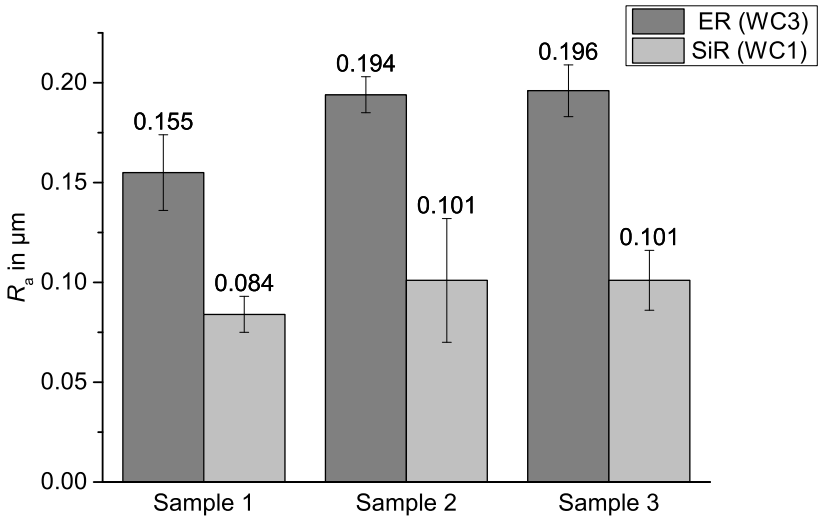

FIGURE 5.3: Measured average surface roughness of SiR and ER specimens

Since the water droplets under tangential E-field stress were found to develop partial discharges earlier than those under normal E-field stress, the investigations are mainly concentrated on tangential E-field stress. However, the investigation results of the water droplet under normal E-field stress have been used to validate the first simulation results of the developed dynamic simulation tool in TP-A5 in frame of the SFB-TRR75 cooperation works.

5.2 Movement Measurement System

The experimental setup for mechanical movement measurements under tangential E-field stress is shown in Figure 5.4. To generate a high voltage of adjustable frequency, a signal generator, a power amplifier and a test transformer are used. The output of the test transformer is connected to the specimen via a resistor. Using a mirror system a "3D-view" video of the water droplet can be captured with the aid of a high speed camera. The sample is placed in front of the camera such that the front view of the water droplet is taken directly by the camera and top and side views are visible in two mirrors, which are placed in appropriate angles to reflect the top and side view pictures of the water droplet towards the camera. Thus, in each frame a "3D-view" is captured. The overall test setup is shown in Figure 5.5.

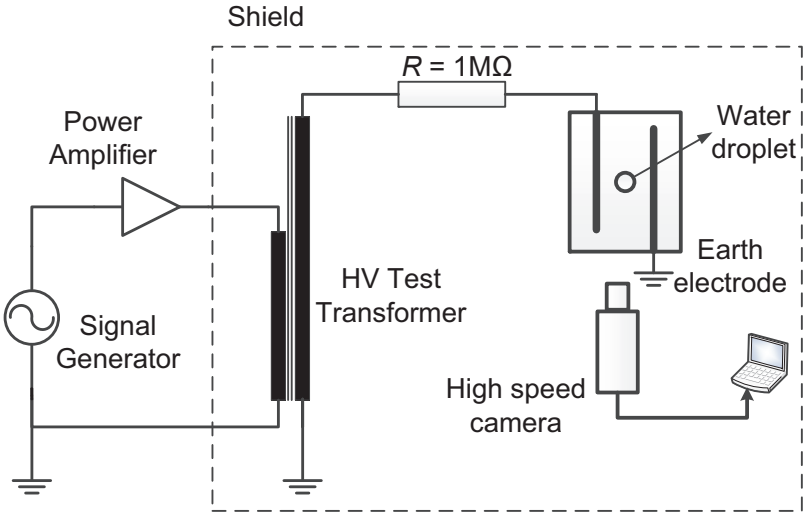

FIGURE 5.4: Experimental setup for oscillation measurement

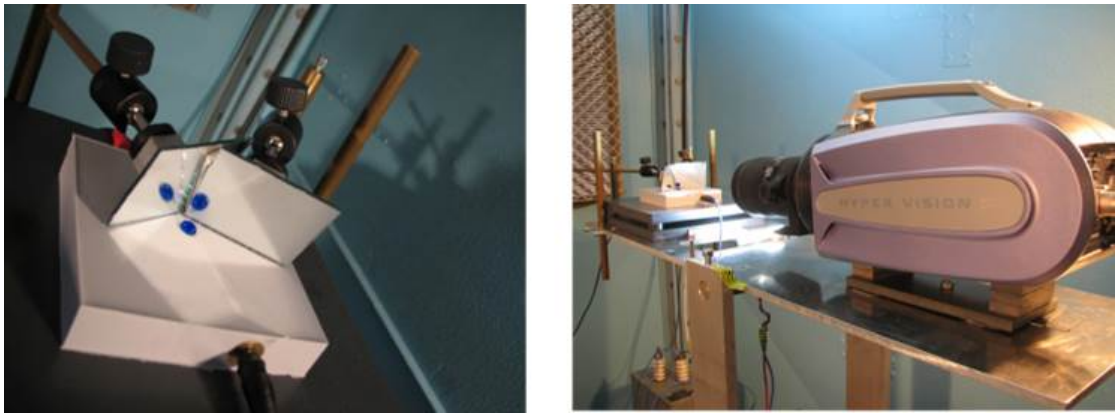

FIGURE 5.5: Test setup with mirror system (left) and high speed camera (right)

A simple FEM simulation confirmed that the mirrors have no effect on the tangential electric field distribution at the location of the droplet. Figure 5.6 compares the results of absolute and tangential components of the electric field on the SiR surface in two cases "with" and "without" mirror system at a test voltage of 1 kV between electrodes. E_{tan} and E_{abs} represent the tangential and the absolute components of electric field and x represent the distance from the center of test object in x-direction. It can be seen that the mirrors just affect the normal component of electric field, which, however, is not interesting for these investigations, whereas the tangential component remains unchanged.

The SHIMADZU Hyper Vision (HPV2) high speed camera with 1000 frames per second is used to capture the videos. The high speed camera saves pictures in any of BMP, JPEG and TIFF formats and videos in AVI format. High intensity illumination is provided by several white power LEDs in order to minimize heat generation, which would affect the droplet volume during measurement. The LEDs are placed at the bottom, and a white paper cover above the setup is used to avoid any light reflections from the surface of the water droplet. The resolution of captured pictures from the camera was 312 (horizontal) x 260 (vertical) pixels, and the recording time interval could be varied from 1 µs to 33 ms based on the available frame per second rates. The recording speed of the camera varies from 1 Mfps to 30 fps. The camera records 102 frames for each of the recording speed. In order to make the water droplet better visible, methylene blue ($C_{16}H_{18}ClN_3S$) is used to colorize the water droplet. Pre-investigations have shown that this has only negligible effect on conductivity and permittivity of the water droplet. Adding methylene blue to the distilled water increased the solution conductivity of

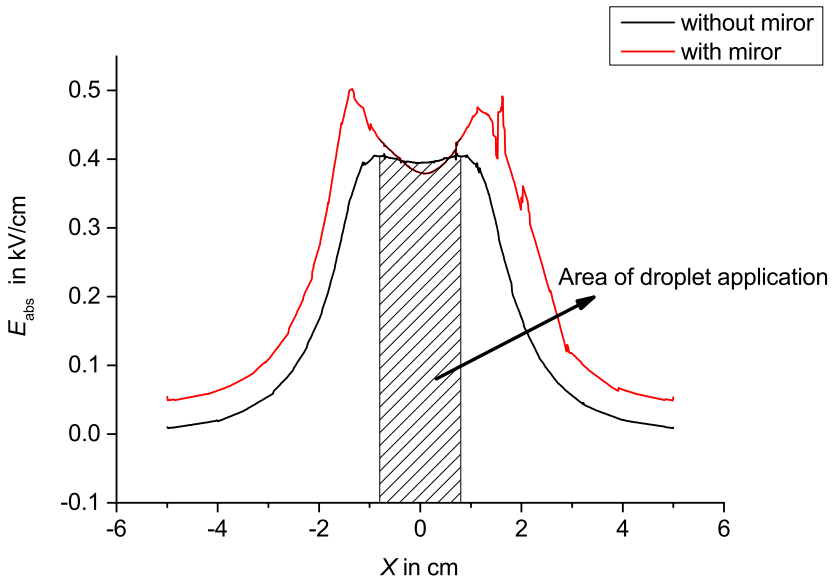

(a) Absolute E-field

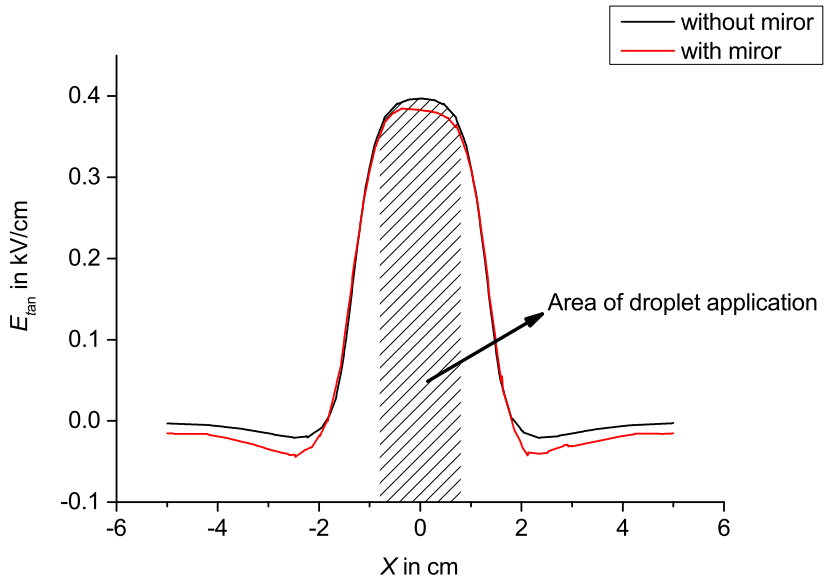

(b) Tangential E-field

FIGURE 5.6: Electric field simulation of the setup with and without mirror system for an applied voltage of 1 kV

35 µS/cm to about 45 µS/cm, which was still in the range of non-conductive droplets[2]. It is also observed that the permittivity of water solution increases by only 1%, adding methylene blue to the distilled water.

For movement measurements, one individual water droplet, having a volume of 20, 40,

[2]Water droplets with conductivities below 70 µS/cm are considered here as a non-conductive water droplets.

60, 80 or 100 µl, is placed on the specimen's surface between the electrodes with the help of a precise pipette. After each measurement the water droplet is replaced by a new one because of its deformation by previous voltage application. The surface is cleaned between the measurements to remove any dust and to provide the same initial value of surface hydrophobicity. Conductivity of the water is measured before each experiment.

5.3 Partial Discharge Measurement

Partial discharge measurements are usually performed with proper shielding inside an electromagnetically shielded cabin, in order to minimize the background noise level [Kue05]. For determining and evaluating partial discharges, optical, acoustical, chemical and electrical methods are available [Koe93]. Except for the electrical method, the other three methods are not suitable for quantitative measurement of partial discharge, but they are essentially used to detect and/or to locate the discharges [IEC00]. In this work, the relevant test circuit mentioned in IEC60270 is used for PD measurements. The most common circuit is illustrated in Figure 5.7, in which the test object is represented as a capacitor C_a. The PD pulses appear across the measuring impedance (quadrupole) via the coupling capacitor C_k. The coupling capacitor C_k serves as a return path for the PD pulses. It is designed in order to withstand the full test voltage and to have a very low self-inductance. The coupling capacitor is PD free and has a high capacitance in comparison with stray capacitances of the test circuit and the test object, providing a high measuring sensitivity. The filter Z between the test object and the high voltage supply prevents interferences and blocks the PD pulses coming from voltage source. Before measuring partial discharges, the test setup has to be calibrated. A pulse source (calibrator) connected to the test object injects a given amount of charge to the circuit, and the displayed charge value on the PD measuring software will be accordingly corrected.

A photomultiplier system has been developed by Feier-Iova [Fei09] to measure the partial discharges of less than 1 pC from water droplets on polymeric insulating surfaces. Optical radiation emitted by the discharge at the water droplet is captured by the photomultiplier module, which is fed by a voltage source, and the output signal is connected to an oscilloscope [Fei09]. The developed photomultiplier system has been calibrated with an existing phase resolved partial discharge measurement system. Since

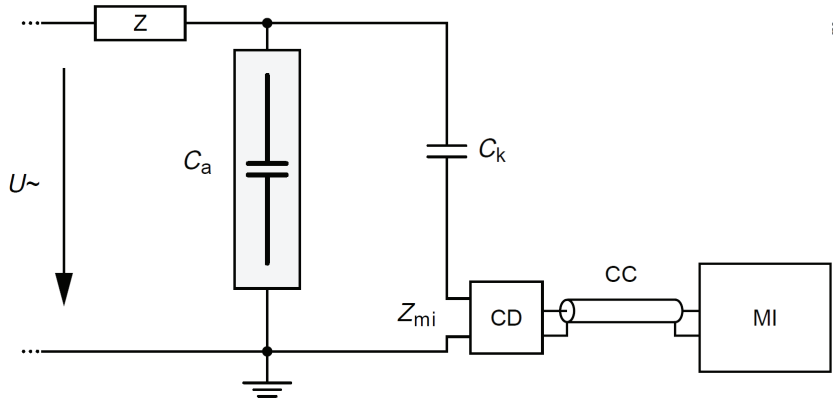

U~	high-voltage supply
Z	filter
C_a	test object
C_k	coupling capacitor
Z_{mi}	input impedance of measuring system
CD	coupling device
CC	connecting cable
MI	measuring instrument

FIGURE 5.7: Basic partial discharge test circuit [IEC00]

the photomultiplier system is very sensitive to any stray lights, it has to be used in an encapsulated dark closed box, equipped with a ventilator to exhaust the generated ozone by electrical discharges out of the box. However, nowadays the new modern partial discharge measuring systems with a very good sensitivity of less than 1 pC are used for sensitive measurements. In this investigation, the MPD 600 Omicron measurement system is used inside a shielded test cabinet with background noise level of less than 1 pC. The technical specification of the Omicron PD-Measuring system is given in detail in Table 5.1. The setup is calibrated for each test at alternating (AC), direct (DC) and combined alternating-direct voltages (AC/DC) individually. After each measurement the surface of the specimen is cleaned, and a new water droplet is carefully placed on the surface symmetrically between electrodes. A large number of measurements for water droplet volumes of 20, 40, 60, 80 and 100 µl in a wide range of frequencies between 20 to 100 Hz is performed.

TABLE 5.1: Specification of Omicron System MPD 600

Input voltage: V input	60 V
Input voltage : PD input	10 V
System noise	< 0.015pC
Measurement accuracy voltage	$\pm 0.05\%$ of calibrated value
Measurement accuracy frequency	± 1ppm $= 10^{-6}$
Measurement accuracy PD-level	$\pm 2\%$ of calibrated value

5.3.1 PD at Alternating Voltage

The test circuit is shown in Figure 5.8. A signal generator, a power amplifier and a test transformer are used to generate the AC high voltage. The voltage is slowly increased in small steps of about 300 V until the first signal of partial discharges (1 pC) is detected. This procedure is repeated six times, and the average value is noted as PD inception voltage. It is assumed that the droplet volume is virtually unchanged during this time. The PD process of an individual water droplet placed on a polymeric insulating surface at alternating voltage is characterized by the inception voltage U_i, apparent sum charge q and phase angle φ_i. The inception voltage U_i is defined as the lowest applied voltage at which the magnitude of a PD pulse quantity becomes equal to or exceeds a specified low value (here: 1 pC) [IEC00]. Furthermore, it is required to identify whether the partial discharge sources are internal or external, which can easily be recognized by the voltage phase angle information φ_i.

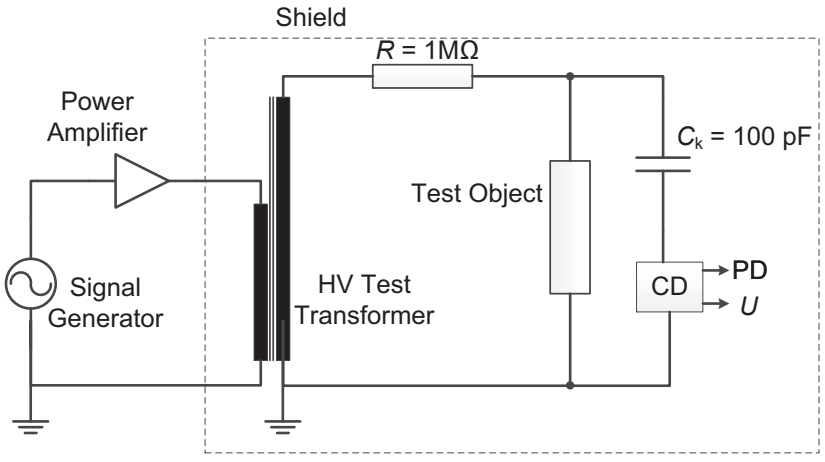

FIGURE 5.8: Partial Discharge measurement test circuit for AC applications

5.3.2 PD at Direct Voltage

For DC tests, the resistor in Figure 5.8 is replaced by a rectifier diode with integrated 500 kΩ resistance, and a smoothing capacitor (1.2 nF) is added to the circuit, which is also used as coupling capacitor for the PD measurements. Under DC stress, the electric field distribution at the beginning is capacitive (distribution based on permittivities) and will then change to resistive (distribution based on conductivities) after a certain time. The transition time depends on the insulator material (or, more precisely, on

its relaxation time constant) and varies from only several seconds to a couple of days. Partial discharges should be measured not before the E-field distribution has reached its final resistive distribution, because the steady state condition shall be investigated. Therefore, the water droplet should be kept under a "pre-stress" voltage for a certain time before PD measurement. Primary pre-investigations showed that for all volumes of the water droplet between 20 µl and 100 µl, the maximum time, which can be used as a "pre-stress" time, is about 30 minutes, as after that the droplet has evaporated too much[3]. It is also observed that at both polarities of the applied direct voltage the first PD signal is detected after a time less than five minutes. So, a five minutes DC "pre-stress" time is later on also used in the AC-DC investigations.

The direct voltage is slowly increased up to a certain specified level and is then kept constant for 30 minutes. This procedure is repeated four times. The same voltage as of the previous attempt, but of opposite polarity is applied to the test object without water droplet after each measurement for one minute to remove possibly accumulated charges on the surface. Once a surface discharge is observed, the PD magnitude as a function of time ($q(t)$) is selected as a PD characteristic of the water droplet at direct voltage.

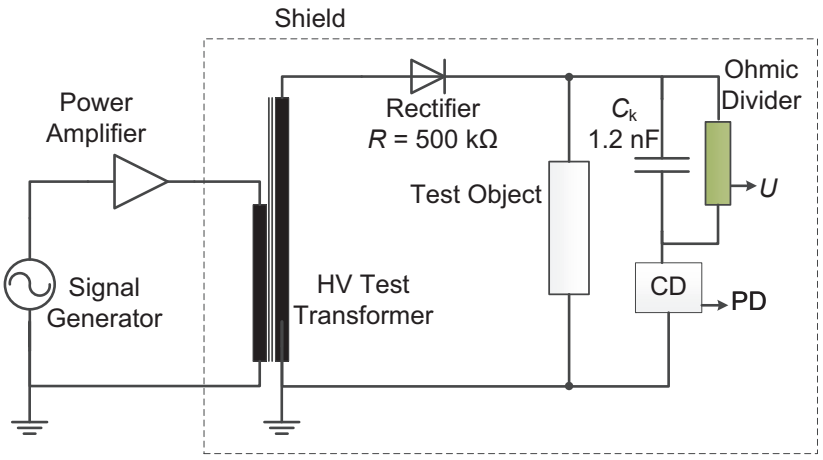

FIGURE 5.9: Partial Discharge test circuit for DC applications

[3]To have an approximate estimation of how much the volume of the water droplet will change during experimental investigations, the sequence snapshots of a 100 µl water droplet locating on a SiR surface without E-field stress in the first 30 minutes of investigations is analyzed. It has been observed that the volume of the water droplet reduces approximately to less than 75% after 30 minutes, while the water droplet keeps more than 93% its volume after 5 minutes.

5.3.3 PD at Combined Alternating and direct Voltage

The combination of two AC and DC test circuits for generation of combined alternating and direct voltages was not possible due to restricted space in the shielded lab. Therefore, the AC test circuit together with a PD-free commercial DC-source (Heinzinger, ± 20 kV, 3 mA) is used in this case (Figure 5.10). In combined AC-DC tests, first a direct voltage of specified value is applied to the test object for five minutes. Then the alternating voltage is slowly increased in small steps of about 300 V until the first signal of partial discharges (1 pC) is detected and continuously increased. This procedure is repeated four times, and the average value of measured alternating voltage is noted as inception voltage at specified AC-DC condition. Figure 5.11 shows the voltage application method at combined alternating and direct voltage. It shall be noted that no polarity reversal in DC has been considered in this work. This is justified by the expected increasing use of VSC (voltage-sourced converter) rather than LCC (line-commutated converter) technology, which does not require polarity reversals for changing the direction of load flow. The DC and combined AC-DC test voltages are chosen to be in line with published combined voltage stress conditions [San14], according to which, for example, a 380 kV AC three-phase system could be combined with a ± 400 kV or ± 500 kV DC system.

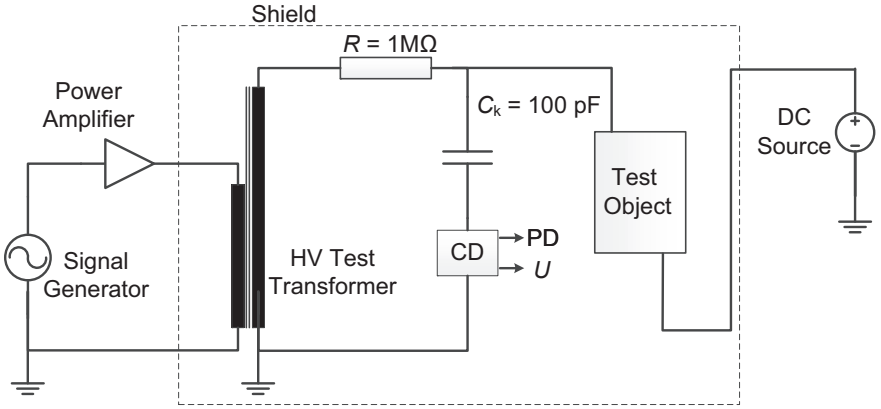

FIGURE 5.10: Partial Discharge test circuit for AC-DC applications

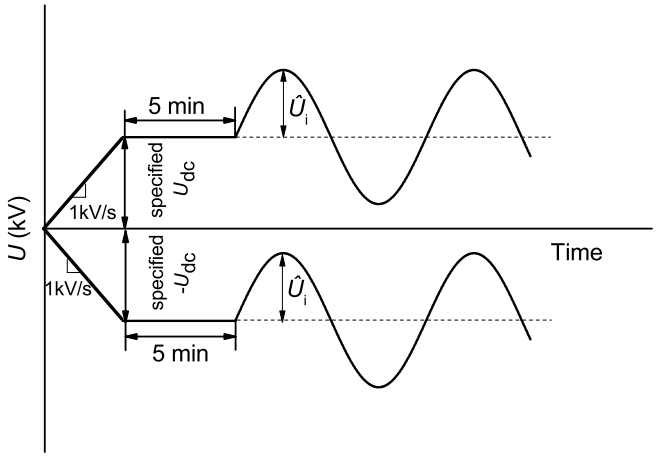

FIGURE 5.11: Voltage application method at combined alternating and direct voltage and definition of inception voltage $\hat{U}_\mathrm{i}$ in case of combined voltage stress

5.3.4 Conversion of Inception Voltage to Inception E-field Strength

All measured PD inception voltages are converted to the PD inception E-field strength on the insulating surface for the sake of generalization. They are also all corrected to normal atmospheric conditions (temperature of 20 °C, pressure of 1013 hPa and humidity of 11 g/cm^3). The converted PD inception E-field strengths refer to the E-field strengths without water droplet considering the scaling factor according to the simulation result of the test setup without water droplet. Figure 5.12 shows the E-field simulation result of the test setup without water droplet. The E-field value at the center of the test object is considered as a constant value of $E_0 = 0.41$ kV/cm when applying a voltage $U = 1$ kV across the electrodes. This resulting E-field E_0 is considered for the scaling factor for conversion of measured PD inception voltages to PD inception E-field strengths, i.e. inception E-field strength values are thus referring to the base field on the surface without a droplet present, and not regarding any field enhancement factors caused by presence of a droplet.

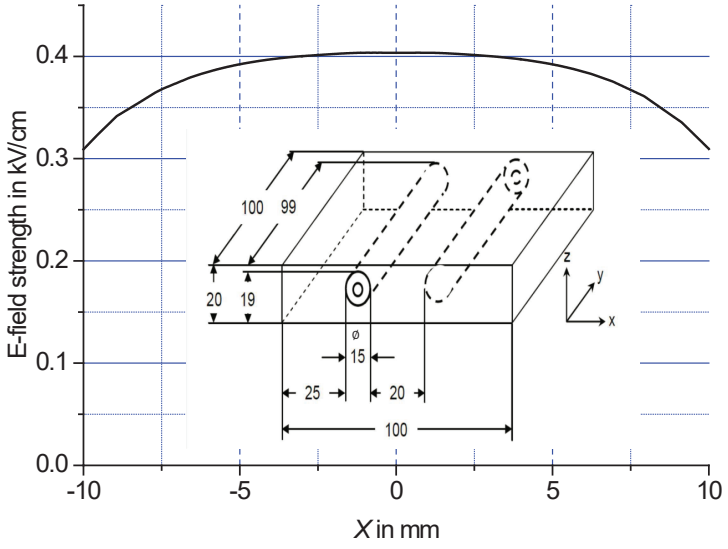

FIGURE 5.12: Tangential E-field of the test setup without water droplet at $U = 1$ kV

5.3.5 UV-Camera

In order to localize partial discharges of water droplets on the insulating surfaces, the ultraviolet camera DayCor SUPERB from OFIL is used to detect the UV emissions of partial discharges. The UV-Camera detects UV radiation in daylight with a sensitivity of $3 \cdot 10^{-18}$ W/cm^2 from a distance of 8 m. To improve the near vision of partial discharges three lenses are specifically developed by the manufacturer of the camera. With help of these lenses, it can be focused on the source of partial discharges in UV mode at a distance ranging from 0.5 m to 3 m. Using a remote control, the screen of the camera can be controlled and captured from outside the high voltage area.

5.4 Variation of Parameters

In order to obtain results close to real conditions, some parameters that are expected to have an effect on the PD inception field strength of water droplets on polymeric insulating surfaces have to be taken into account. There is a large number of parameters that can be varied, the most important ones being volume of water droplet, number of

water droplets and distance between them (in case of several water droplets), conductivity and viscosity of water droplets, inclination angle of the surface as well as surface hydrophobicity, which are investigated experimentally in this work. Of course, there are some further complex effects like collision or fragmentation of the drops, UV radiation or surface roughness, which are not considered here.

5.4.1 Volume of Water Droplet

Different typical size (volume) for water droplets under rain, fog or dew is reported in the literature. Water drops larger than 0.5 mm in diameter i.e. larger than 0.065 µl are classed as rain [Off]. Raindrops with an average diameter between 0.5 to 5 mm (average volume between 0.065 to 65 µl) are reported in [Ele01, Wes81], depending on different parameters like the fall velocity of droplets, the rain type and the complex collision-coalescence process. Raindrops of 8 mm diameter (268 µl droplets) are known to occur rarely [Niu10]. Larger sizes do not normally occur because the raindrop particles simply break up or collide with other neighboring particles [Ele01]. Typical average diameter of water droplets under fog condition varies between 1 to 100 µm [Spi12], which is related to the drops up to 0.5 nl. Variation of temperature and humidity leads also to the condensation of very small dew droplets on the surface, which are important not only for outdoor, but also for indoor insulation. The size of water droplets provoking "naturally" by a condensation process depends on the surface properties [Bra07]. Dziubek et al. has observed a diameter range between 0.2 to 0.4 mm (volume of 4 to 33 nl) on two different insulating surfaces, some even reaching 1 mm in diameter (volume of 0.5 µl) [Dzi05]. Dew droplets are clearly smaller than single droplets in the range of 10 to 100 µl, which possess diameters of about 6 mm.

In this investigation, water droplets with a volume of 20, 40, 60, 80 and 100 µl are placed on the surface of the test object using an accurate microliter pipette from SOCOREX. The pipette has a volume range from 1 µl to 100 µl and an accuracy of ±0.1 µl [SOC]. In addition, the method of condensation described in [Bra07] is used for PD investigations under dew conditions. The air is kept nearly saturated with a relative humidity of 98% at a temperature of 10 °C for one hour, using a WK3-180/40 climate chamber from WEISS. The temperature is raised then to 35 °C for half an hour at a given relative humidity, causing condensation on the surface [Bra07].

5.4.2 Water Droplet Conductivity

Unless otherwise specified, non-conductive (distilled) water with a conductivity of less than 30 µS/cm is used in the experiment. To vary the conductivity over a wide range common salt (NaCl) is added to the water, and the conductivity is thus varied from 30 µS/cm to 120 mS/cm, covering the range of conductivity that exists in nature from rain water to salted fog conditions. To get an idea about typical water conductivities, different water conductivities are listed in Table 5.2. The conductivity of different types of water at 25 °C are also reported in [SAS], so pure, deionized and rain water have, respectively, conductivities of about 0.055, 1 and 50 µS/cm. Drinking water has a conductivity of 500 µS/cm [SAS], and conductivity of industrial waste water can reach up to 10 mS/cm [Sut90]. In our experiment, water droplets with conductivity of 30 µS/cm and 120 mS/cm are used, respectively, as "non-conductive" and "conductive" droplets. The conductivity of samples are measured with a conductivity probe HANNA, which

Table 5.2: Conductivity of different kinds of water [Sut90]

Water type	Conductivity in µS/cm
Deionized water	$0.5 \cdots 3$
Pure rainwater	<15
Freshwater rivers	$0 \cdots 800$
Marginal river water	$800 \cdots 1600$
Brackish water	$1600 \cdots 4800$
Saline water	>4800
Sea water	51500
Industrial waters	$100 \cdots 10000$

measures conductivity up to 3999 µS/cm at temperatures up to 60 °C. Conductivities of more than 3999 µS/cm have been considered with the reference correlation between amount of salt in water and its conductivity given in IEC 60507 [IEC13]. Figure 5.13 shows that adding the salt to the water solution has no impact on water droplet viscosity.

5.4.3 Viscosity of Water Droplet

The viscosity is an important property in fluid dynamics that represents the frictional resistance within the fluid against deformations. There are two related measures of fluid viscosity; the dynamic (or absolute) viscosity μ in mPa · s or centiPoise (cP) and the

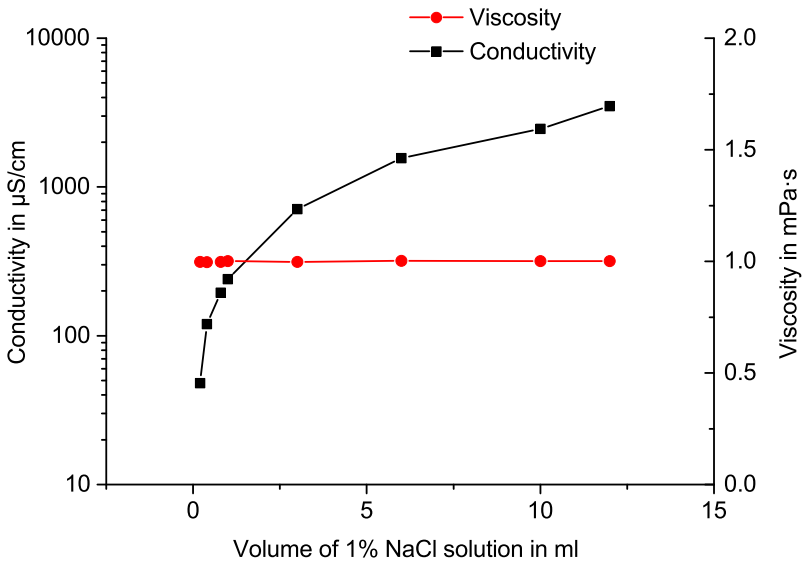

FIGURE 5.13: Measured relation of viscosity and conductivity at room temperature (by adding salt to distilled water)

kinematic viscosity ν in m^2/s. Dynamic viscosity or just viscosity is the more commonly used measure, that measures the resistance of a fluid to flow. Kinematic viscosity, by contrast, measures the resistance of the liquid to flow in the presence of gravity. The kinematic viscosity is the ratio of the dynamic viscosity to the density. To observe the effect of viscosity of water droplets on the partial discharge inception field, the dynamic viscosity of water droplets is varied in a wide range. It is important to mention that the viscosity of rain waters change within a narrow band, depending on the temperature. However, a wide range of viscosity has been investigated in this work to provide a data bank, which can be used to validate the dynamic simulation package developed in subproject TP-A5 in frame of the SFB-TRR75 research center. The initial idea was to vary the temperature as the viscosity of water varies with temperature. But the viscosity has a low value, varying from 1.317 mPa · s up to 0.315 mPa · s when the temperature is varied from 10 °C to 100 °C [Kes78]. Within that range the inception voltage stays almost constant, and it is not sufficient to investigate the effect of viscosity on inception voltage [Hig12]. Also, it is not possible to say that the inception voltage is affected by viscosity only, as temperature has an effect on inception voltage as well. So to vary the viscosity in a wide range, starch sugar made of maltose ($C_{12}H_{22}O_{11}$) is added to the distilled water. Maltose up to 40% by weight at room temperature varies the viscosity of distilled water in a wide range from 0.9 mPa · s up to 5.7 mPa · s

[Hig12]. All the values of viscosity are measured at room temperature of 22.5 °C with a HAAKE MARS III viscometer from Thermo Fisher Scientific[4]. The viscometer has a torque range of 0.01 µN · m to 200 mN · m and can measure the viscosity of 0.5 mPa · s to 10,000 mPa · s in the temperature range of −150 °C to +600 °C. The equipment consists of a moving plate at top which is pulled down and the water droplets are placed between the two plates with a syringe. The maltose with different percentage by weight is added to distilled water to form a maltose water solution. The viscosity measurement is started with 0% maltose by weight and is gradually increased by 5% by weight up to 40% by weight till the solution reaches saturation. The water droplet volume for each measurement is 10 milliliter. The two plates provide a shear stress on the sandwiched water volume, and thereby the viscosity is measured. After each measurement the surface is cleaned with a tissue paper before the next water droplet is placed on the surface. The variation of conductivity with the maltose percentage by weight is represented graphically in Figure 5.14. It can be seen that adding the maltose does not affect the conductivity of the solution. The measured value of conductivity at the highest concentration of maltose is less than 25 µS/cm, which is almost like that of distilled water.

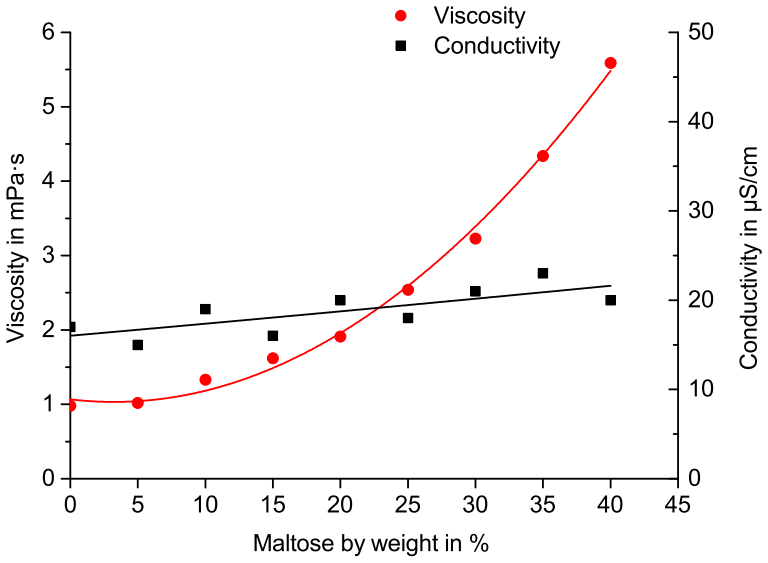

FIGURE 5.14: Measured relation of viscosity and conductivity at room temperature (by adding maltose to distilled water)

[4]Many thanks to the institute of printing science and technology, TU Darmstadt for providing the viscometer and performing the measures.

5.4.4 Inclined Surfaces

On an inclined surface of polymeric insulating material water droplets are subjected to gravitational force, $\vec{f}_{\mathrm{g}}$, in addition to the dielectric force, $\vec{f}_{\mathrm{e}}$. The water droplet is distorted not only due to the electric field but also due to the gravitational force. Figure 5.15 shows three configurations with inclined surfaces under tangential and normal E-field stress. Arrangement X represents water droplets under tangential E-field stress, where the force due to E-field $\vec{f}_{\mathrm{e}}$ and the force due to gravity $\vec{f}_{\mathrm{mech}}$ are perpendicular to each other, while in arrangement Y, $\vec{f}_{\mathrm{e}}$ and $\vec{f}_{\mathrm{mech}}$ are in the same direction. Inclined surface orientation under normal E-field stress is illustrated in arrangement Z.

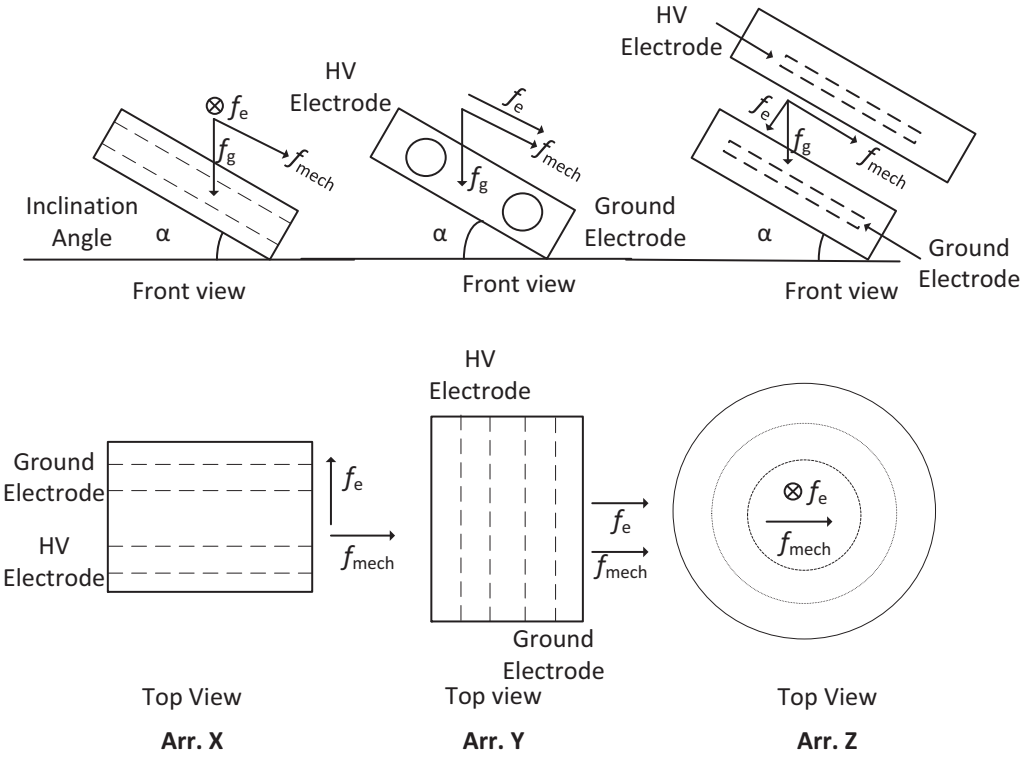

FIGURE 5.15: Inclined surface orientations under tangential and normal E-field stress;
(left) Arr. X: the force due to E-field ($\vec{f}_{\mathrm{e}}$) and the force due to gravity ($\vec{f}_{\mathrm{mech}}$) perpendicular to each other
(middle) Arr. Y: the force due to E-field ($\vec{f}_{\mathrm{e}}$) and the force due to gravity ($\vec{f}_{\mathrm{mech}}$) in the same direction
(right) Arr. Z: inclined surface orientations under normal E-field stress

5.4.5 Multiple Drops

To investigate the effects of multiple drops on the PD inception E-field strength, different configurations according to Figure 5.16 are chosen. The numeric assignment in the

water droplet configuration represents the number of the droplets, and the alphabetic assignment is for the distance between them. "A" stands for 4 mm distance, whereas "B" stands for 8 mm distance. For instance, "3A" means that there are three droplets at 4 mm distance to each other. All configurations discussed here are placed in the uniform tangential electric field.

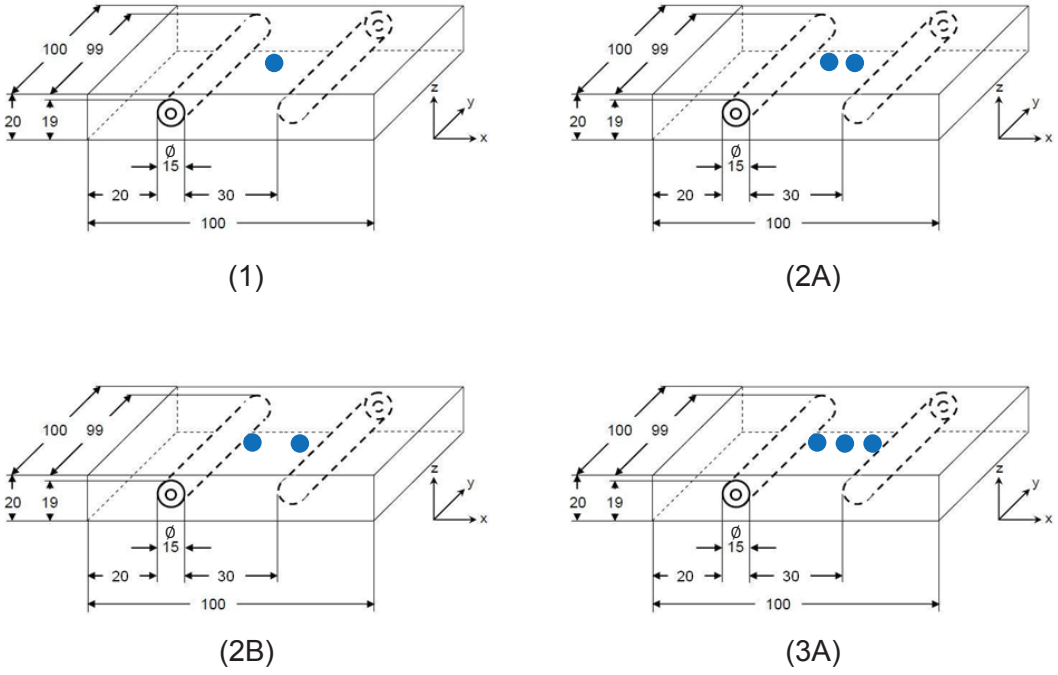

FIGURE 5.16: Different multiple water drops configurations

Chapter 6

Experimental Results and Discussion

6.1 Introduction

Deformation of water droplets during application of different types of an electric field as well as electric partial discharges at the water droplets under variation of a large set of parameters are experimentally investigated in this chapter.

Comparing the PD inception E-field strengths of all volumes of water droplet at all frequencies under horizontal (tangential) and vertical (normal) E-field stress showed that the tangential E-field provides lower PD inception values. Figure 6.1 shows a comparison between tangential and normal E-field inception field strengths for water droplets of 20, 60 and 100 µl volume on a silicone rubber surface. The water droplets under tangential E-field stress were found to develop partial discharges earlier than those under normal E-field stress, which is in good agreement with the results found by [Sar11]. Partial discharges occur at triple lines under tangential E-field stress, while they occur often at the top of the water droplet under normal E-field stress. Due to the severity of tangential E-field, in large part of this work only a merely tangential E-field is being considered.

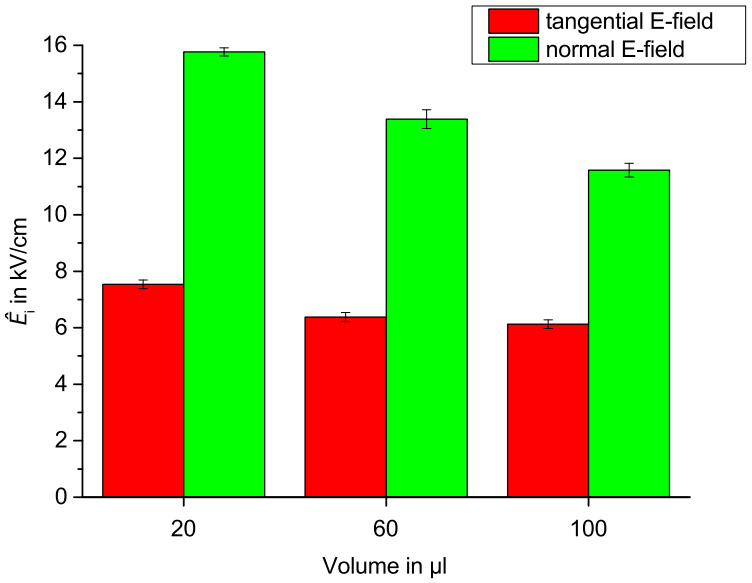

FIGURE 6.1: Inception E-field of water droplet on silicone rubber surface under tangential and normal E-field stress (50 Hz)

6.2 AC Investigations

At first the behavior of water droplets located on polymeric insulating surfaces at alternating voltage are investigated. These behaviors are analyzed considering the oscillation of water droplets under the impact of high electric field as well as their partial discharge characteristics under variation of a large set of parameters.

6.2.1 Oscillation Modes

The experimental setup for mechanical oscillation measurements is shown in Figure 5.4. A large set of videos with water droplet volumes varying from 20 to 100 µl in the frequency range of 20 to 100 Hz on the two different surface materials (SiR and ER) are captured. Comparison of the captured videos shows that four dominant oscillation modes develop on the SiR surface with its high degree of hydrophobicity, while on the ER surface, due to its lower degree of hydrophobicity, almost all of the modes seem to be identical. Four different oscillation modes of the water droplet dominantly occur on the SiR surface, which are named mode No.1 to mode No.4. They are illustrated in Figure 6.2.

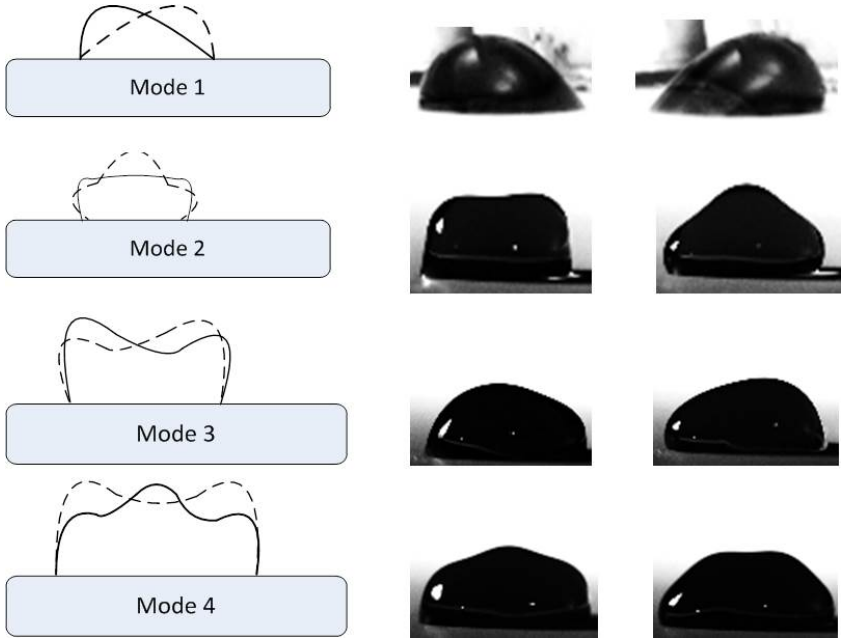

FIGURE 6.2: Four dominant oscillation modes of a water droplet on SiR surface under tangential E-field stress

In mode No.1 the water droplet periodically develops sharp edges on one side and elongates towards the electrodes two times per cycle of the applied electric field. In this case the water droplet has two different peaks on its shape, each one related to one half-cycle. Mode No.2 consists of two up and down shrinking positions. The water droplet stretches upwards and then shrinks back down two times per cycle. In mode No.3 the water droplet moves in a way that two different peaks occur in its left and right part during one half-cycle each of the applied electric field. Stronger oscillation at top of the water droplet can be seen in mode No.4, which has periodically three or more peaks on its shape during oscillation.

Mode analysis in the range of 20 to 100 Hz shows an increasing trend of mode number with frequency for all investigated volumes (Figure 6.3). Comparing the captured videos of conductive and non-conductive water droplets additionally shows that conductivity, varied in the range of 30 µS/cm to 120 mS/cm, has no effect on the pattern of water droplet oscillation under tangential E-field stress.

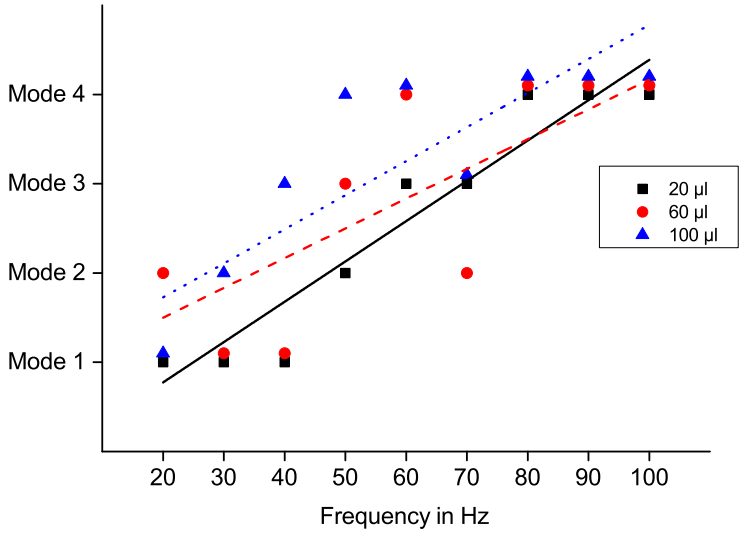

FIGURE 6.3: Mode number vs. frequency for 20, 60 and 100 µl non-conductive water droplets

6.2.2 Frequency analysis

In order to find the critical frequencies in respect of the water droplet oscillation under tangential electric field stress, "3D" recorded frames are analyzed. Figure 6.4 shows sample "3D" recorded frames of water droplet oscillation during one cycle of the applied sinusoidal E-field. By measuring the dimensions of the water droplet in each frame according to Figure 6.5 the value of an A_{dn} factor can be derived in each frame. The A_{dn} stands for the A_{d} factor in each frame, normalizing by the reference value A_{d0} before voltage application. The critical frequencies can be found as frequencies, at which the higher A_{dn} values are observed.

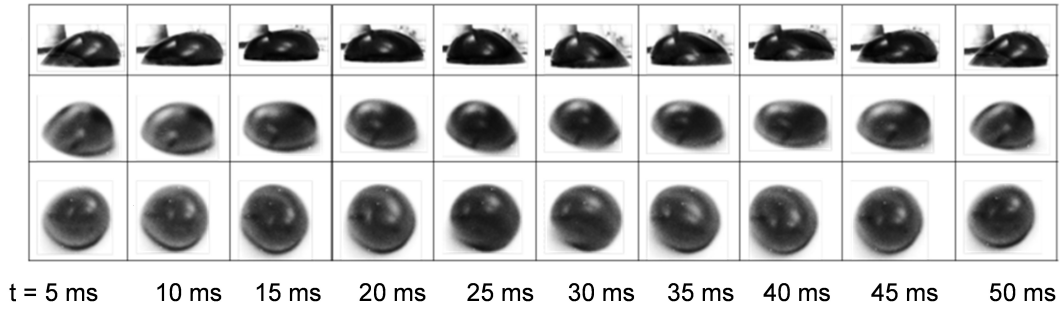

FIGURE 6.4: "3D" recorded frames of a 20 µl water droplet oscillation during one cycle of applied 20 Hz sinusoidal E-field (first row: front view, second row: side view and third row: top view)

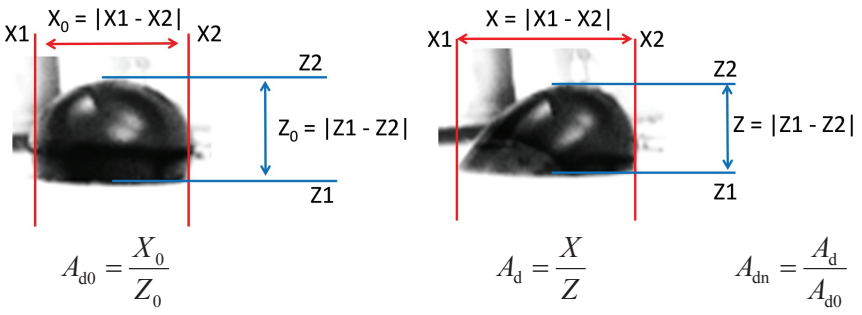

FIGURE 6.5: A_{dn} factor definition

Figure 6.6 exemplarily shows the resulting A_{dn} factors in ten recorded frames of one oscillation cycle for a 20 µl water droplet in the investigated range of frequencies. The 20 µl water droplet has an increase in A_{dn} at 20 Hz, which is due to the difference in mode numbers at different volumes and frequencies. The 20 µl water droplet oscillates at mode number 1 at 20 Hz, at which the water droplet elongates towards the electrodes. Increase in length of the droplet consequently leads to a bigger value of A_{dn}. Figure 6.7 shows the maximum A_{dn} values of each volume at different frequencies between 20 and 100 Hz. By increasing the volume of the water droplet, the mode number of oscillation increases, so for large volumes resonance occurs at high mode numbers, which leads to a lower but still considerable difference between the A_{dn} values at different frequencies. For example, the difference between A_{dn} values of 100 µl water droplet at 60 Hz, which oscillates at mode number 4, is considerable in comparison with the other frequencies.

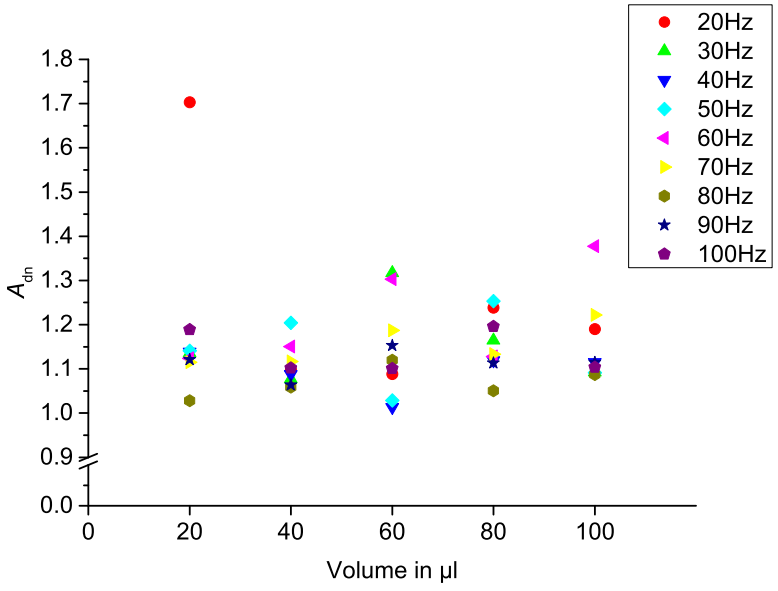

FIGURE 6.7: Summarized critical frequencies in respect of the water droplet oscillation

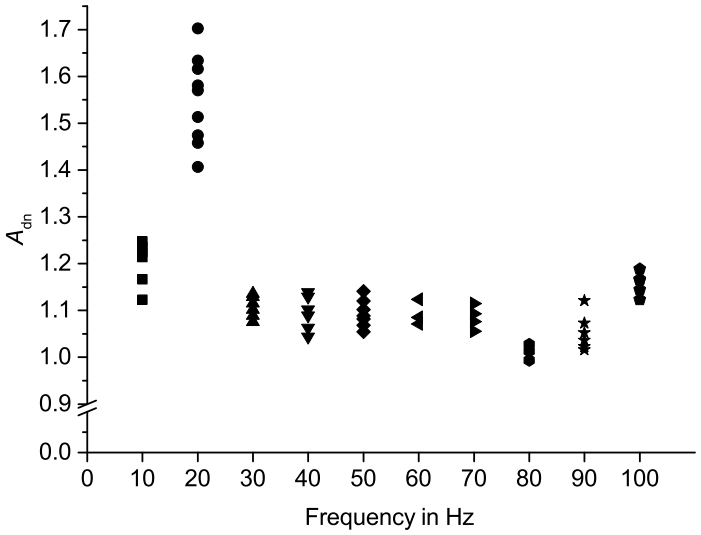

FIGURE 6.6: Resulting A_{dn} factors for a sample 20 µl water droplet

Considering the three highest A_{dn} values for each volume, the critical frequencies in respect of different oscillation modes for all investigated volumes of the water droplet between 20 and 100 µl are depicted in Figure 6.8.

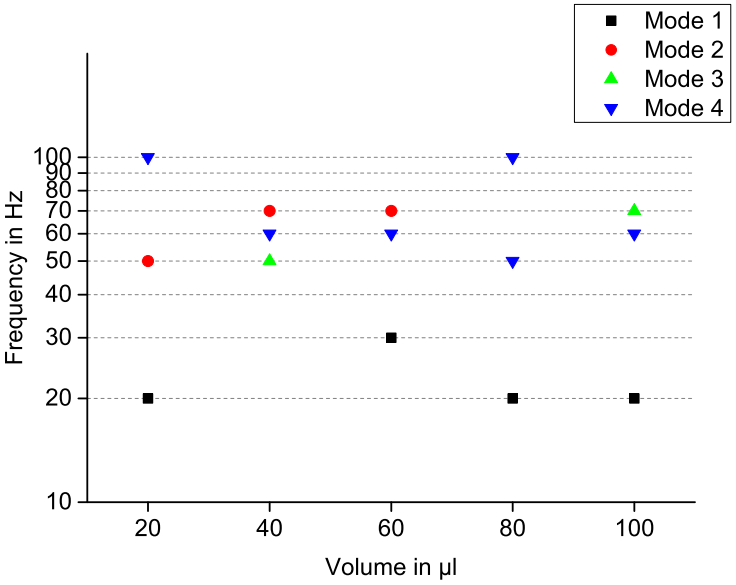

FIGURE 6.8: Critical frequencies in respect of different oscillation modes of the water droplet for all volumes between 20 and 100 µl

The frequency of water droplet oscillations has also been compared with the applied voltage frequency. It is observed that in some cases the water droplet vibrates with

twice the frequency of the applied voltage, but, in some other cases the frequency of water droplet oscillation is the same as the applied voltage frequency. Figures 6.9 and 6.10 show two typical vibrations. In these figures the calculated A_{dn} factor of the water droplet in one or two cycles of its oscillation is plotted. Figure 6.9 shows a movement of a 20 µl water droplet at 20 Hz applied voltage oscillating at 40 Hz, while Figure 6.10 shows a movement of a 60 µl water droplet at 70 Hz applied voltage oscillating at 70 Hz.

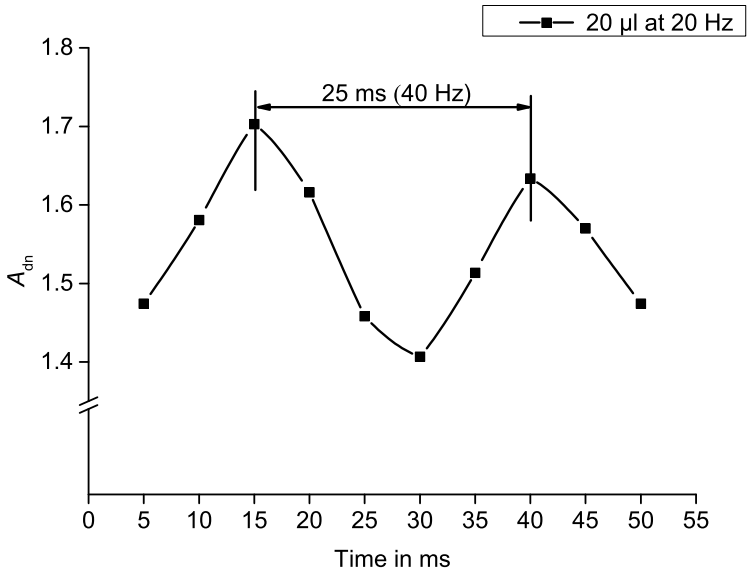

FIGURE 6.9: Vibration of a 20 µl water droplet at 20 Hz: mechanical oscillation at twice the frequency of applied voltage

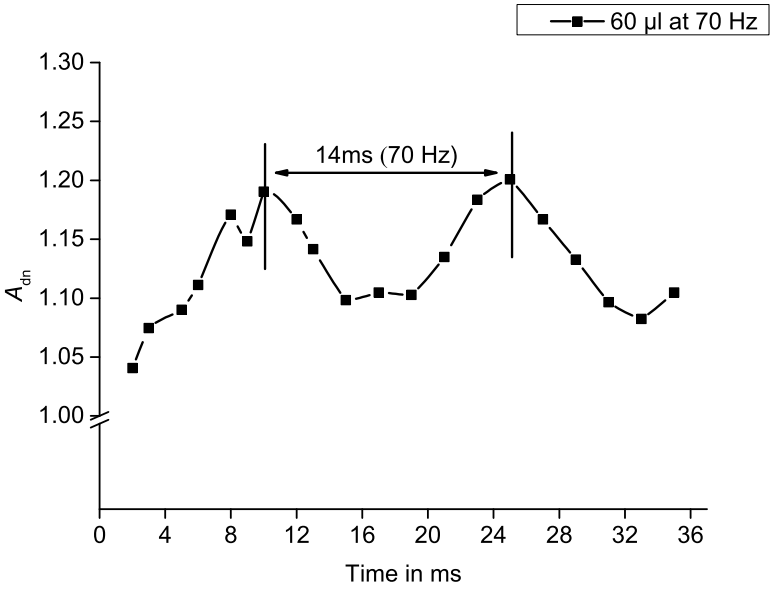

FIGURE 6.10: Vibration of a 60 µl water droplet at 70 Hz: mechanical oscillation at the frequency of applied voltage

Considering that water droplets oscillate with twice the frequency of the applied electric field [Fuj10, Kei03a, Yam03, Sch90, Hig02], the first reason of oscillation with the fundamental frequency is most probably due to the charging of the water droplet with existing free charge carriers in the lab or polarization of the droplet, as reported earlier by [Fuj10, Miz01]. The electric charge on the surface of the water droplet reduces the surface tension, so the charged water droplet has a lower surface tension in comparison with the uncharged water droplet. Lower surface tension leads consequently to the lower oscillation frequency of the drop under E-field stress [Fro00].
Fuji et al. [Fuj10] suggest a mass-spring-damper mechanical model for the water droplet on the surface. According to this model, the kinetic equation is expressed by [Fuj10]:

$$M \cdot \frac{\mathrm{d}^2 x}{\mathrm{d}t^2} + \mathrm{D} \cdot \frac{\mathrm{d}x}{\mathrm{d}t} + \mathrm{K} \cdot x = F \tag{6.1}$$

where M, D and K are mass, damping constant and spring constant, respectively. x is the displacement of the representative point on the water droplet and t represents the time. F is the main external force which can be expressed by the Maxwell tensor for uncharged droplets and by the Coulomb force for charged droplets [Fuj10]. Considering the Maxwell tensor in case of an uncharged drop results in:

$$F \propto \frac{E^2}{2} \propto \frac{E^2}{2} \cdot \sin^2 \omega t = \frac{E^2}{4} \cdot (1 - \cos 2\omega t) \tag{6.2}$$

where E is the electric field and ω is the angular frequency of the applied voltage. Solving Equation 6.1, considering only the steady state condition, results in displacement with twice the frequency of E:

$$x_{\mathrm{ss}}(t) = \mathrm{A} + \mathrm{B} \cdot \cos(2\omega t - \alpha) \tag{6.3}$$

where A, B and α are constants.
In case of a charged droplet and considering the Coulomb force, we have [Fuj10]:

$$F \propto q \cdot E \propto q \cdot E \cdot \sin \omega t \tag{6.4}$$

which leads to the water droplet displacement with the same frequency as that of the applied electric field:

$$x_{\mathrm{ss}}(t) = \mathrm{C} \cdot \cos(\omega t - \beta) \tag{6.5}$$

where C and β are constants.

As it can be seen, according to the theory of [Fuj10], the theoretically "uncharged" and "charged" water droplets oscillate with twice and the same frequency of applied electric field, respectively. However, a reliable method for quantitative measurement or calculation of the charges on the surface of water droplets under the impact of high electric field is still required. On the other hand, comparing the calculated resonance frequencies of the sessile droplet according to equation (3.11) for different modes of oscillation with experimentally found critical frequencies, at which the water droplet oscillates with the fundamental frequency only, shows also a reasonable similar pattern (Figure 6.11). Recently Songoro [Son15] has also pointed out that this phenomenon is caused by underdamped droplet oscillations, which originate in the transient regime [Son15]. It can be therefore concluded that this assumption that the water droplet oscillation with the fundamental frequency of applied electric field is due to the charging of the water droplet with existing free charge carriers in the lab or is due to the resonance frequencies of the sessile droplet stays still as an open question and has to be more investigated in future works.

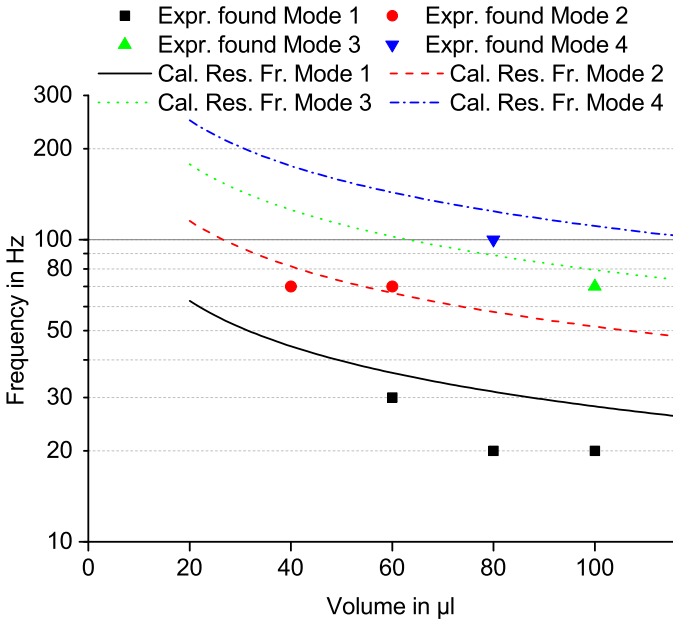

FIGURE 6.11: Experimentally found critical frequencies, at which the water droplet oscillates with the fundamental frequency of applied electric field and theoretical resonance frequencies of a sessile droplet

6.2.3 PD Inception Analysis

The test circuit of partial discharge measurement is shown in Figure 5.8. A large number of measurements for water droplet volumes of 20, 40, 60, 80 and 100 µl in a wide range of frequencies between 20 to 100 Hz is performed. Figure 6.12 compares the results of PD inception E-field strength of a non-conductive water droplet depending on volume on SiR ($\theta = 90°$) at 50 Hz with other results in the literature [Phi99b, Lop01]. The observed results are similar to the results obtained by Phillips et al. [Phi99b] and Lopez et al. [Lop01].

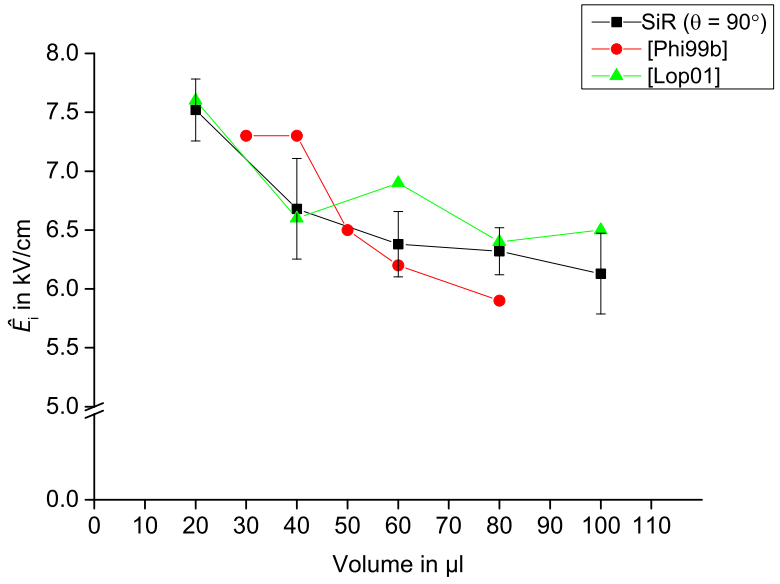

FIGURE 6.12: PD inception E-field strength of a single water droplet as a function of water droplet volume for SiR surface at 50 Hz

As it can be seen, the applied E-field required for PD inception decreases with increasing water droplet volume. This is also reported in [Gua05, Zhu03], where the maximum E-field enhancement factor at triple lines of larger water droplets under tangential E-field stress has been found to be higher than that of small droplets. Considering that larger volumes provide lower contact angles on the surface in comparison with small volumes, the higher E-field enhancement i.e. the lower inception E-field strength for larger droplets is expected. The PD inception E-field strength is reduced to 81% by increasing the droplet volume from 20 µl to 100 µl. However, the PD inception E-field strengths of large volume droplets (80 and 100 µl) are almost constant, as they are oscillating at a higher oscillation mode (mode No.4), at which only the top of the droplet

oscillates, while the bottom including the triple line stays virtually unchanged. It can be concluded that the PD inception E-field strength of water droplets decreases when the volume of the droplet increases. However, this dependency is not linear and depends also on the oscillation modes of the water droplet with different volumes.

6.2.3.1 Frequency Analysis

Figure 6.13 presents the average value of measured PD inception E-field strengths of non-conductive water droplets on SiR ($\theta = 90°$) as a function of water droplet volume and for different frequencies. Comparing the results of Figure 6.13 with A_{dn} values depicted in Figure 6.7 shows that the resonance condition does not always lead to lower partial discharge inception E-field strengths. For example, the 40 and 100 µl water droplets have the lowest PD inception E-field strength at 30 and 20 Hz, respectively, which are different from the main obtained critical frequencies of 50 and 60 Hz, which can be seen as higher A_{dn} values in Figure 6.7.

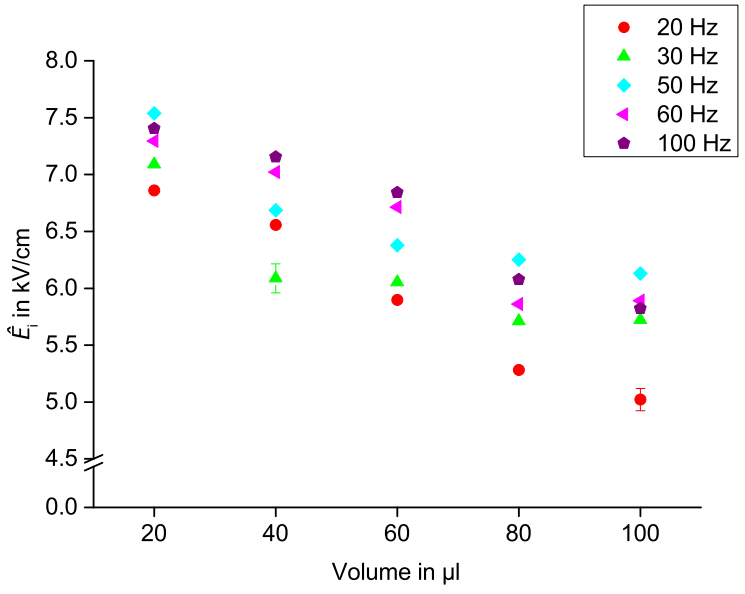

FIGURE 6.13: PD inception E-field strength as a function of water droplet volume for different frequencies

Another result is obtained by comparison of PD inception E-field strengths for different volumes at different frequencies. Obviously for small droplets (20, 40 and 60 µl), by increasing the frequency, the PD inception E-field strength increases. This follows the

trend of mode numbers depending on frequency. The reason is that at higher frequencies the upper part (the peak) of a small water droplet is moving more than the rest. Regarding that partial discharges would start in the triple zone of the water droplet (see, e.g., [Fei09]) and that the bottom part of water droplet stays unchanged at high frequencies, higher values of PD inception E-field strengths are expected. The PD inception E-field strength of large volume droplets (80 and 100 µl) increases also by increasing the frequency up to 50 Hz. At higher frequencies there is a large deviation but small differences in PD inception E-field strength of large water droplets. The reason could be due to similar oscillation modes of large water droplets at high frequencies. Reducing the distance between the water droplet and the electrodes leads to large deviation in PD inception E-field strengths of large volume droplets. Figures 6.14 and 6.15 show the frequency analysis of PD inceptions for a non-conductive water droplet on SiR under tangential E-field stress for small and large volumes, respectively.

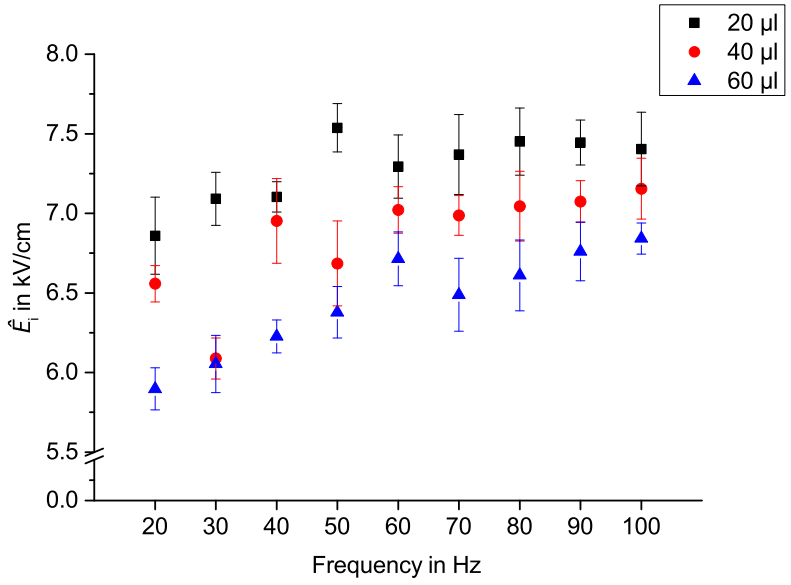

FIGURE 6.14: Frequency analysis of PD inceptions for a non-conductive water droplet on SiR under tangential E-field stress (small volumes)

The most interesting result is that PD inception E-field strength makes a step when the oscillation mode of the water droplet changes. For example, a 20 µl water droplet has oscillation mode numbers 1, 2 and 3, respectively, at 40, 50 and 60 Hz. Distinct differences in PD inception E-field strength at these three frequencies are detected (Figure 6.16). The reason can be explained by the different shapes of water droplet oscillations at different modes. As can be seen in Figure 6.2, the contact angles of water droplet at mode

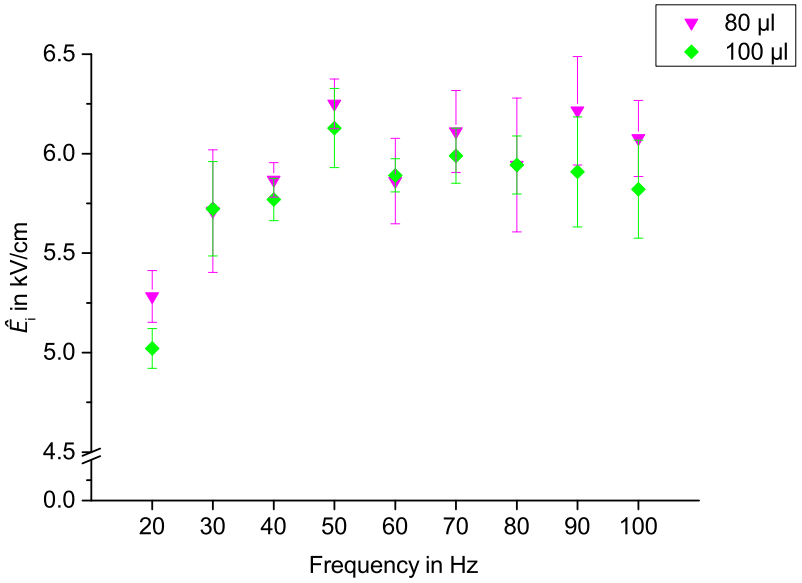

FIGURE 6.15: Frequency analysis of PD inceptions for a non-conductive water droplet on SiR under tangential E-field stress (large volumes)

numbers 1 and 3 are lower than those at mode numbers 2 and 4. Comparison of PD inception E-field strengths and mode numbers in several cases shows that mode numbers 1 and 3 result in lower values of PD inception E-field strength than mode numbers 2 and 4. More investigations have shown that the other steps in inception E-field strengths are also correlated to differences in mode numbers.

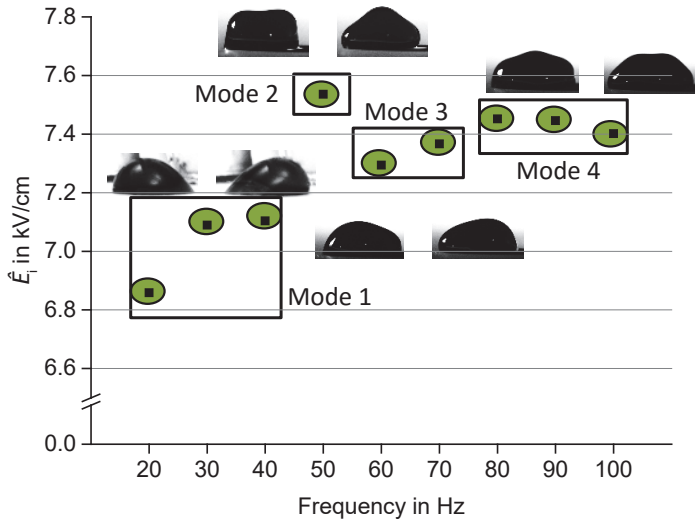

FIGURE 6.16: Typical steps in PD inception field strength when the oscillation modes change, depending on the frequency of applied voltage; (exemplary results for a 20 µl water droplet)

6.2.3.2 Water Droplet Conductivity Effect

As described in section 2.3.2 water droplets on hydrophobic insulating surfaces absorb pollutants and become conductive. Growing the conductive electrolyte layer short out the insulator, causing a flashover [Far09]. Therefore the conductivity of water droplets has an influence on flashover voltages. But it turns out that the conductivity of water droplets has no effect on the inception E-field strength on SiR surfaces having a high degree of hydrophobicity (WC≈1) with contact angles $\theta \geq 80°$. A conductive droplet on an ER surface with a lower degree of hydrophobicity (WC≈3) with contact angles of about 45°, results however, in marginally lower inception E-field strengths. In the following, the angle given in parenthesis indicates the contact angle. Figures 6.17 and 6.18 compare the results of PD inception E-field strength of conductive (120 mS/cm) and non-conductive (30 µS/cm) water droplets on SiR(90°) as well as on ER(45°) for 20 µl and 100 µl water droplets at three frequencies (20, 50 and 100 Hz) of the applied electric field. The PD inception E-field strengths of 20 µl non-conductive water droplets on SiR(90°) are measured as 6.86 kV/cm, 7.54 kV/cm and 7.42 kV/cm (peak) at 20 Hz, 50 Hz and 100 Hz, respectively. The PD inception E-field is the average value of six measurements with standard deviation of approximately 0.23 kV/cm at all three mentioned frequencies. A 20 µl non-conductive water droplet on ER(45°) results in PD inception E-field strengths of 5.68 kV/cm, 6.49 kV/cm and 6.46 kV/cm with standard deviation of 0.16 kV/cm, 0.16 kV/cm and 0.11 kV/cm from six measurements at 20 Hz, 50 Hz and 100 Hz, respectively. As it can be seen, PD inception E-field strength on the ER(45°) is lower than on the SiR(90°) due to its lower class of hydrophobicity as well as its higher permittivity, which provides higher E-field enhancement factor at the triple lines. Difference between PD inception E-field strength of conductive and non-conductive droplets on the SiR (90°) are very small (0.6% for 20 µl at 100 Hz or 1% for 100 µl at 20 Hz), but on the ER(45°) with lower degree of hydrophobicity, the conductive droplet has a marginal lower value of PD inception E-field strength. Difference in this case is observed to be 5.3% for 20 µl at 100 Hz and 4% for 100 µl at 20 Hz.

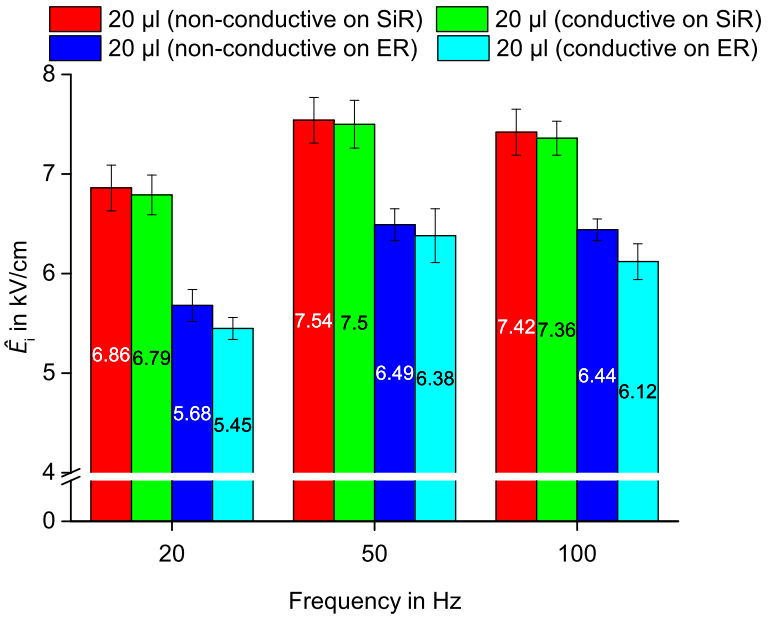

FIGURE 6.17: Effect of water droplet conductivity on PD inception E-field strength for SiR and ER (20 µl)

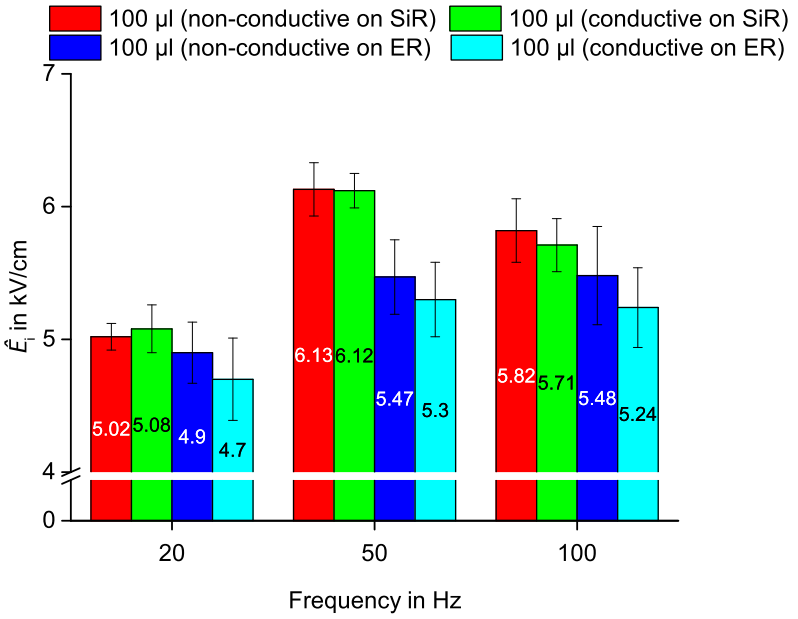

FIGURE 6.18: Effect of water droplet conductivity on PD inception E-field strength for SiR and ER (100 µl)

As a conclusion it can be pointed out that the conductivity of water droplets has a very low influence on the PD inception E-field strength of polymeric insulating surfaces. The inception E-field strengths of three different volumes of a single water droplet on a SiR surface at 50 Hz alternating voltage in a wide range of conductivities are also measured and depicted in Figure 6.19.

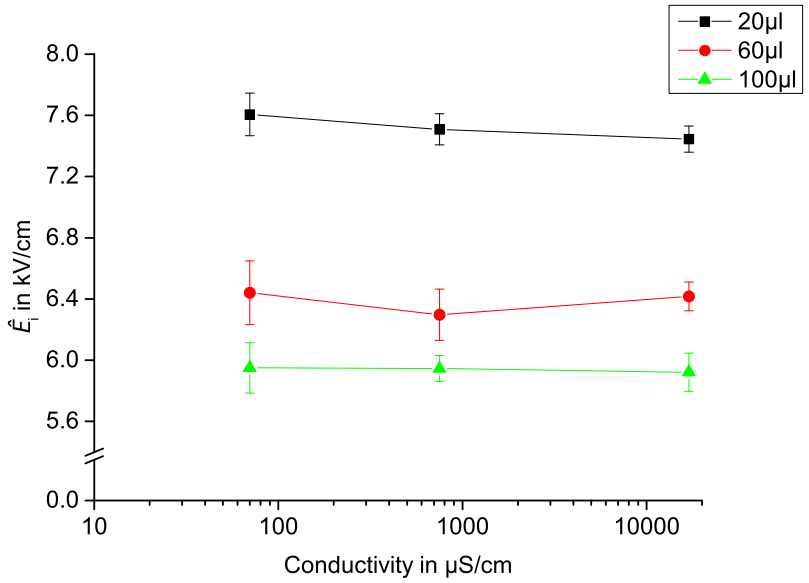

FIGURE 6.19: Effect of conductivity on PD inception E-field strength of a single water droplet on a silicone rubber surface at alternating voltage (50 Hz)

6.2.3.3 Surface Hydrophobicity Effect

In order to compare two materials, the PD inception E-field strength of a non-conductive water droplet at 20 and 100 Hz on the surface of SiR and ER are illustrated in Figures 6.20 and 6.21. As can be seen, on the surface of both materials, the PD inception E-field strength decreases when the volume of a water droplet increases. The reason is that larger water drops provide lower contact angles, which increases the electric field at triple lines and consequently leads to the lower PD inception. Comparing the PD inception E-field strength results of a 20 µl non-conductive water droplet on SiR (90°) and on ER (45°) shows that at 20 Hz, there is a difference of about 1.16 kV/cm (17%) in PD inception E-field strength. This difference reaches to 0.12 kV/cm (2.4%) for 100 µl droplet. The similar investigation at 100 Hz shows a difference of 0.93 kV/cm (12.7%) in PD inception E-field strength for 20 µl water droplet which reduces to 0.35 kV/cm (5.8%) for 100 µl droplet. The reason is that by increasing the water droplet volume, the contact angle of drop on SiR surface decreases. In other words, larger drops result in lower degrees of hydrophobicity on SiR surface, so the larger the water droplet, the smaller will be the difference between hydrophobicity class of SiR and ER surfaces. Therefore the smaller droplets have a bigger difference of PD inception E-field strength on two different surfaces.

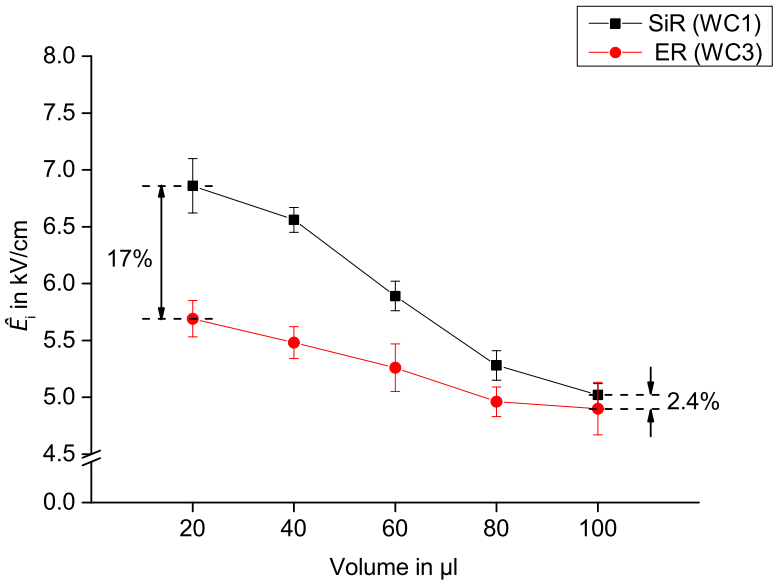

FIGURE 6.20: PD inception E-field strength of a non-conductive water droplet on the surface of SiR and ER (20 Hz)

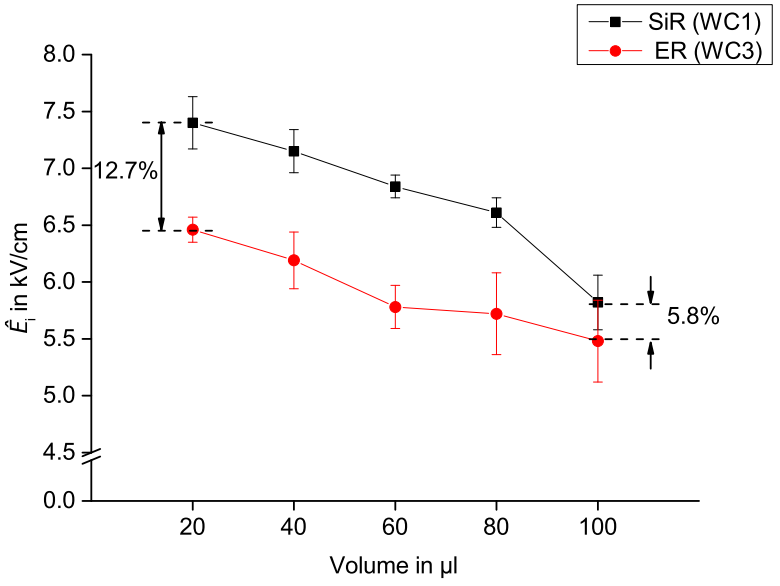

FIGURE 6.21: PD inception E-field strength of a non-conductive water droplet on the surface of SiR and ER (100 Hz)

The reduction in PD inception E-field strength with increase in the wettability of surfaces is expected, as the surface roughness of ER(WC3) was obviously higher than that of SiR(WC1) (see Figure 5.3). The higher the surface roughness, the lower will be the contact angle and the degree of hydrophobicity, which leads to a higher leakage current and consequently lower PD inception E-field strength. The results are also in good

agreement with the earlier findings by Philips et al. [Phi99b], in which it has been approved that better hydrophobicity leads to smaller droplet diameters for the same droplet volume and a higher curvature strain in the droplet, consequently results in higher E-field inception strength values.

6.2.3.4 Water Droplet Viscosity Effect

Figure 6.22 shows the effect of water droplet viscosity on inception E-field strength values. As it can be seen, the inception values increases by increasing the water droplet viscosity. This is due to the fact that the mobility of water droplets is reduced when viscosity is increased. The cone formation of water droplets under the impact of electric field is delayed due to high viscosity. The water droplet with higher viscosity starts to deform at higher E-field strength compared to the distilled water droplet until it reaches inception at the triple zones causing the higher inception E-field strength.

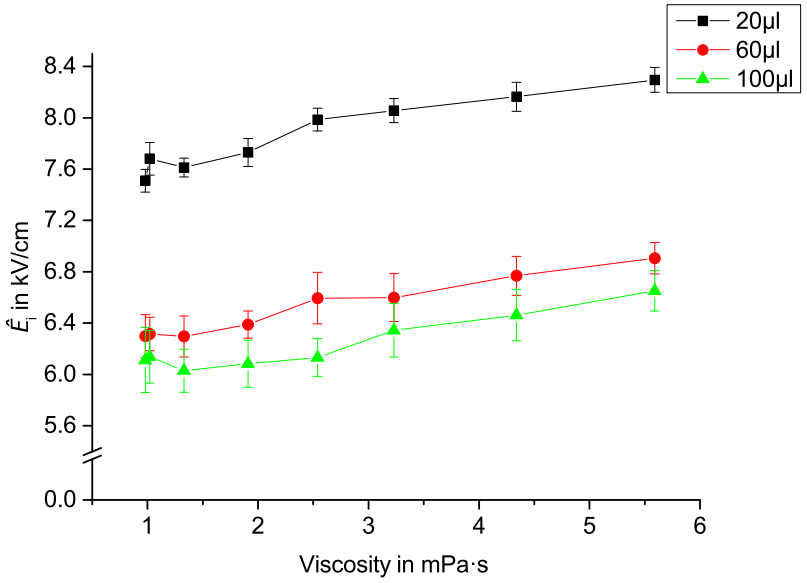

FIGURE 6.22: PD inception E-field strength depending on droplet viscosity

6.2.3.5 Multiple Drops

Figure 6.23 shows the results of the measured PD inception E-field strength for 20 µl and 40 µl water droplets in different configurations illustrated in Figure 5.16. As it can be seen, the higher the number of water droplets, the lower will be the PD inception

E-field strength. In case of two water droplets, the PD inception field strength of water droplets closer to each other is lower than that of droplets far from each other, because the PD starts between the droplets (see section 6.2.4 as well as sections 7.2.4, 7.2.5 and 7.2.6). The PD inception E-field strength of three water droplets is also lower than that of two droplets.

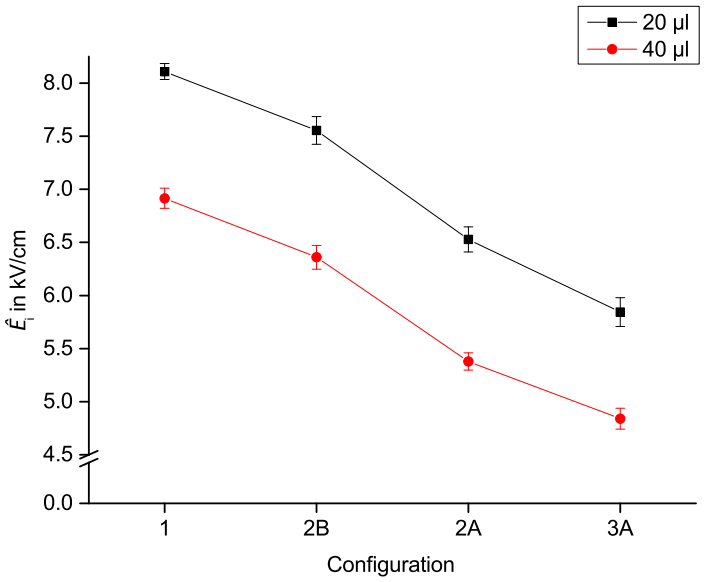

FIGURE 6.23: Comparison of PD inception E-field strengths of multiple drops arrangements (for definition of configurations see figure 5.16)

In order to investigate the effect of multiple droplets on PD inception E-field strengths closer to the reality, PD inceptions of a random spray of water droplets and dew droplets on the region of homogeneous E-field between electrodes on the surface is also measured. In random spray, water droplets with different volume and distance between them have been provided on the surface, using a prepared stencil and a flower sprayer. The number of water droplets in all random sprays were more than 100 drops. The average value of six measured PD inceptions is considered as the PD inception E-field strength. A method suggested by Braunsberger [Bra07] is also used for generating dew droplets. The method is described in section 5.4.1. Much more tiny droplets are formed under dew condition (see Figure 6.24). Figure 6.25 shows the results of PD inception E-field strength under random spray and dew conditions in an extended graph of Figure 6.23. It can be seen that the reduction in PD inception E-field strength will be saturated by increasing the number of water droplets. For random spray and dew conditions the inception E-field strength is measured as 5.07 and 4.54 kV/cm (peak value), respectively.

The average PD inception E-field strength under dew condition is lower than that of random spray but in deviation ranges. Figure 6.26 compares the results of PD inception E-field strength of multiple droplets under random spray and dew conditions on SiR surface with the results reported in the literature. A good agreement is noticeable.

FIGURE 6.24: Water droplets under random spray and dew conditions on SiR surface; stencil on the surface (left), random spray (middle) and dew droplets (right)

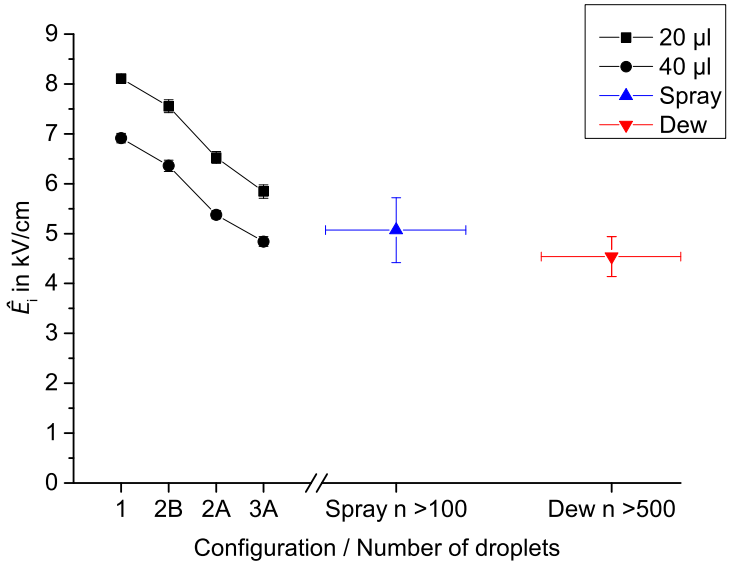

FIGURE 6.25: PD inception E-field strength of random spray and dew droplets on SiR surface

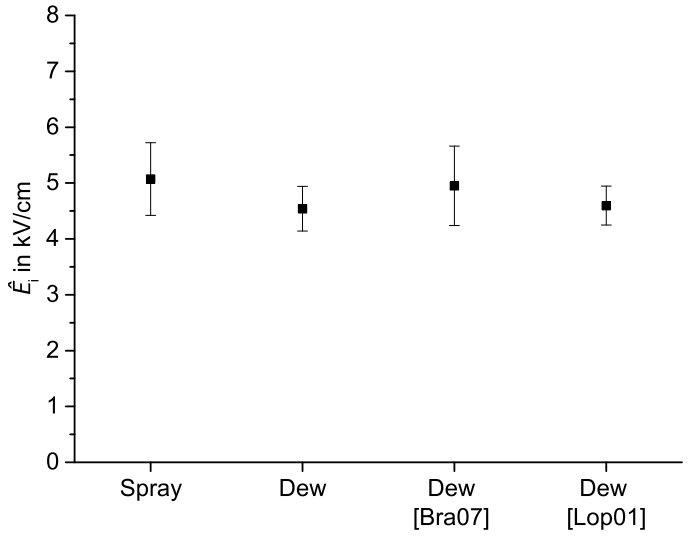

FIGURE 6.26: PD inception E-field strength of multiple droplets on SiR surface

6.2.3.6 Inclined Surfaces

Figure 6.27 presents the average value of the six measurements of the PD inception field strength with their standard deviations for 20 µl and 40 µl water droplets in arrangements X and Y according to Figure 5.15. In arrangement X (forces due to E-field and gravity perpendicular to each other), it can be observed that the inception E-field strength for both of the water droplet volumes increases linearly up to a certain inclination angle. Thereafter, the water droplets start rolling downwards. This tendency is clearly visible, though with high values of the standard deviations at higher inclination angles. Reason for the increase of the inception field strength with inclination angle is that the electric force and the force due to gravity in this arrangement are perpendicular to each other. Thus at higher inclination angles the force due to gravity tends to generate a tip at the edge of the water droplet, which is not in direction of the E-field force. As partial discharges start at the triple line, at higher inclination angles higher E-field forces are required to form a tip. Therefore, inception field strength increases with increasing inclination angle. For the same reason, the inception E-field strength for water droplets in arrangement Y (forces due to E-fields and gravity in same direction) decreases linearly up to a certain inclination angle, because in this arrangement E-field force and the force due to garvity are in the same direction. However the PD inception values in arrangement Y for both volumes of 20 µl and 40 µl start to decrease firstly from 5 degree

inclination angle. Although the physical reason behind this phenomenon (higher PD inception E-field strength at 5 degree inclined angle) is not yet fully understood, based on the experimentally found results and considering the worst case of arrangement Y, the PD inception E-field strength is reduced when the inclination angle is increased.
In arrangement Z according to Figure 5.15 (inclined surface orientations under normal E-field stress) no significant change is observed in PD inception by increasing the inclination angle (see Figure 6.28). The reason is assumedly that partial discharges always start at the top of the water droplets rather than at the triple line in this configuration. Therefore, changing the inclination angle has no effect on the distance between top of the water droplet and the upper electrode, and consequently the same PD inception voltages would be measured.

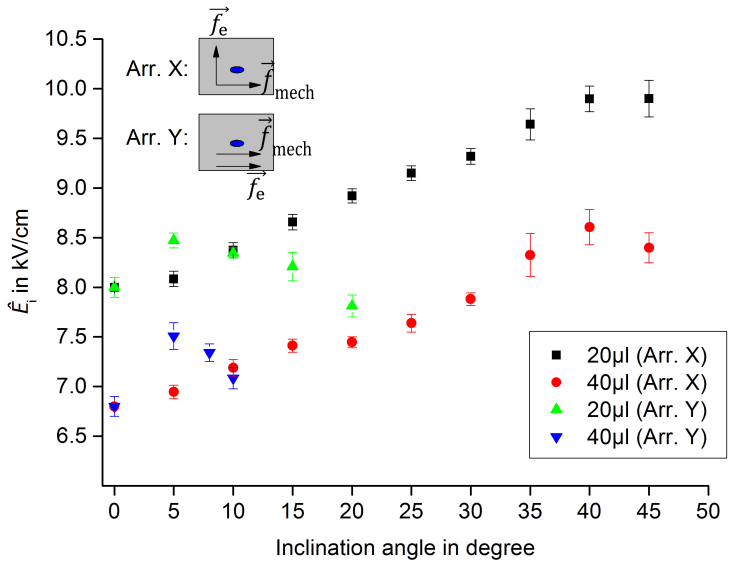

FIGURE 6.27: PD inception field strengths of water droplets in Arr. X and Y

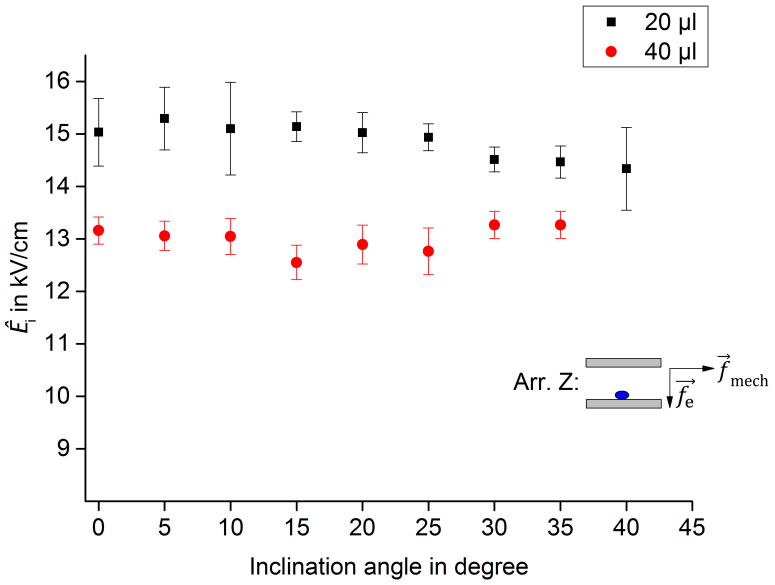

FIGURE 6.28: PD inception field of water droplets in Arr. Z

6.2.3.7 Multiple Drops on an Inclined Surface

Figure 6.29 compares the inception E-field strength of different water droplet configurations typically for a 20 µl water droplet at 0°, 10° and 20° inclination angles in Arr. X. A 20 µl water droplet in Arr. X results in PD inception E-field of 8.11 kV/cm, 7.76 kV/cm, 6.53 kV/cm and 5.84 kV/cm (all in peak value) at "1", "2B", "2A" and "3A" droplet configurations at flat position, respectively and are increased to 9 kV/cm, 8.94 kV/cm, 7.46 kV/cm and 7.30 kV/cm at 20° inclination angle. As it can be seen, the PD inception E-field of a 20 µl water droplet is increased about 11%, 13.2%, 14.2% and 20% at "1", "2B", "2A" and "3A" droplet configurations, respectively by increasing the inclination angle from 0° to 20°. Figure 6.30 represents the inception E-field for a 20 µl water droplet at different inclination angles in Arr. Y. The inception E-field at 5° inclination angle is the highest for all configurations. However when the inclination angle is increased from 5° to 10° a decrease to 98%, 94%, 89% and 92% in PD inception E-field strength is observed for "1", "2B", "2A" and "3A" water droplet configurations, respectively.

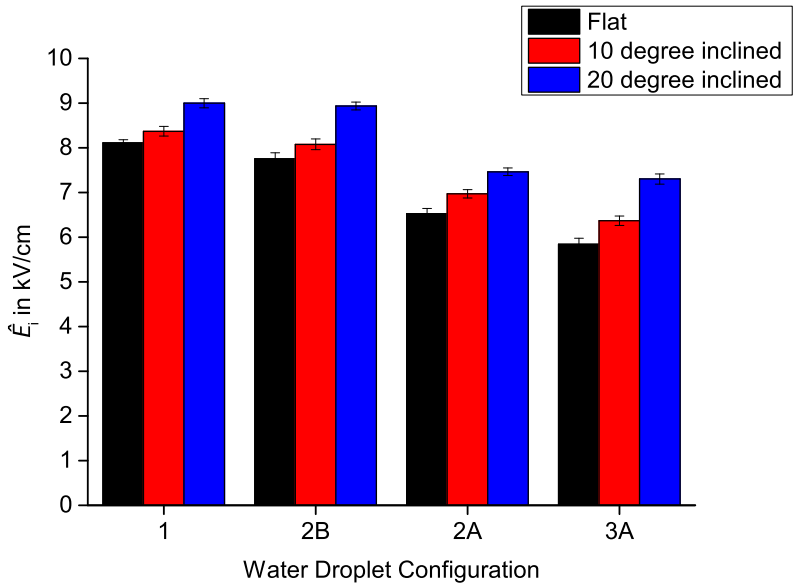

FIGURE 6.29: Comparison of inception E-field strength of 20 µl water droplet in Arr. X at different inclination angles

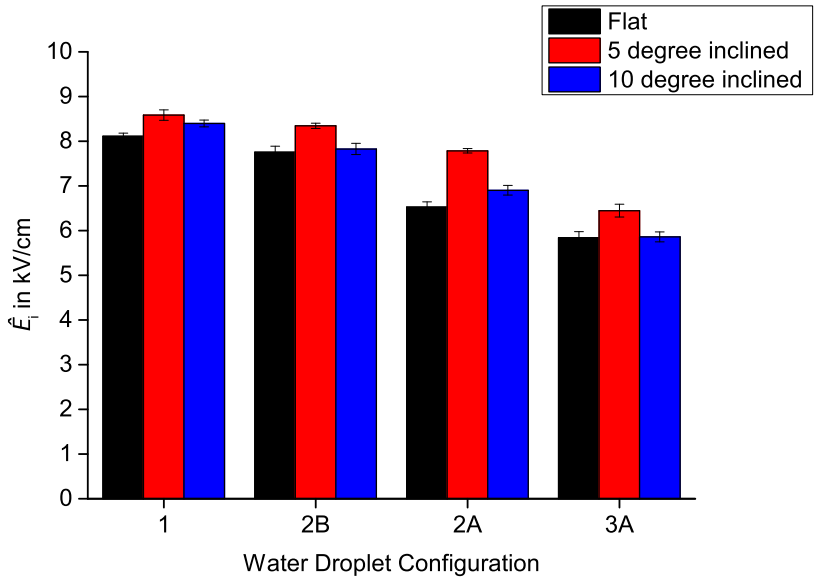

FIGURE 6.30: Comparison of inception E-field strength of 20 µl water droplet in Arr. Y at different inclination angles

It can be concluded that increasing in inclination angles will reduce the PD inception E-field strength of water droplets in Arr. Y, in which the forces due to E-field and gravity are in same directions. This is valid for single as well as for multiple droplets on inclined surfaces.

6.2.4 PD Localization

The partial discharges of single and multiple water droplets at different configurations are localized using a day-light UV-camera. Figure 6.31(a) shows the location of partial discharges of a single water droplet on the flat surface of silicone rubber under tangential E-field stress. As expected for a single droplet, the PD starts from the triple lines towards the electrodes (i.e. in E-field direction). For two water droplets, the first occurrence of PD is localized at the position between the droplets, which is confirmed by simulation results (see Chapter 7). By increasing the E-field further PDs are also detected at the triple lines towards the electrodes. Some snapshots with voltage increasing are depicted in Figure 6.31(b). PD localization of three droplets in triangle configuration shows that at first PD starts from the inside triple lines between two water droplets, which are in direction of the electric field. By increasing the voltage PDs from other triple lines are also obtained. The PD development can be seen in Figure 6.31(c).
The PD inception voltage under normal E-field stress starts at first from the top of the droplet, because of high E-field stress at this point. By increasing the voltage, PD at triple lines is also detected. The snapshots of the UV-camera for single and two water droplets under normal E-field stress are shown in Figure 6.32. The streamer channel (blue columns at the top of water droplets) can also be observed at very high level of PDs in Figure 6.32.

(a) Single droplet

(b) Two droplets

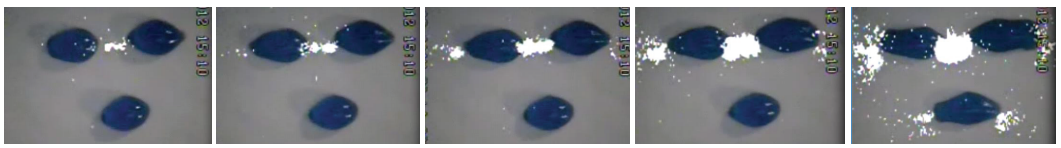

(c) Triangle droplets

FIGURE 6.31: PD localization of water droplets under tangential E-field stress; in each case increasing voltage from the left to the right

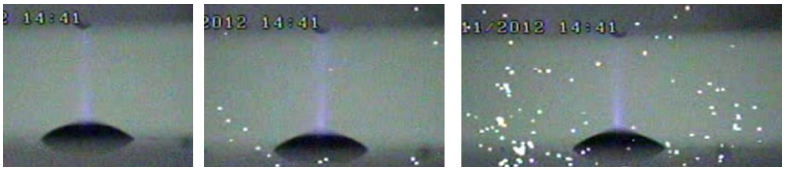

(a) Single droplet

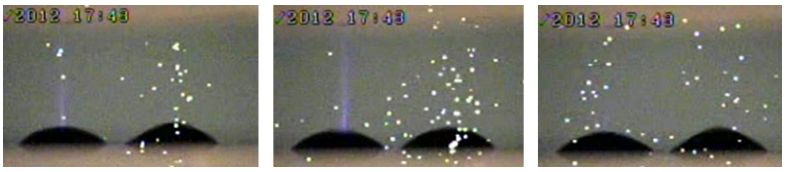

(b) Two droplets

FIGURE 6.32: PD localization of water droplets under normal E-field stress; in each case increasing voltage from the left to the right

Figure 6.33 and 6.34 show also the sequence snapshots of PD localization for random spray as well as for dew droplets. As it can be seen, the PD starts at first between droplets on the surface. By increasing the E-field, PDs are trying to reduce the gap between electrodes. A trace of discharges between two electrodes can be finally observed.

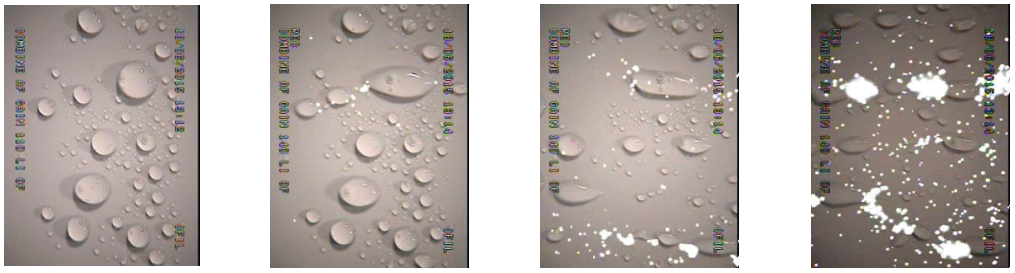

FIGURE 6.33: PD localization of random spray water droplets

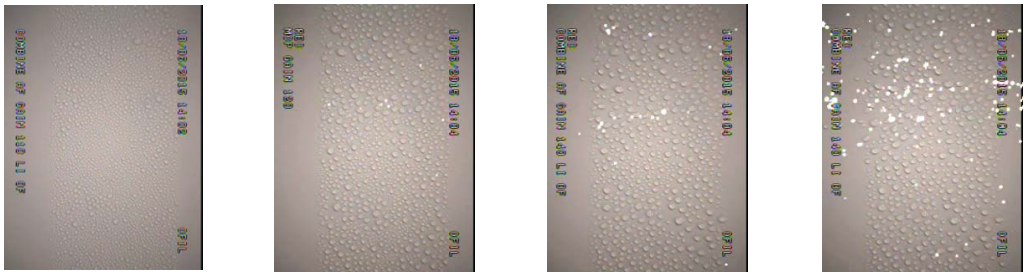

FIGURE 6.34: PD localization of dew droplets

6.2.5 Summary AC Investigations

The behavior of water droplets on polymeric insulating surfaces under alternating E-field stress is experimentally investigated. A single water droplet oscillates in four different oscillation modes on the SiR surface. The PD inception E-field strength of water droplets is dependent on the oscillation modes and a step (jump) in PD inception E-field strength is observed when the oscillation mode of the water droplet changes. Mode numbers 1 and 3 have been found to result in lower values of PD inception E-field strength rather mode numbers 2 and 4.

The water droplet vibrates with twice the frequency of the applied voltage, however, in some cases the frequency of water droplet vibration is found to be the same as the applied voltage frequency. The reason is assumedly either due to the charging of the water droplet with existing free charge carriers in the lab or due to resonance frequencies of the sessile droplet. This is still an open question and has to be investigated in future works.

Resonance condition does not always lead to lower partial discharge inception E-field strengths of water droplets. The maximum allowable E-field strength tangential to a polymeric insulating surface in presence of a single water droplet on the flat surface of WC1 is found to be between 6 and 7.5 kV/cm (peak). This value reduces to about 4.5 kV/cm (peak) for more water droplets on the surface like random spray and dew droplets.

Conductivity of water droplets has a very low influence on the inception E-field strength values. The reduction in PD inception E-field strength with increase in the wettability of surfaces is also observed. The PD inception E-field strength of water droplets increases by increasing the water droplet viscosity.

Three different inclined surface arrangements are investigated. In arrangement X, in which forces due to E-field and gravity were perpendicular to each other, the inception E-field strength increases with increasing the inclination angle, while in arrangement Y, in which forces due to E-fields and gravity were in same direction, the inception E-field strength decreases. In arrangement Z (inclined surface orientations under normal E-field stress) no significant change is observed in PD inception E-field strengths by increasing the inclination angle. It is also found that water droplets under tangential E-field stress develop partial discharges earlier than those under normal E-field stress.

By localizing partial discharges, it is observed that the PD starts from the triple lines

towards to the electrodes under tangential E-field. For two water droplets, the first occurrence of PD is localized at the position between droplets. Under normal E-field stress, it is found that the partial discharge starts at first from the top of the water droplet.

6.3 DC Investigations

6.3.1 Movement Analysis

Captured videos of the water droplet movement at direct voltages have shown that the water droplet does not oscillate on the surface. It elongates slowly towards one electrode and is suddenly deformed at a certain time. This process of elongation and deformation can happen again after a while. Figure 6.35 shows a typical movement of a single water droplet at high direct voltage. For generalization of the analysis in this section, the terms "positive DC" and "negative DC" are defined in a way that the earth electrode is always the same and only the polarity of the high voltage electrode is changed. A polarity-dependent elongation/deformation of water droplets is observed. In case of positive DC, the water droplet elongates towards the earth electrode and deforms (jumps) to the opposite side at a certain time. This process is vice versa for the negative polarity of direct voltage. The droplet elongates towards the high voltage electrode and deforms (jumps) to the opposite side at the time of deformation (see Figure 6.36). No reasonable explanation could be found so far for this polarity dependent behavior. Comparing the elongation of different volume water droplets shows also that smaller droplets elongate faster than larger drops. Figure 6.37 shows the normalized elongation factor (the ratio of the water droplet length under the impact of E-field to its initial length without E-field) for two different volumes of water droplets. It can be seen that the normalized elongation factor for larger droplets is lower than that for small droplets and the elongation process takes longer time for larger drops.

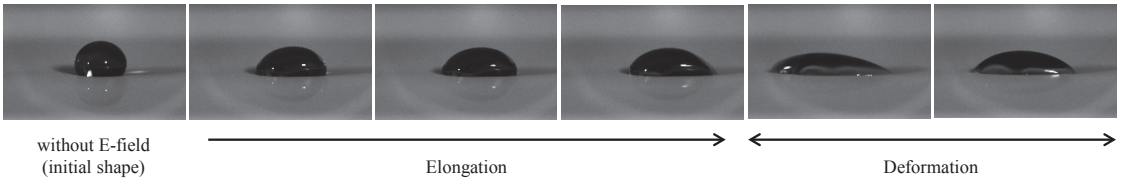

FIGURE 6.35: Typical movement of a single water droplet at direct voltage (positive DC in left side and earthed electrode in right side); from left to right: constant voltage at the moment of deformation (results for 20 µl)

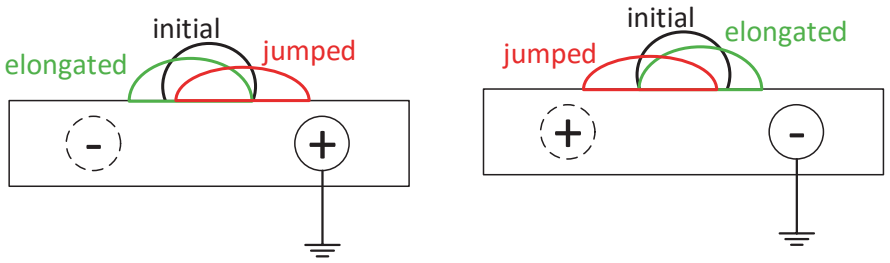

(a) Negative (b) Positive

FIGURE 6.36: Water droplet movement at positive and negative direct voltage

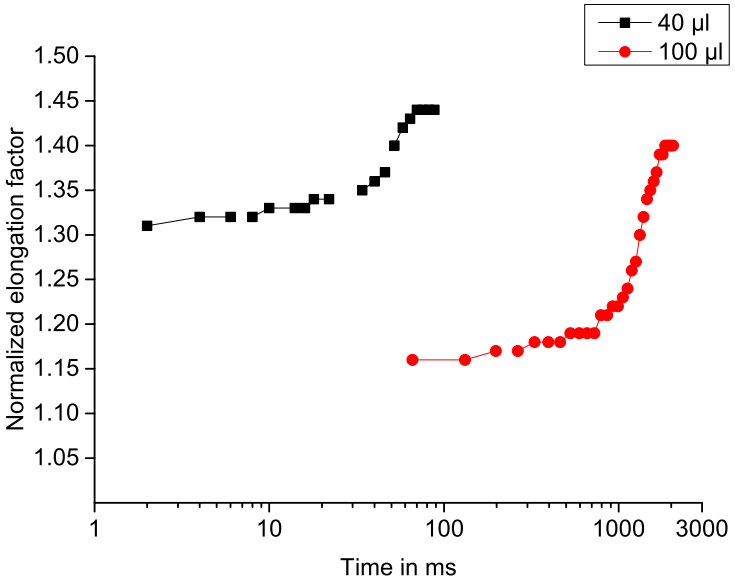

FIGURE 6.37: Normalized elongation factor of a single water droplet at direct voltage

6.3.2 PD Characteristics

A set of PD measurements at both positive and negative polarities of high direct voltage for a 100 µl water droplet are taken during 30 minutes of applied voltage at levels of about

80%, 100% and 120% of the respective AC inception E-field strength ($\hat{E}_{\mathrm{i,ac}}$). Figure 6.39 shows the typical results of apparent charge of individual PD pulses. Although the PD characteristics of water droplets under DC stress follows a statistic process and is not completely reproducible, following properties are found to be noticeable;

- Based on the homogeneity of the E-field on the surface no big difference between both polarities is expected. However, and as it can be seen in Figure 6.39, at 80% of $\hat{E}_{\mathrm{i,ac}}$, the PD signals are detected only at negative polarity. The reason can be due to the movement of water droplet, which can affect the homogeneity of the electric field distribution on the surface. Such behaviors are also reported in the literature under inhomogeneous E-field stress (e.g. [Fro95b, Bey02]).

- At both polarities of the applied direct voltage the first PD signal is detected after a time of less than five minutes.

- Mostly, the PD signals consist of two or more different discrete PD levels, which may be explained by the differently sharped edges of the deformed water droplet under DC stress (see Figure 6.38 as an example).

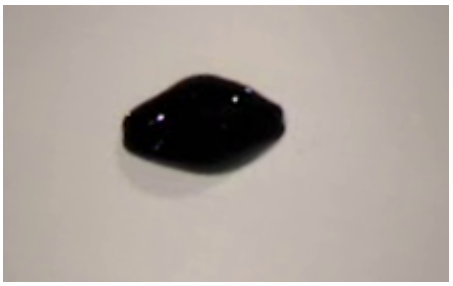

FIGURE 6.38: Differently sharped edges of the deformed water droplet under DC stress (top view snapshot)

- At higher electric fields ($1.0 \cdot \hat{E}_{\mathrm{i,ac}}$ and $1.2 \cdot \hat{E}_{\mathrm{i,ac}}$) the charge magnitude at positive polarity of the direct voltage is higher than that at negative polarity, while the number of discharges at positive polarity is less than that at negative polarity. Figures 6.40 and 6.41 show also typical accumulated apparent charges as well as the typical histogram of PD pulse count against apparent charge intervals for a non-conductive 100 µl water droplet at both positive and negative direct voltage corresponding to $1.0 \cdot \hat{E}_{\mathrm{i,ac}}$ as recommended in new amendment of [IEC00]. These are also in agreement with the pattern results obtained for corona discharges at direct voltages in [Fro95b].

- It is also observed that by increasing the voltage to values above the respective AC inception E-field strength, charge magnitudes and number of discharges increase (at both polarities), which proves that the detected PD signals are originating from surface discharges.

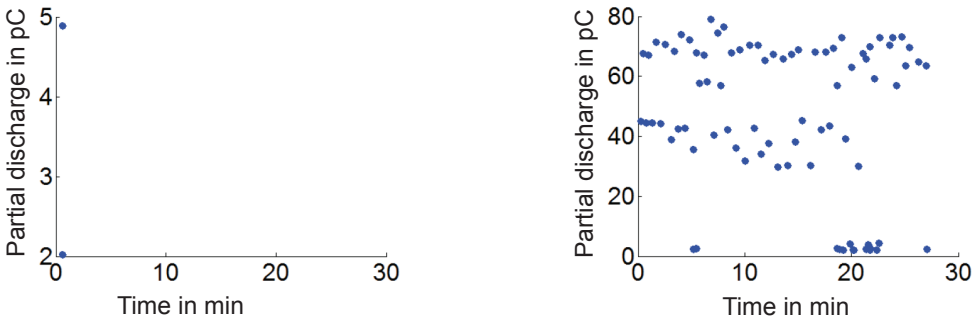

(a) $E_{\mathrm{dc}} = 0.8 \cdot \hat{E}_{\mathrm{i,ac}}$

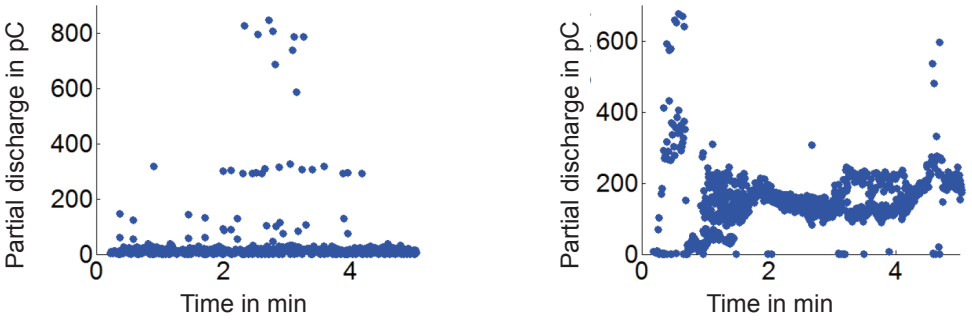

(b) $E_{\mathrm{dc}} = 1.0 \cdot \hat{E}_{\mathrm{i,ac}}$

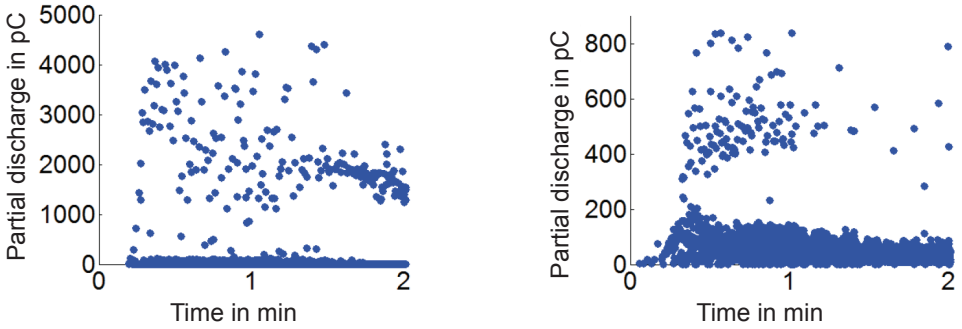

(c) $E_{\mathrm{dc}} = 1.2 \cdot \hat{E}_{\mathrm{i,ac}}$

FIGURE 6.39: Apparent charge of individual PD pulses for a non-conductive 100 µl water droplet at direct voltage; left: positive DC and right: negative DC (Note: different scales of the y-axes)

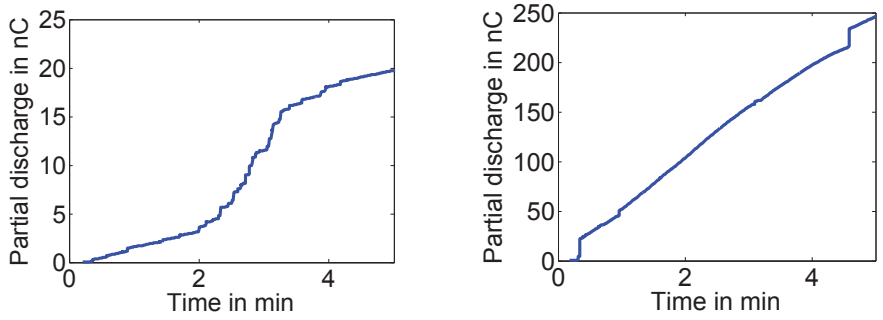

(a) Positive DC (b) Negative DC

FIGURE 6.40: Accumulated apparent charge for a non-conductive 100 µl water droplet at direct voltage correspond to $1.0 \cdot \hat{E}_{\mathrm{i,ac}}$

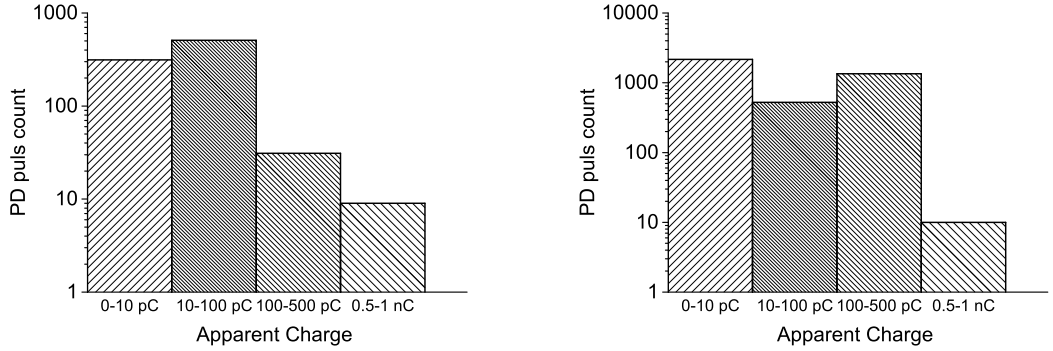

(a) Positive DC (b) Negative DC

FIGURE 6.41: Histogram of PD pulse count against apparent charge intervals for a non-conductive 100 µl water droplet at direct voltage correspond to $1.0 \cdot \hat{E}_{\mathrm{i,ac}}$

6.3.3 Conductivity Effect at Direct Voltage

Figure 6.42 shows the PD measurement results for a 100 µl conductive single water droplet (120 mS/cm) at direct voltages of about 80%, 100% and 120% of $\hat{E}_{\mathrm{i,ac}}$ at both positive and negative polarities. The difference between PD signal levels for non-conductive and conductive water droplets is assumedly because of the different shapes of the deformed water droplets on the surface. Each PD level refers to corona of the one of sharped edges of the deformed water droplet. Different contact angles of the deformed water droplets on the surface provide different PD signal levels at each condition. At higher conductivity, it seems that at increased field stress $1.2 \cdot \hat{E}_{\mathrm{i,ac}}$ the charge magnitude increases more at negative polarity.

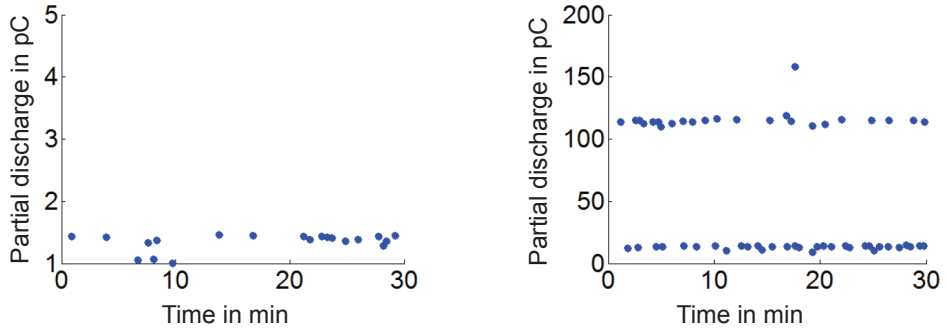

(a) $E_{\mathrm{dc}} = 0.8 \cdot \hat{E}_{\mathrm{i,ac}}$

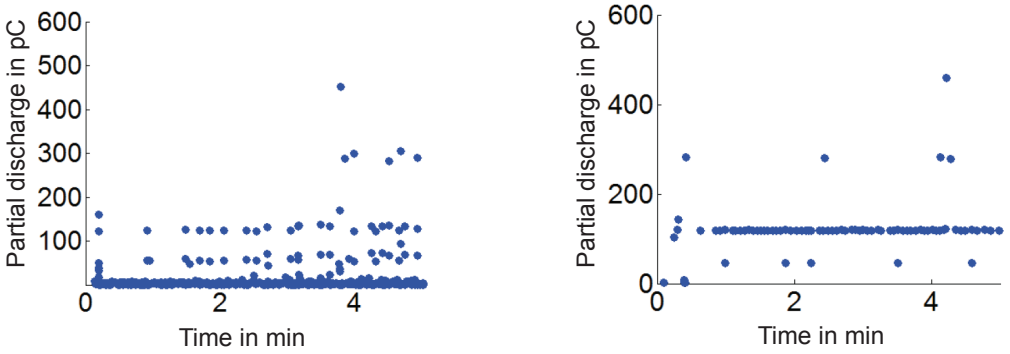

(b) $E_{\mathrm{dc}} = 1.0 \cdot \hat{E}_{\mathrm{i,ac}}$

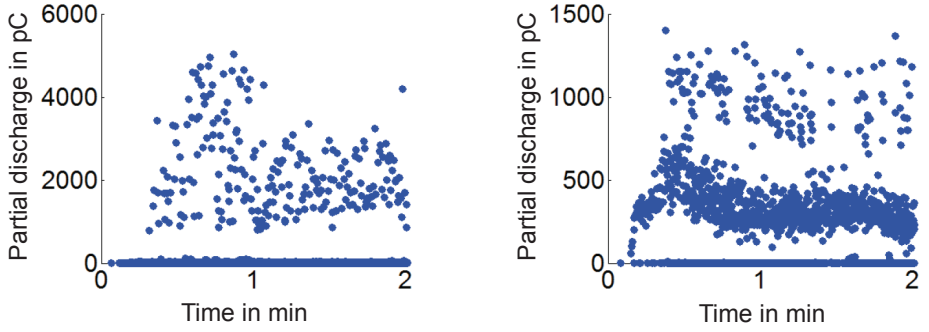

(c) $E_{\mathrm{dc}} = 1.2 \cdot \hat{E}_{\mathrm{i,ac}}$

FIGURE 6.42: Apparent charge of individual PD pulses for a conductive 100 µl water droplet at direct voltage; left: positive DC and right: negative DC

6.4 Combined AC/DC Investigations

6.4.1 Movement Analysis

Water droplet movement at combined alternating/direct voltage consists of an oscillation superimposed to an elongation towards the electrodes. Figure 6.43 compares two frames of a recorded video with different deformations of the water droplet, which are typical for an 80 µl water droplet at combined alternating/direct voltage under both positive and negative DC polarities. The main observation is that the water droplet elongates towards the AC electrode when the polarity of DC applied source is negative, while it elongates towards the DC electrode in case of positive applied direct voltage. The investigation of discharge initiated by water droplet on epoxy nanocomposites under direct voltage by Sarathi et al. [Sar13] also shows a similar behavior of the water droplet at a different geometry. It has been pointed out that a droplet moves towards the ground electrode under a negative direct voltage, whereas it moves towards the high voltage electrode under a positive direct voltage [Sar13].

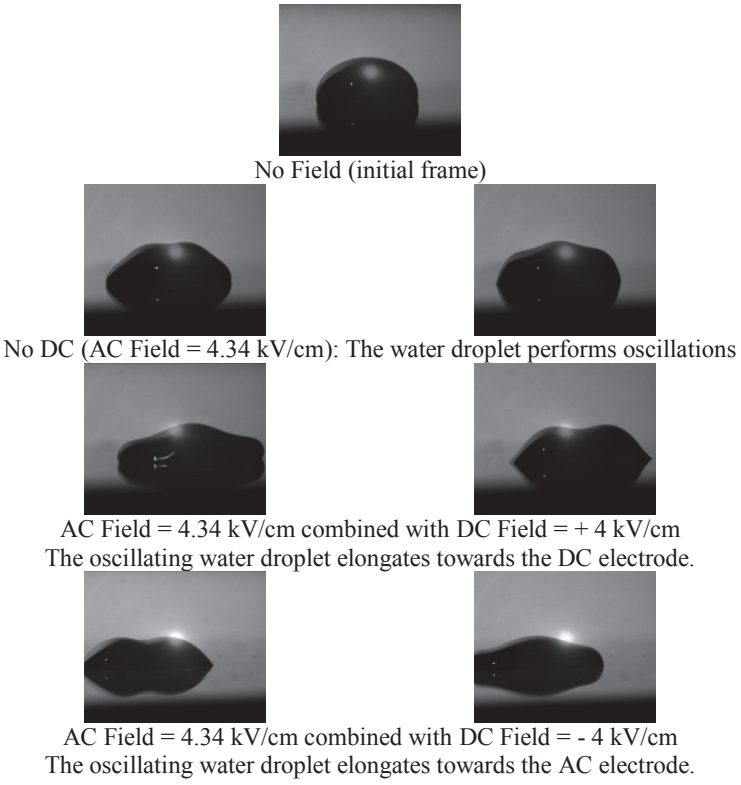

FIGURE 6.43: Deformation of a water droplet (80 µl) at combined alternating/direct voltage

An intensive analysis of water droplet movements at combined alternating/direct voltage is performed, selecting ten frames of one cycle of captured videos for a wide droplet volume range from 20 µl to 100 µl. The length of the water droplet, its left and right (i.e. those oriented towards the electrodes) contact angles as well as their distances from both electrodes are measured at each frame. Three parameters - the minimum contact angle, the maximum elongation and the minimum distance to the opposite electrode - are calculated and normalized based on their initial positions (without E-field). Since the water droplet elongates towards different electrodes at positive and negative polarities of the combined AC-DC stress, and in order to be able to compare this elongation at both polarities, the opposite electrode is considered as the AC electrode in case of negative direct voltage and the DC electrode in case of positive direct voltage. These normalized parameters are calculated for all volumes under 4.34 kV/cm (peak) AC E-field (at which it was found earlier that the water droplet performs periodical oscillations) and under 1, 2 and 3 kV/cm positive and negative DC electric field stress. Results are summarized in Figure 6.44. As it can be seen, by increasing the DC component of combined alternating/direct voltage, the minimum normalized contact angle of the water droplet decreases while its elongation factor increases. This means that at higher direct voltages, the water droplet does not only elongate more but that it also has a lower minimum contact angle, which can be the reason for the lower PD inception E-field strength. The minimum distance to the opposite electrode (which is the AC electrode in case of negative direct voltage or the DC electrode in case of positive direct voltage) is evaluated for positive and negative DC source polarities (Figure 6.45). The water droplet elongates towards the opposite electrode at combined alternating/direct voltage. One exception is, however, the 20 µl droplet, which does not move towards the electrodes at both polarities. The reason is assumedly due the larger ratio of adhesion to electric force.

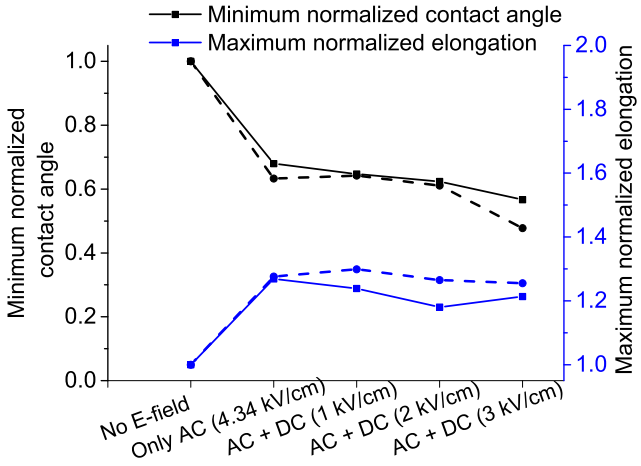

(a) 20 µl

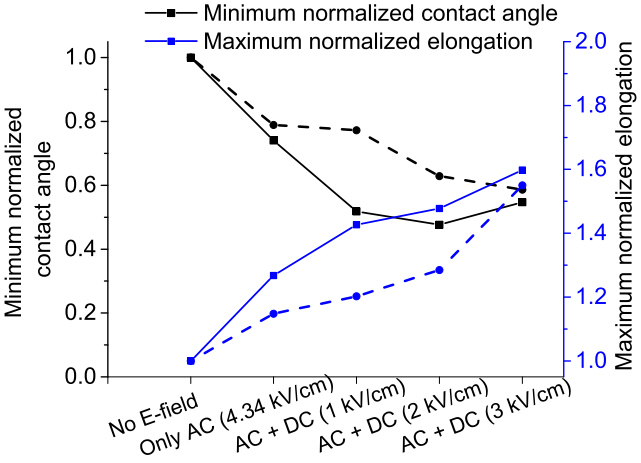

(b) 60 µl

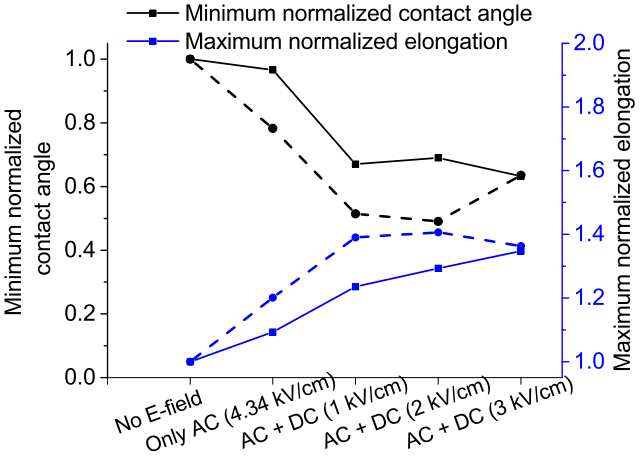

(c) 100 µl

FIGURE 6.44: Minimum normalized contact angle and maximum normalized elongation for different droplet volumes; solid lines: at positive DC, dashed lines: at negative DC voltage

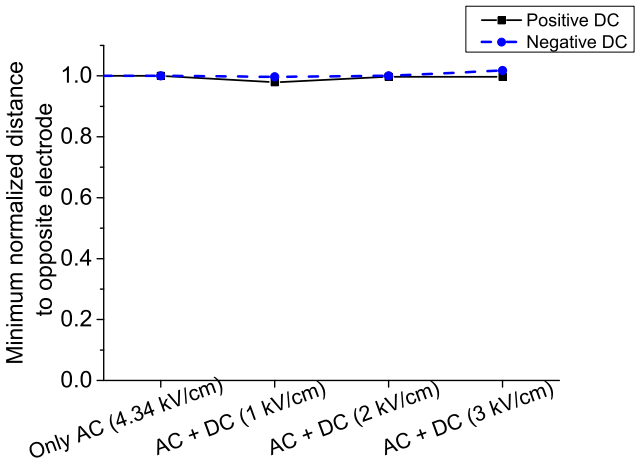

(a) 20 µl

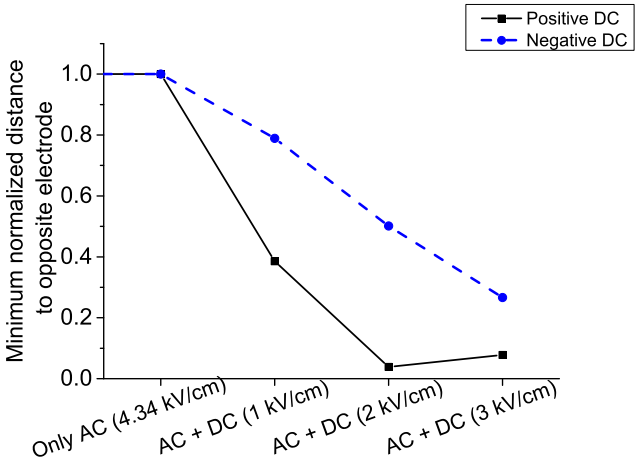

(b) 60 µl

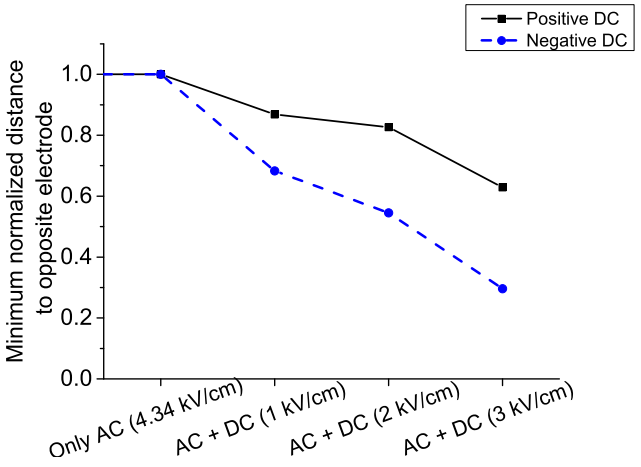

(c) 100 µl

FIGURE 6.45: Minimum normalized distance to the opposite electrode for different droplet volumes; solid lines: at positive DC, dashed lines: at negative DC voltage

6.4.2 PD Characteristics

Figure 6.46 shows PD inception results of 20 and 100 µl water droplets at combined alternating/direct voltages. The PD inception E-field strength is reduced when the DC component of the voltage is increased at both positive and negative polarities. The inception E-field strength of a 20 µl water droplet is relatively higher than that of a 100 µl at both polarities. Figure 6.47 shows the polarity effect on PD inception E-field of water droplets at combined alternating/direct voltage. As can be seen, water droplets at positive polarity of DC electric field have relatively lower inception values. The reason can be explained as follows. Near the AC electrode, the charges injected to the surface due to external E-field stress during the positive half cycle will be swamped out in the negative half cycle, leading to minimum amount of charge accumulation on the surface. But near the DC electrode, more accumulated charges can enhance the E-field at the edge of the water droplet, leading to lower inception voltage. Therefore, when the water droplet moves towards the DC electrode (at positive direct voltage) a lower inception field strength is resulting in comparison with the case that it moves towards the AC electrode (at negative direct voltage). It was also observed that at positive and negative polarities of direct voltage, PD starts first at the time instant of the negative and positive peak value of the voltage shape, respectively.

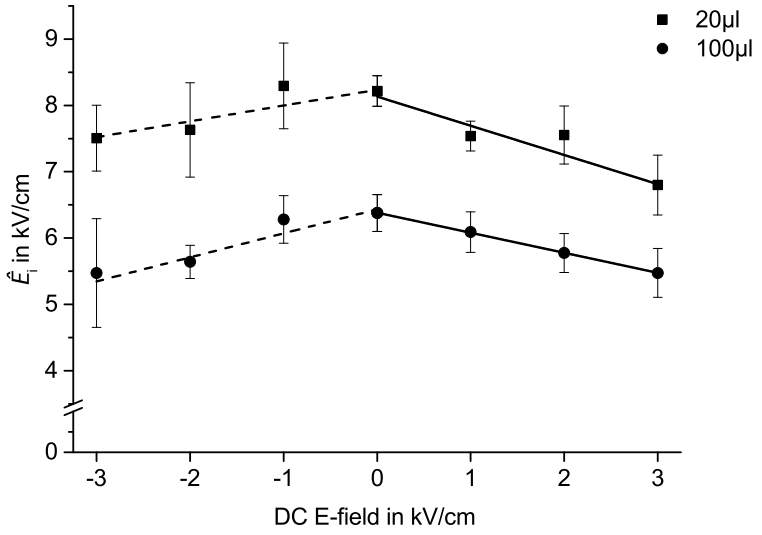

FIGURE 6.46: PD inception E-field strength of water droplets at combined alternating/direct voltage

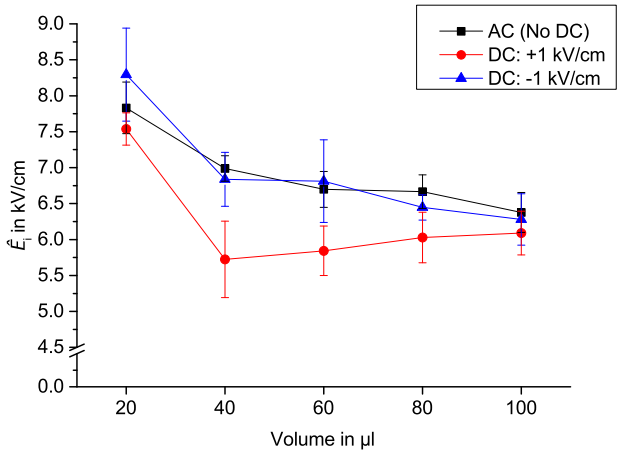

(a) DC Field = 1 kV/cm

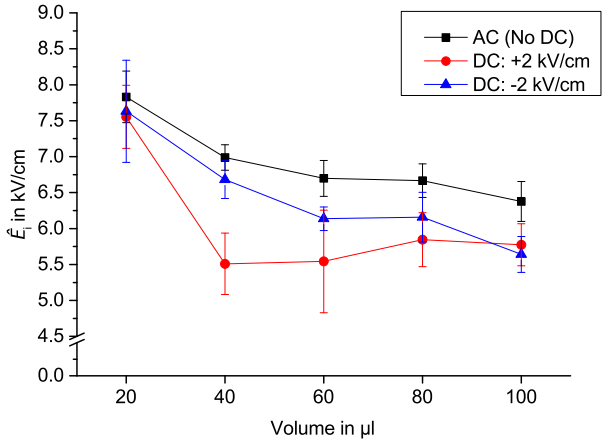

(b) DC Field = 2 kV/cm

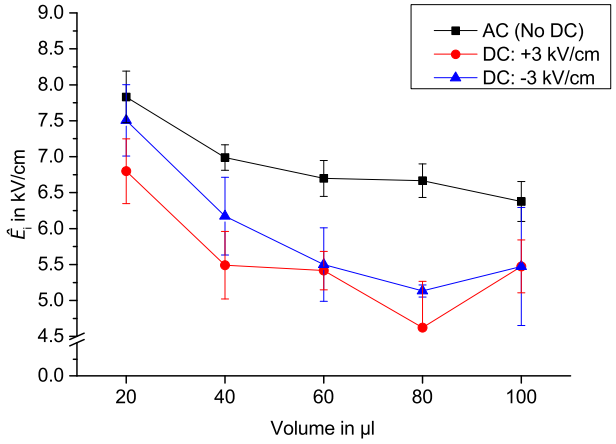

(c) DC Field = 3 kV/cm

FIGURE 6.47: Polarity effect on PD inception E-field strength of water droplets at combined alternating/direct voltage

6.4.2.1 Frequency Effect at Alternating/Direct Voltage

As described in Chapter "AC investigations", the water droplet oscillates in different oscillation modes at alternating voltage, which are frequency dependent. For instance, a 20 µl water droplet oscillates in mode numbers 1, 2 and 4 at 20 Hz, 50 Hz and 100 Hz, respectively. This behavior has an influence on PD inception E-field strength of the water droplet at alternating voltages (Figure 6.16). In order to analyze the frequency effect on PD inception E-field strength of the water droplet at combined alternating/direct voltages, the results of PD measurements of a 20 µl water droplet with different DC E-field components and at three different frequencies of alternating voltage (20, 50 and 100 Hz) are presented in Figure 6.48. The pattern of frequency effect at alternating/direct voltage is almost similar to that at alternating voltage (compare Figure 6.16): inception field strength increases in the order 20 Hz - 100 Hz - 50 Hz.

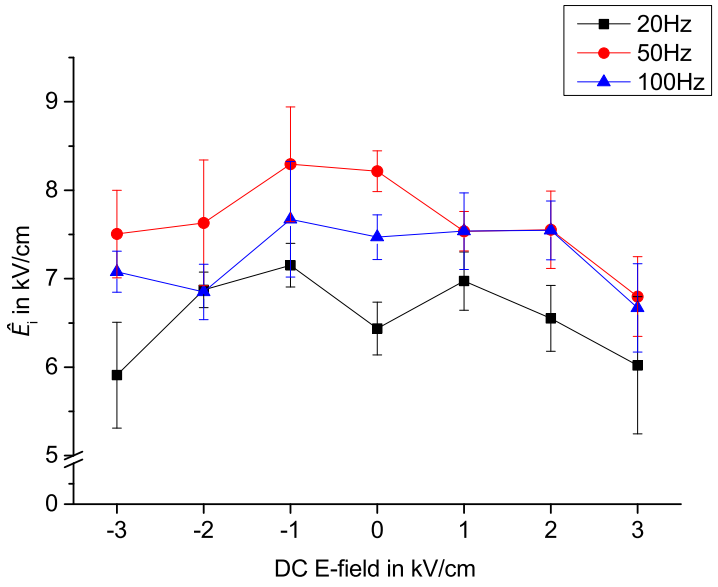

FIGURE 6.48: Frequency effect on PD inception E-field strength of water droplets at combined alternating/direct voltage (results for 20 µl water droplet)

6.4.2.2 Conductivity Effect at Alternating/Direct Voltage

Figure 6.49 shows the influence of water droplet conductivity on the inception E-field strength of 20 µl and 100 µl water droplets. It is obvious that although conductivity has no effect at alternating voltage (DC E-field = 0), conductive water droplets have lower PD inception values in comparison with non-conductive ones when increasing the

DC component at both polarities. This might assumedly be due to induced surface charges on the insulating surface due to movement of the water droplet, which lead to a lower inception E-field strength. Another possible explanation is due to the big difference between water droplet and air conductivities, which affects the E-field distribution under DC stress. The reduction in inception E-field strength is more severe at negative direct voltages.

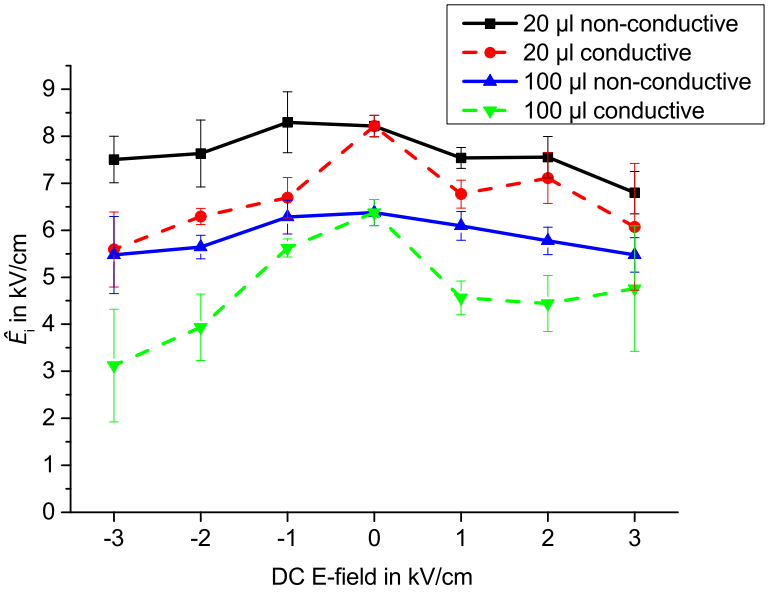

FIGURE 6.49: Effect of conductivity on PD inception E-field strength of a single water droplet on a silicone rubber surface at alternating/direct voltage

6.5 Summary of Experimental Investigations

A systematic experimental investigation on the deformation of water droplets located on polymeric insulating surfaces as well as their PD inception characteristics at alternating, direct and combined alternating/direct voltages were presented and discussed. Following results were obtained:

- At alternating voltage:
  - Water droplets oscillate in different oscillation modes, which has an influence on PD inception E-field strength.
  - PD inception E-field strength is reduced to 81% by increasing the volume of water droplet from 20 µl to 100 µl. However, a very low reduction in PD

inception E-field strength of large water droplets (larger than 60 µl) could be observed.

  - Conductivity of the water droplet has a very low influence on the PD inception E-field strength, when the surface is hydrophobic.
  - On inclined surfaces, PD inception E-field strength can be reduced to about 90%, depending on the direction of dielectric and gravitational forces on the droplet.
  - Multiple droplets on the surface as well as random spray and dew droplets will reduce the PD inception E-field strength to ca. 4.5 kV/cm (peak).
  - On the surface of WC 3 (contact angle of about 45°) the PD inception field strength can reduce to about 85% rather the surface of WC 1 (contact angle of about 90°).

- At direct voltage:
  - Water droplets do not oscillate on the surface. They elongate slowly towards one electrode and suddenly deform at a certain time. This process can happen after a while again.
  - There is no definition for partial discharge inception E-field strength at direct voltage. Charge magnitude over time can be used as a PD characteristic.
  - Charge magnitude at positive polarity of direct voltage is higher than at negative polarity, whereas the number of discharges at positive polarity of direct voltage is less than at negative polarity.
  - By increasing the applied direct voltage to values above respective AC inception E-field strength ($\hat{E}_{\mathrm{i,ac}}$), charge magnitude and number of discharges is increased for both polarities.
  - By increasing the water droplet conductivity at high field stress it seems that the charge magnitude increases more at negative polarity.

- At combined alternating/direct voltage:
  - Water droplet deformation consists of an oscillation superimposed to an elongation towards the electrodes.

- The water droplet elongates towards the AC electrode when the polarity of applied direct voltage is negative, while it elongates towards the DC electrode in case of applied positive direct voltage.
- For both positive and negative polarities of direct voltage, PD inception E-field strength is reduced when the DC component of the combined alternating/direct voltage is increased.
- Water droplets at positive polarity of DC electric field have relatively lower PD inception values in comparison with negative direct voltage.
- For both polarities of direct voltage, by increasing the DC component, conductive water droplets have lower PD inception levels in comparison with non-conductive ones. This dependency is more severe at negative direct voltages.

Chapter 7

Simulations

7.1 Introduction

In this chapter electric field distributions of single and multiple water droplets on a polymeric insulating surface under both tangential and normal E-field are simulated and compared with the experimental results. The test setup is illustrated in Figure 5.1. Since the electrodes are embedded in insulating material, which is surrounded by air, electric field lines and equipotential lines are refracted at the surface. E-field distribution is simulated in the following parts using CST EM-Studio® and COMSOL Multi-Physics® softwares. Unless otherwise specified, the applied voltage in simulation cases is 1 kV. In order to find a better accuracy of the results, a thin ring of silicone rubber at the position of water droplets on the insulating surface is considered, which makes the software able to refine the mesh quality at triple points. It is important to mention that the software has a singularity problem at triple lines. The electric field vector becomes infinite at the points where the materials with different permittivities are in contact. So the point field values along the contact line do not converge numerically [Fei09]. Therefore the maximum E-field strength values especially at the triple line have a considerable uncertainty, which cannot be considered as a valid value for prediction of partial discharges. However, with considering the same initial conditions and defining the mesh quality step size as a constant parameter in all simulation cases, the simulated/calculated E-field enhancement factors can be compared relative to each other. A qualitative correlation between experimentally found PD inception E-field strengths as well as PD

localization results and the relative calculated E-field enhancement factors is discussed in this chapter.
The part project "dynamic E-field simulation package", which has been developed recently by Songoro [Son15] as a member of TP-A5 in frame of the SFB-TRR75, is also briefly introduced in this chapter.

7.2 Tangential E-field

7.2.1 Without Water Droplet

A simulation result of the test setup without water droplet is shown in Figure 5.12. The E-field between electrodes and at the position of water droplet is almost tangential (parallel to the surface). This E-field value at the center of the test object can be considered as a constant value of 0.41 kV/cm as a reference E-field, E_0.

7.2.2 Single Water Droplet

Due to the hydrophobicity effect of the insulator surface, a water droplet is approximately hemispherical at initial condition. After applying a voltage, the water droplet deforms, and its shape changes to become non-hemispherical. Two shapes of water droplet, at initial condition and at a certain time instant during voltage application, where it is extremely deformed, are depicted in Figure 7.1. Simulation results of this case without water droplet, with initial water droplet and with deformed water droplet are shown in Figure 7.2. The maximum E-field, E_m at each kind of initial and deformed shapes of the water droplet (as exemplary marked in Figure 7.2) is normalized by the constant E-field at initial condition (E_0). So the field enhancement factor k is defined as $k = \frac{E_\mathrm{m}}{E_0}$. For the initial shape of water droplet with contact angle of about 90 ° the maximum E-field increases by a factor of 4. When the water droplet deforms, the length of the droplet increases and the distance between droplet and electrodes decreases. The sharp edge of the deformed water droplet also reduces the contact angle, which leads to an E-field enhancement factor of more than 7. It shall also be noted that due to uncertainty of the simulation package, sometimes the results of symmetric arrangements are not totally symmetric, which can be solved by increasing the mesh quality. But increasing

the mesh quality takes a lot of computation time. Since the results are to be compared with each other, these asymmetric shapes in some following results have been found to have no effect on comparison results.

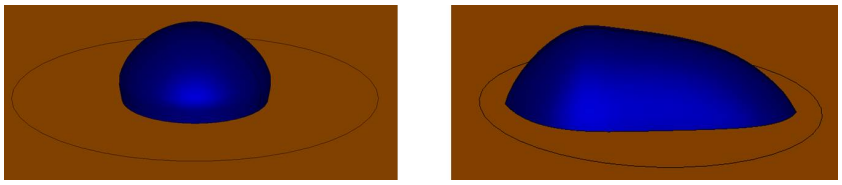

FIGURE 7.1: Initial (left) and deformed shape of water droplet (right); obtained form experimental captured videos

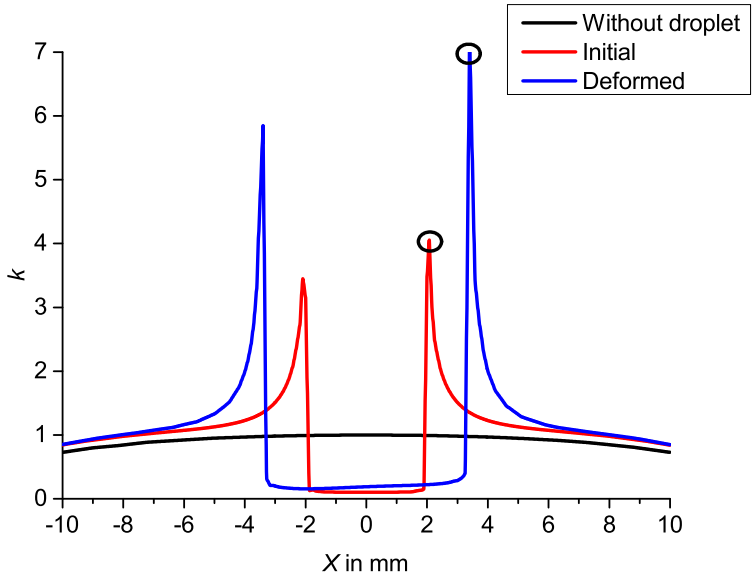

FIGURE 7.2: E-field enhancement factor for a single water droplet under tangential E-field stress along the insulating surface (the field strengths at the points marked by circles have been used for evaluation)

7.2.3 Oscillation Modes

Since the water droplet oscillates under AC electric field stress periodically, one cycle of this oscillation is analyzed. With the help of the captured videos four different frames of water droplet oscillation during one cycle of each mode are selected from experimental results as an input for simulations (See Figure 7.3). Dimensions of the water droplet are measured in each frame. The water droplet at initial condition has 4 mm length, while after applying voltage and due to elongation towards the electrodes its length reaches 5 mm at mode 1 and 4.4 mm at modes 2, 3 and 4. Four oscillation modes of a single

water droplet on the surface are compared, considering same initial conditions and mesh qualities in all simulation cases. The average E-field value at 0.1 mm distance from the triple line and from three different mesh qualities is considered as the maximum E-field value E_{m}[1].

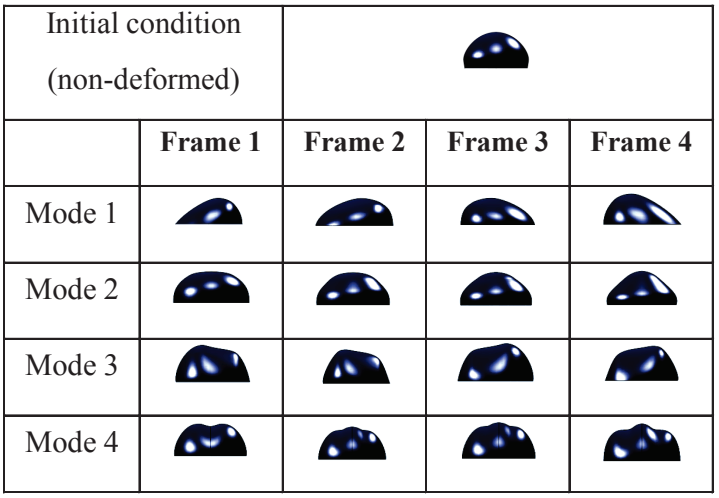

FIGURE 7.3: Four different shapes of a 20 µl water droplet under one cycle of tangential AC E-field stress (front view)

The simulation of an initial water droplet results in a maximum tangential E-field at 0.1 mm distance from the triple line of 1.15 kV/cm. Thus, presence of the water droplet on the surface increases the tangential component of the E-field at the converge point by factor of about 2.9 (i.e. 1.15/0.4). Since the water droplet shape changes differently at different modes, four different kinds of water droplet oscillation at four modes based on Figure 7.3 are simulated. The maximum E-field obtained from simulation of different shapes of the water droplet are compared with the maximum E-field of a water droplet at initial condition (non-deformed droplet). The E-field enhancement k factors for different degrees of deformation are calculated and summarized in Table 7.1. As can be seen, the k factor for mode 1 in all of the four cases is higher than in the other modes. The reason is firstly the length of the water droplet, which is bigger than that of the other modes, and secondly the low contact angle of water droplet at mode 1 in comparison with the other modes. Considering the maximum k factor, it seems that the deformation of water

[1]Simulation results in [Fei09] have shown that considering the E-field value at the converge point of 0.1 mm distance from the edge of the water droplet instead of at the triple line is a first option to solve the singularity problem. Considering the E-field value at the converge point is, in principle, physically correct, because a discharge in the triple zone needs a certain minimum volume to develop an avalanche of electrons.

TABLE 7.1: Enhancement factor of different frames at different modes

	E-field enhancement factor k				
	Frame 1	Frame 2	Frame 3	Frame 4	Maximum
Mode 1	3.45	3.36	3.25	3.51	3.51
Mode 2	3.10	3.07	3.04	3.02	3.10
Mode 3	3.22	3.19	3.16	3.13	3.22
Mode 4	3.16	3.02	3.04	3.07	3.16

droplet at mode 1 increases the local E-field at the convergence point by a factor of 3.51, which is 22% more than the maximum E-field in presence of a non-deformed water droplet on the surface. The enhancement factor is k = 3.10, 3.22 and 3.16 for mode numbers 2, 3 and 4, respectively. It shall be noted that these enhancement factors are only those due to the different shapes of water droplet, whilst the lengths of the water droplets are constant. Mode numbers 2, 3 and 4 are found to have only little differences of their k factors at different frames. It is also visible that the field enhancement is higher for lower contact angles of the water droplet, oscillating in mode number 1. Figure 7.4 compares the maximum k factors of four modes. A good agreement can be found with experimental results, where it was found that water droplets oscillating at mode Nos.1 and 3 have lower PD inception voltage in comparison to mode Nos.2 and 4.

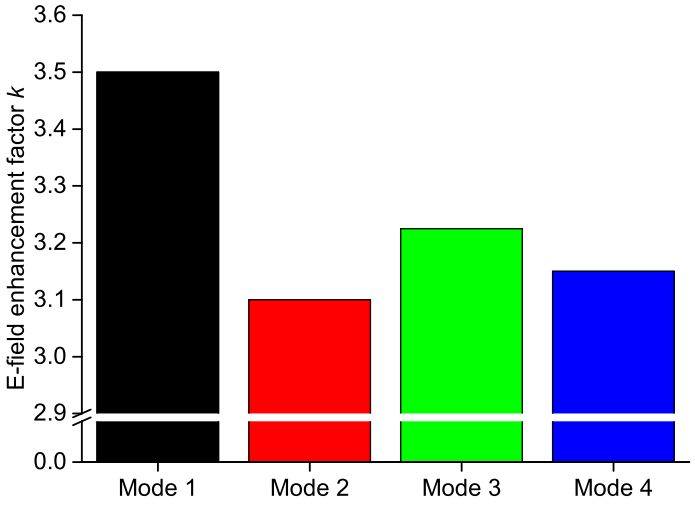

FIGURE 7.4: Enhancement factor k for different modes

7.2.4 Two Water Droplets Close to the Electrodes

Figure 7.5 shows the simulation results of two water droplets located close to the electrodes and in 10 mm distance to each other. In the initial condition, because of the high contact angle at the edges, the maximum E-field strength with an enhancement factor of about 4 can be found at the triple lines, which are closer to the electrodes. In case of deformed droplets (the same deformation as shown in Figure 7.1 right is assumed), although the droplets are closer to the electrodes, the maximum E-field with an enhancement factor of more than 7 arises between the droplets due to their very sharp edges and low contact angles of triple lines between droplets. In this case the droplets are elongated towards each other, and the distance between them is reduced to 7 mm. These and the following deformation and movement values are taken as typical cases from video recordings. The higher E-field strength between droplets shows a good agreement with experimental PD localization results, where the first signal of partial discharges has been found between droplets (Figure 6.31).

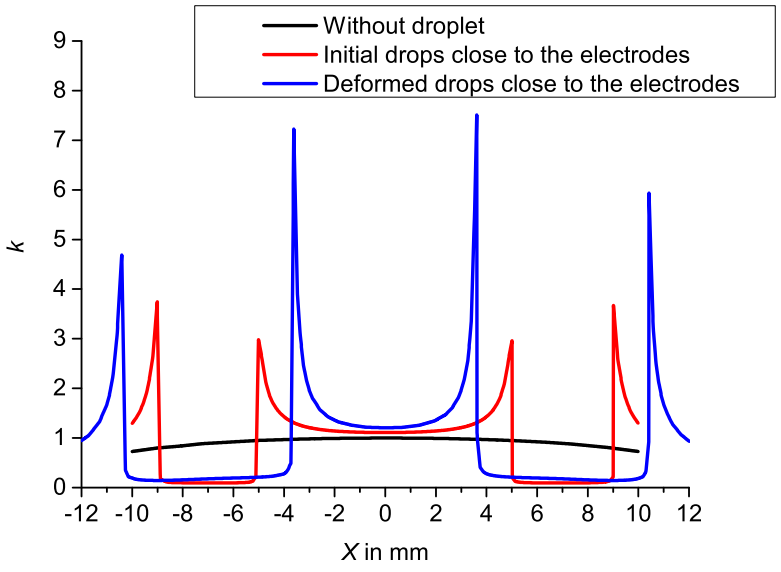

FIGURE 7.5: E-field enhancement factor for two water droplets under tangential E-field stress "droplets close to the electrodes"

7.2.5 Two Water Droplets far from Electrodes

Two water droplets are located far from the electrodes and close to each other with 4 mm distance at initial condition. The maximum E-field increases by a factor of 4.5 at

those triple lines that are closer to the electrodes. By applying voltage and deforming droplets, they move towards each other up to approximately 2 mm distance and the maximum E-field arises between the droplets with an enhancement factor of about 8 (Figure 7.6).

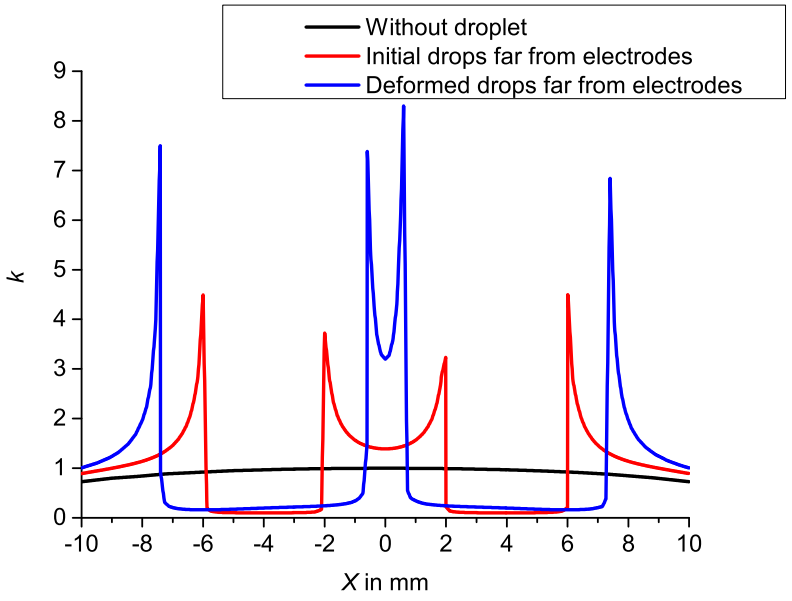

FIGURE 7.6: E-field enhancement factor for two water droplets under tangential E-field stress "droplets far from electrodes"

7.2.6 Three Droplets in Triangle Configuration

To investigate the triangle configuration, three water droplets are placed on the surface in triangular shape. The shapes of deformed water droplets are taken from video recordings. Two droplets, which are in direction of the E-filed, are placed in 2 mm distance. A single droplet is also placed in the center of the specimen about 5 mm behind the two droplets, also in direction of the E-field. The E-field distribution is simulated and its magnitude is evaluated along the four lines 1, 2, 3 and 4 according to Figure 7.7. Results are shown in Figure 7.8. Comparing the four lines, the higher E-field enhancement factor can be found to be always on line 1 and 4, at which the droplets are aligned in the E-field direction. In this case also the higher E-field enhancement factors are observed to occur between the droplets and also at triple lines of single droplet.

Summarizing, it can be noted that in case of multiple droplets on the insulator surface, the maximum E-field stress under tangential applied E-field arises between the droplets

and in direction of the applied E-field. So electric partial discharges are expected to be localized at first between the droplets, which is in good agreement with experimentally investigated PD localization results (see Figure 6.31).

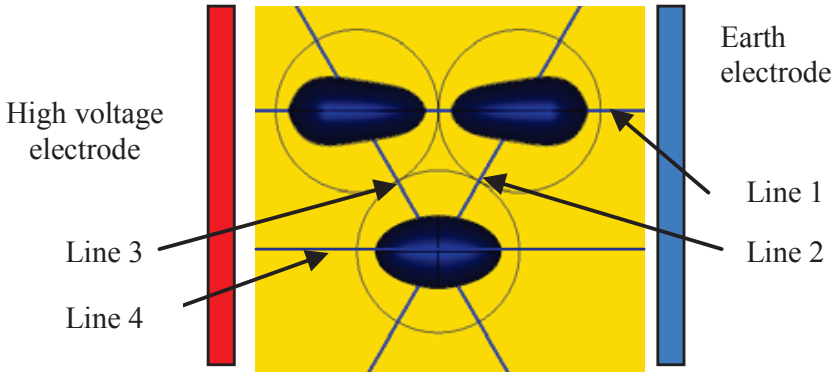

FIGURE 7.7: Three water droplets in triangle shape and evaluation lines 1, 2. 3 and 4

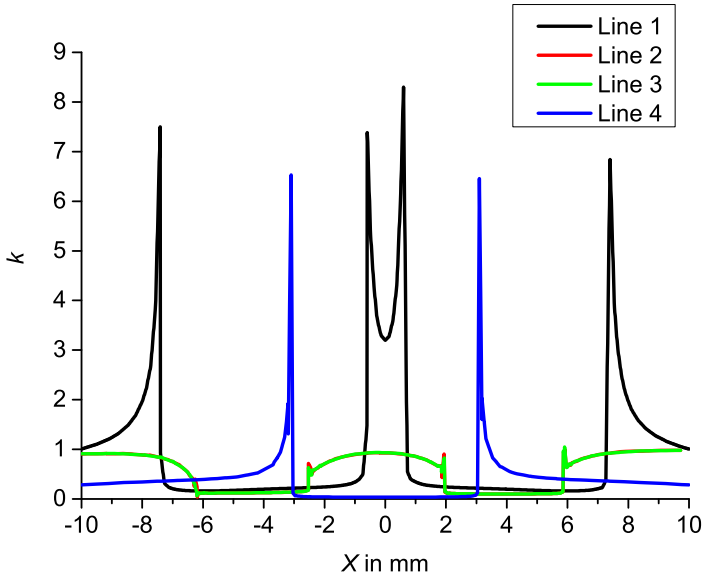

FIGURE 7.8: E-field enhancement factor for triangle deformed water droplets

7.3 Normal E-field

7.3.1 Without Water Droplet

Considering the arrangement of the normal configuration according to Figure 5.1(b), there are three regions in series, made of silicone rubber, air and again silicone rubber

with different heights. Figure 7.9 shows the configuration in 2D. The electric field in the air region can be easily calculated according to a voltage divider as follows:

$$U = U_\mathrm{s} + U_\mathrm{a} + U_\mathrm{s} \tag{7.1}$$

$$U_\mathrm{a} = U \cdot \frac{\frac{d_\mathrm{a}}{\epsilon_\mathrm{ra}}}{\frac{d_\mathrm{a}}{\epsilon_\mathrm{ra}} + 2 \cdot \frac{d_\mathrm{s}}{\epsilon_\mathrm{rs}}} \tag{7.2}$$

$$E_\mathrm{a} = \frac{U_\mathrm{a}}{d_\mathrm{a}} = U \cdot \frac{\frac{1}{\epsilon_\mathrm{ra}}}{\frac{d_\mathrm{a}}{\epsilon_\mathrm{ra}} + 2 \cdot \frac{d_\mathrm{s}}{\epsilon_\mathrm{rs}}} = \frac{U}{d_\mathrm{a} + 0.69 \cdot d_\mathrm{s}} \tag{7.3}$$

where U, E and d are respectively applied voltage, electric field strength and distances. Indices a and s refer to air and silicone rubber, respectively. This calculation is valid without any water droplet on the surface, which results in a reference E_0 equal to 1 kV/cm, applying a voltage of 1 kV between electrodes.

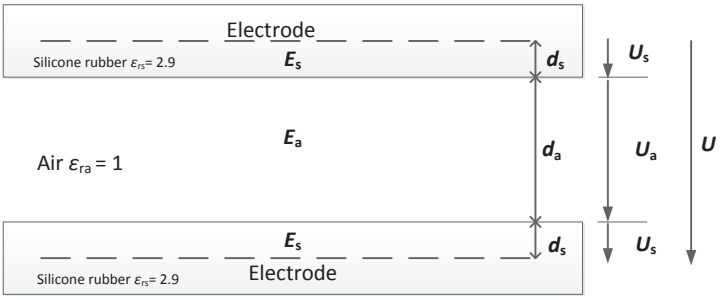

FIGURE 7.9: Normal E-field arrangement

7.3.2 With Water Droplets

The E-field distribution in case of existing water droplets has to be determined by simulation. Since the water droplet is exposed to normal E-field stress, there are two regions, which are important for partial discharge development and electric field calculation point of views. These two regions are the top of the water droplet, which is in the direction of the normal E-field as well as the triple lines, which produce tangential E-field stress. The E-field enhancement factor k for normal configurations is calculated as a ratio of the maximum E-field, E_m at each kind of initial and deformed shapes of the water droplet to the reference calculated $E_0 = 1$ kV/cm. Figure 7.10 shows the E-field enhancement

factor for normal component of E-field distribution across a line perpendicular to the electrodes for an arrangement with only one droplet. The E-field enhancement factor for tangential component of E-field distribution across a line parallel to the electrodes, for an arrangement with one and two droplets is shown in Figure 7.11.

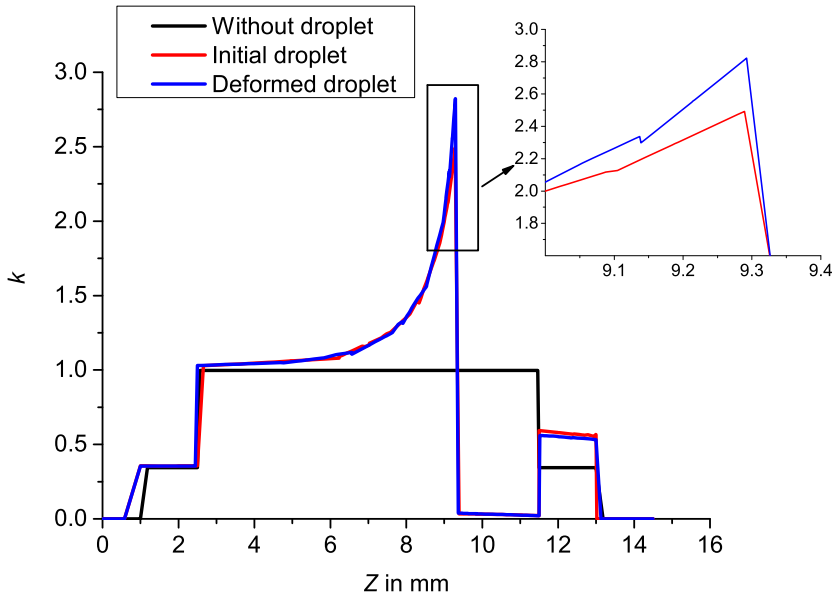

FIGURE 7.10: E-field enhancement factor for normal component of E-field distribution across a line perpendicular to the electrodes

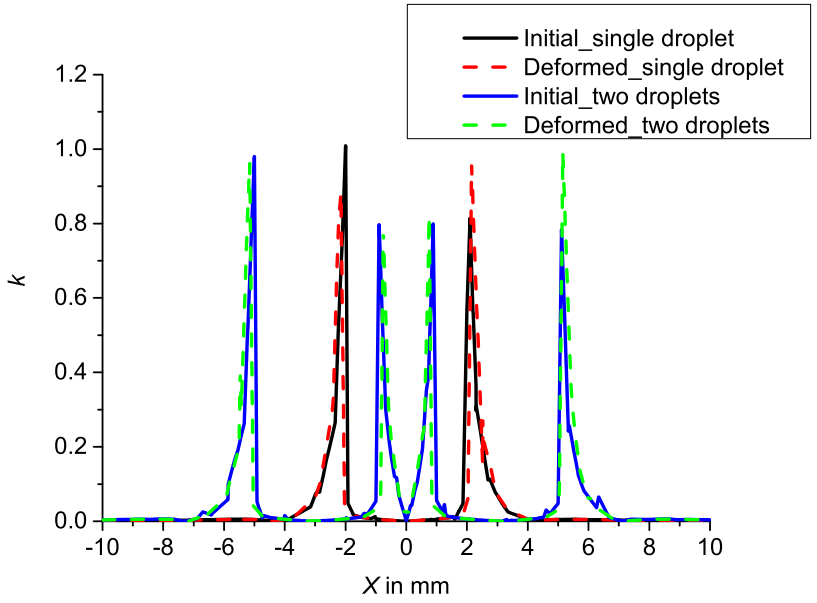

FIGURE 7.11: E-field enhancement factor for tangential component of E-field distribution across a line parallel to the electrodes

As it can be seen, the normal component of the E-field at the top of water droplet is higher the tangential component at the triple lines. All in all the droplet increases the maximum electric field at its top with an enhancement factor of ca. 2.8, whereas the maximum enhancement for a tangential component of E-field is less than 1.1. Since the height of deformed water droplet is higher than that for the initial water droplet, the normal component of the E-field for the deformed droplet is bigger than that for the initial water droplet. Simulation results are in good agreement with experimentally investigated PD localization of Figure 6.32.

7.4 Dynamic Simulation Package

In this section the part project "dynamic simulation package", which is prepared by TP-A5 in frame of the SFB-TRR75, is briefly introduced.
In the presence of an external electric field, the time-dependent electric force density $\vec{f}_{\mathrm{e}}$ tends to distort the interface of the water droplet while the gravitational force density $\vec{g}$ and the surface tension force $\vec{f}_{\mathrm{s}}$ tend to bring back the droplet to its equilibrium shape as shown in Figure 7.12 [Son15].

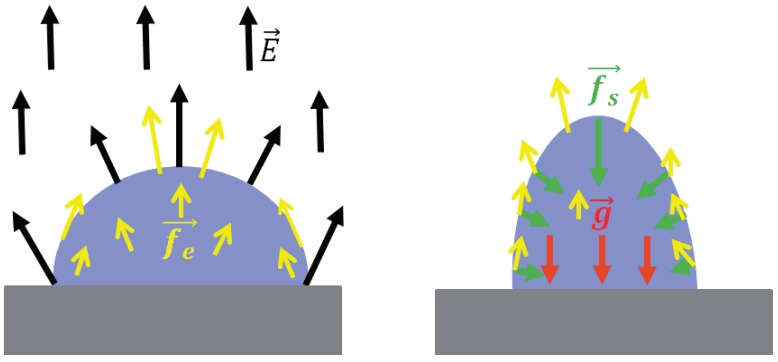

FIGURE 7.12: Electrical and mechanical forces acting on a water droplet [Son15]

The electric force density (force per volume) can be expressed as the divergence of the Maxwell stress tensor $\vec{T}_{\mathrm{e}}$ [Son15]:

$$\vec{f}_{\mathrm{e}} = \vec{\nabla} \cdot \vec{T}_{\mathrm{e}} = \vec{\nabla} \cdot \begin{bmatrix} D_{\mathrm{x}} \cdot E_{\mathrm{x}} - \frac{1}{2}\epsilon_0 E^2 & D_{\mathrm{y}} \cdot E_{\mathrm{x}} & D_{\mathrm{z}} \cdot E_{\mathrm{x}} \\ D_{\mathrm{x}} \cdot E_{\mathrm{y}} & D_{\mathrm{y}} \cdot E_{\mathrm{y}} - \frac{1}{2}\epsilon_0 E^2 & D_{\mathrm{z}} \cdot E_{\mathrm{y}} \\ D_{\mathrm{x}} \cdot E_{\mathrm{z}} & D_{\mathrm{y}} \cdot E_{\mathrm{z}} & D_{\mathrm{z}} \cdot E_{\mathrm{z}} - \frac{1}{2}\epsilon_0 E^2 \end{bmatrix} \tag{7.4}$$

However, due to the discontinuity at the interface between two dielectrics (such at the droplet surface), calculating the electric force from the Maxwell stress tensor requires special treatments [Son15]. A common approach is to consider only the normal surface force density $\vec{f_s}$ at the interface, which leads to the same surface force density due to E-field stress reviewed in Chapter 3.

$$\vec{f_s} = \vec{n} \cdot \frac{1}{2}\epsilon_0 E^2 \tag{7.5}$$

It is obvious that the surface force density is proportional to the squared electric field, while the force per volume is proportional to the divergence of the squared electric field stress. However, which type of the force densities is exactly acting as a dominant electric force, deforming the shape of the water droplet is still not clear.

7.4.1 The Electrical Problem

At power-frequencies (50 Hz, 60 Hz), the electrical properties of the polymer insulator and of rainwater are described by linear constitutive relations. Rainwater has a relative permittivity of about 80 and an electrical conductivity in the range of 0.5 to 70 µS/cm. The polymeric insulator has a relative permittivity typically between 2 and 3. The frequency of the externally applied electric field is so low that magnetic induction can be neglected. Under these conditions Maxwells equations reduce to the electro-quasistatics (EQS) equations as [Son11b, Son12b]:

$$-\vec{\nabla} \cdot \left(\frac{\partial \epsilon \cdot \vec{\nabla} V}{\partial t} \right) = \vec{\nabla} \cdot \left(\sigma \vec{\nabla} V \right) \tag{7.6}$$

$$\vec{E} = -\vec{\nabla} V \tag{7.7}$$

7.4.2 The Fluid Dynamics Problem

The interface between water droplet and air is a freely moving surface, which can be deformed by the dielectric force. This poses a two-phase flow problem that is governed by the incompressible Navier-Stokes (NS) equations 7.8 and 7.9.

$$\frac{\partial \rho \vec{u}}{\partial t} + \vec{\nabla} \cdot (\rho \vec{u} \vec{u}) - \vec{\nabla} \cdot \mu \vec{\nabla} \vec{u} = -\vec{\nabla} p + \rho \vec{g} + \vec{f_s} + \vec{\nabla} \cdot \vec{T_e} \tag{7.8}$$

$$\nabla \cdot u = 0 \tag{7.9}$$

where u, p and ρ are the fluid velocity, pressure and mass density, respectively. μ is the fluid dynamic viscosity, and g is the acceleration of gravity. $\vec{f}_{\mathrm{s}}$ and $\vec{T}_{\mathrm{e}}$ represent the water droplet surface tension force and the Maxwell stress tensor, respectively [Son11b, Son12b].

7.4.3 Multiphysics Coupling

A computational approach based on the finite element method on a moving mesh for the electrical part and on the finite volume method on a fixed mesh for the fluid mechanical part of the problem has been developed by Songoro [Son15]. The computational domain of the fluid dynamics simulation is discretized by a fixed Cartesian grid. The interface between water and air is captured by using the Volume of Fluid (VOF) method [Hir81]. The EQS problem is solved on a moving curvilinear mesh by the finite element method. The numerical procedure used for the dynamic package adopted to the droplet shape is described in detail in [Son13c].

7.4.4 Results of Dynamic Package

Two arrangements of a water droplet on an insulating surface placed in a normal and tangential externally applied electric field according to Figure 5.1 are used to verify the simulation results of the dynamic package. In order to obtain the same electric field stress at both tangential and normal arrangements, the applied voltage (r.m.s. value) between the electrodes was 7.5 kV and 3 kV in the tangential and in the normal configuration, respectively. Figure 7.13 shows the simulated field strengths for the two configurations when no water droplet is present. It can be seen that the externally applied electric field for both tangential and normal field configurations, in the area between electrodes, has approximately the same value of 4.34 kV/cm (r.m.s. value).

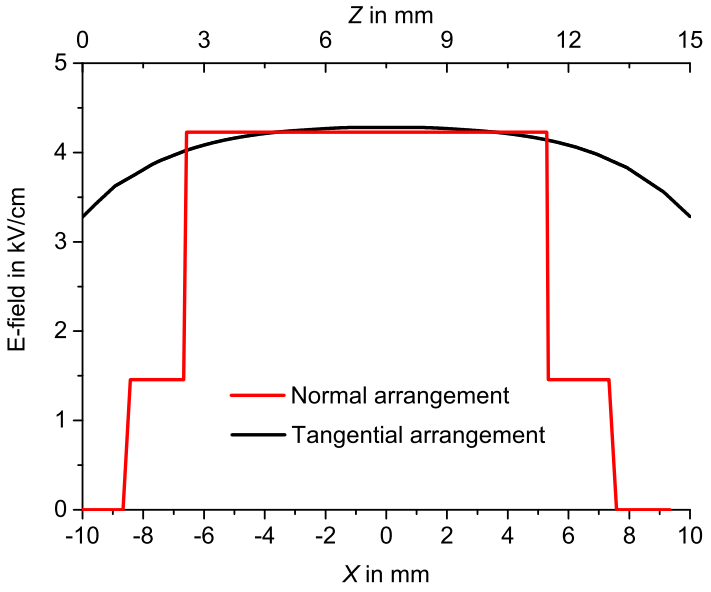

FIGURE 7.13: Simulated electric field stress without water droplet at $U = 7.5$ kV for the tangential field and $U = 3$ kV for the normal field configuration, respectively

Figure 7.14 shows the simulated field strengths for the tangential configuration in the presence of a 20 µl water droplet[2]. The E-field distribution at different shapes of the water droplet can be observed at the triple lines. Considering the maximum E-field strength at the time instant of the maximum voltage, the E-field distribution across a line in parallel to the surface for tangential configuration and across a line perpendicular to the surface for normal configuration can be evaluated (see Figure 7.15). Considering the 4.25 kV/cm E-field strength without water droplet as a background reference value, it is obvious that the E-field strength is increased with an enhancement factor of about 3 and 2.3 for tangential and normal configurations, respectively.

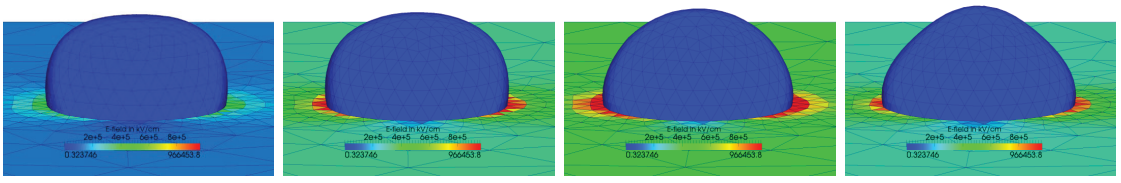

FIGURE 7.14: E-field distribution at different shapes of the water droplet; 20 µl water droplet, $U = 7.5$ kV, tangential field configuration acc. to [Son15]

[2]Many thanks to Dr. Harald Songoro from TEMF institute (as a member of TP-A5 in frame of the SFB-TRR75) for providing simulation data, which have been used as basis for the evaluations shown in figures 7.13 through 7.17.

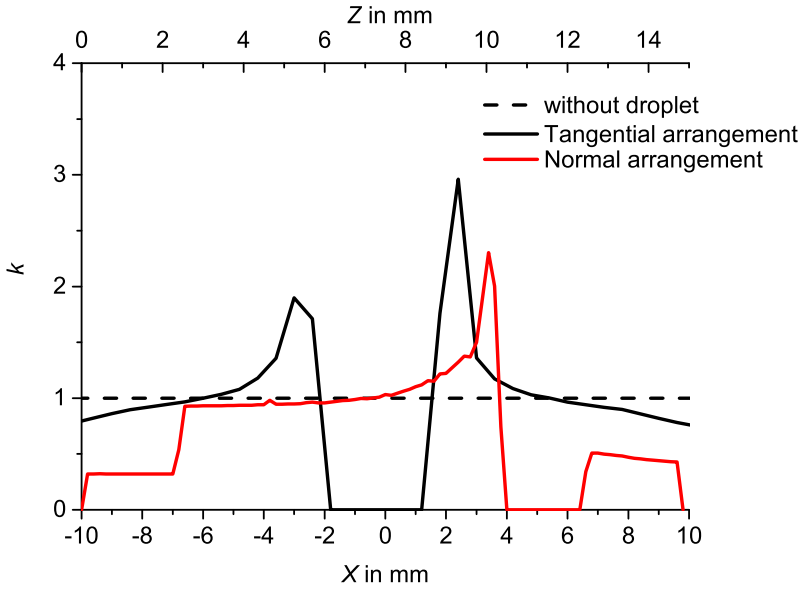

FIGURE 7.15: Tangential and normal E-field at the time instance of the maximum voltage in the presence of a 20 µl water droplet

In order to analyze the oscillation frequency, the normalized height of the water droplet at each frame of its oscillation is also calculated and compared with experimental results. The latter is defined as the ratio of the time dependent height of the water droplet under field stress to its initial height. The simulation and experimental results for this quantity (see Figures 7.16 and 7.17) are in good agreement. As can be seen in Figures 7.16 and 7.17, the frequency of water droplet oscillation is almost twice the frequency of the applied electric field for both tangential and normal configurations at 50 Hz E-field stress. According to experimental results in chapter 6, in some cases the frequency of water droplet oscillation was observed to be the same as the applied voltage frequency, which is assumed to be due to the charging of the water droplet with existing free charge carriers in the lab or due to the resonance frequencies of the sessile water droplet. Songoro [Son15] has pointed out that the vibrations of the droplet occurring at frequencies below $2f_{\mathrm{AC}}$ are not necessarily due to the presence of free charges induced by phenomena such as ionization or accidental charging of the water droplet, rather, they may be caused by underdamped droplet oscillations which originate in the transient regime [Son15]. This is also in correlation with the resonance frequencies of the sessile droplets oscillating freely. However, and since there is no quantitative information about the possible charges, which can be absorbed by the water droplet, the oscillation with the fundamental frequency of applied electric field cannot be proved by the dynamic

simulation package, so far. In addition, different oscillation modes of the water droplet in tangential E-field at different frequencies are also not observed in the dynamic simulation package results. These and the evaluation of simulation results, considering the variation of some important properties of the water droplet have to be considered in the future work as a close cooperation between TP-A5 and TP-C5 in frame of the SFB-TRR75.

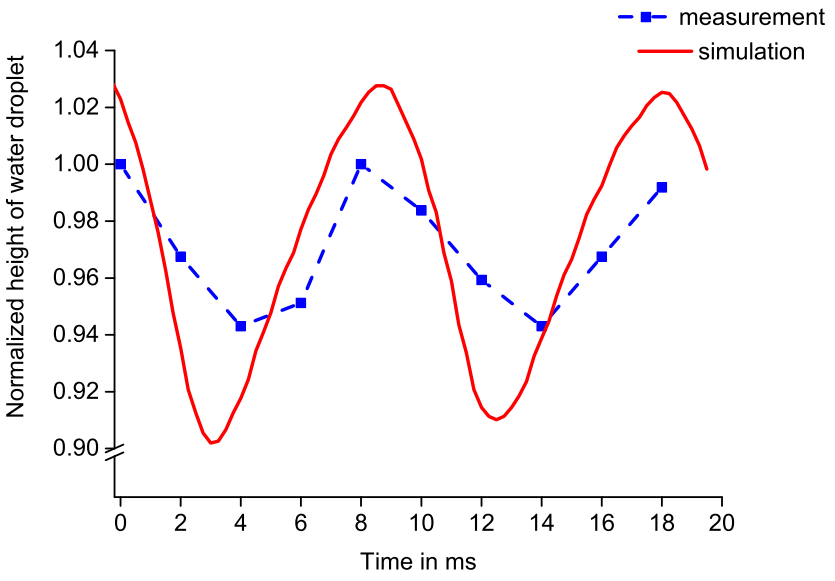

FIGURE 7.16: Simulated and measured normalized droplet heights typically for a 20 µl water droplet under tangential E-field stress

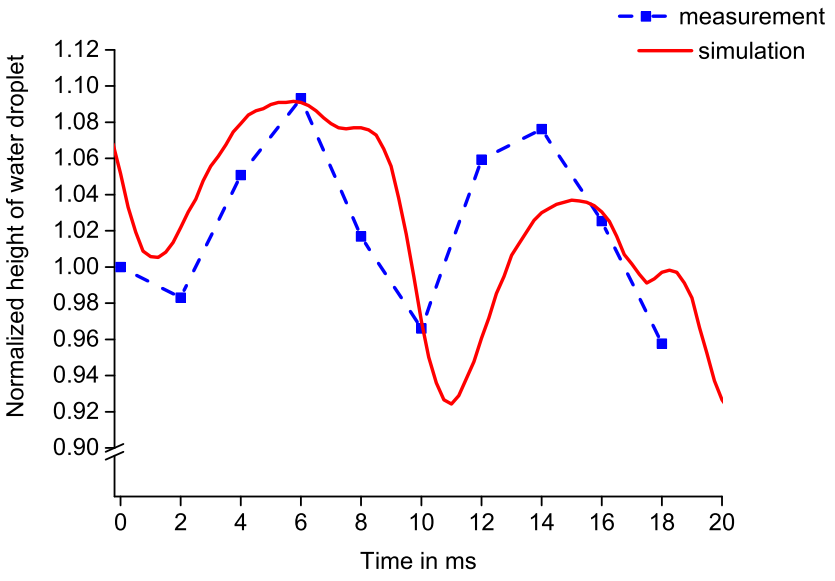

FIGURE 7.17: Simulated and measured normalized droplet heights typically for a 20 µl water droplet under normal E-field stress

7.5 Summary of Simulation Results

Following results can be summarized from the simulation:

- The E-field enhancement factor for the normal configuration was notably lower than that for the tangential configuration. It shows a good agreement to experimental results, at which it has been observed that the PD inception E-field strength of water droplets under normal E-field stress is much higher than that under tangential E-field stress (Figure 6.1).
- The simulated/calculated E-field enhancement factors cannot be considered as a valid value for prediction of partial discharges due to the singularity problem at triple lines. However, simulation results can be compared relative to each other and a qualitative correlation between experimental and simulation results can also be obtained.
- According to simulation results, it is expected that:
  - In case of a single water droplet, PD appears firstly at the triple lines under tangential E-field but at the top of the water droplet at normal E-field stress.
  - In case of two water droplets, PD starts at first in the region between the droplets under tangential E-field, but at the top of the droplets at normal E-field.
  - In case of triangle droplets, PD starts at first always in the direction of E-field stress.

  Simulation results are in good agreement with experimentally investigated "PD localization" results in Figures 6.31 and 6.32.
- Comparing the oscillation modes of a single water droplet under tangential AC stress shows that mode Nos.1 and 3 provide higher electric field strength at the triple zone in comparison to mode Nos.2 and 4, which is also in good agreement with experimental results.
- A new approach of numerical modeling of water droplet deformations under field stresses was proposed by Songoro [Son15] and partly validated with the experimental results in frame of the common research project of the SFB-TRR75. Simulation

results of the dynamic package show good agreement between simulations and experiments so far, however, more cooperation between TP-A5 and TP-C5 is still required to validate the developed simulation package.

Chapter 8

Conclusions and Recommendations

8.1 Conclusions

The study was set out to explore the systematic experimental investigations on the behavior of water droplets under the impact of high electric field stress. The deformation of the water droplet, the intensified E-field stress at the triple lines as well as the partial discharge inception E-field strengths of water droplets at different voltage shapes and under variation of a large set of parameters have been studied and discussed. The main experimental findings and the subsequent analysis were summarized within the previous chapters and this section will synthesize them to answer at least these research questions:

1. Which parameters can affect the PD inception E-field strength of polymeric insulating surfaces in the presence of water droplets?
2. What is the main difference between the behavior of water droplets on the hydrophobic insulating surface at AC, DC and combined AC-DC stress?
3. Is it possible to find the critical background E-field strength experimentally, below which no partial discharge occurs?

Three categories of parameters have been investigated in this study; (1) parameters of the water droplet like volume, conductivity and viscosity, (2) parameters of the insulating surface like hydrophocity and inclination angle and (3) parameters of the E-field

stress like frequency, direction of the electric field (tangential or normal) and the type of applied voltage (AC, DC and combined AC-DC).

As a result of these investigations, it can be pointed out that water droplets under tangential E-field stress provide lower PD inception values than those under normal E-field stress. The PD starts from the triple line under tangential E-field stress, but from the top of the water droplet under normal E-field stress. It seems to be more effective to consider only tangential component of the E-field stress in the design procedure of the polymeric insulators. The water droplet at alternating voltage has been found to have a tendency of vibrating at critical frequencies which were volume dependent; however critical frequencies in respect of the water droplet oscillation did not always lead to lower partial discharge inceptions. Conductivity of the water droplet on hydrophobic surfaces had also no influence on either oscillation modes or PD inception E-field strengths.

The behavior of water droplets at AC, DC and combined AC-DC stress was analyzed and compared, particularly in deformations and PD characteristics point of views. Water droplets at alternating voltage oscillate at different oscillation modes, while they elongate towards electrodes at direct voltage. The deformation under combined alternating/direct voltage consists of an oscillation superimposed to a polarity-dependent elongation towards the electrodes. Increasing the DC component of the combined alternating/direct voltage provided a lower PD inception E-field strength.

The maximum allowable E-field strength along a polymeric insulating surface of wettability class WC 1 for a single water droplet on a flat surface has been estimated experimentally to be between 6 and 7.5 kV/cm (peak). However, the PD inception E-field strength was reduced to about 4.5 kV/cm (peak) for more water droplets on the surface like random spray and dew droplets. On inclined surfaces, the PD inception E-field strength has been found to be reduced to about 90%, depending on the direction of electric field and gravitational forces on the droplet.

A close cooperation between subprojects TP-A5 and TP-C5 in frame of the SFB-TRR75 research center is established with the goal to develop a simulation tool for droplets deforming under the impact of an applied external E-field and the consequences with regard to partial discharge inception E-field strengths. Preliminary results of the dynamic simulation package show a good agreement between simulations and experimental results so far, however more cooperation is still needed to complete the the software package validation.

8.2 Future Work

The study has offered an evaluative perspective on experimental investigations on the PD inception E-field strength of polymeric insulating surfaces in the presence of water droplets, and was conducted in a real environment through the variation of some important parameters. As a direct consequence of this methodology, the study encountered a number of limitations, which needs to be considered furthermore. To generate achievable policy strategies and development targets with regards to the design of polymeric insulators considering their long-term reliability, there is still a need of more investigations to allow further assessment of subject design. Exploring the following as future research strategies can facilitate the attainment of this goal:

- **Validation of the dynamic simulation package**

The software recently developed by Songoro [Son15] is concentrated on the deformation of the water droplet under the impact of high electric field stress. The results are partly compared with experimental results of this study, however, different oscillation modes of the water droplet in tangential E-field at different frequencies are not observed in dynamic simulation package results. These and the evaluation of simulation results, considering the variation of some important properties of the water droplet, concentrating on E-field calculations (and not only on deformation shapes) have to be considered in the future work as a close cooperation between TP-A5 and TP-C5 in frame of the SFB-TRR75.

- **Charge measurement**

Experimental results have shown that under AC field stress, in some cases the water droplet vibrates with twice the frequency of the applied voltage, but, in some other cases the frequency of water droplet oscillation was the same as for the applied voltage frequency. The reason was assumed to be either due to charging the water droplet with existing free charge carriers in the lab, which was also reported in [Fuj10, Miz01], or due to the resonance frequency of sessile droplets. Recently Songoro [Son15] has also concluded that this phenomenon is caused by underdamped droplet oscillations, which originate in the transient regime. Finding out the reason of this behavior will improve

the actual physical understanding of the discharge phenomenon. This can also be used for the development of a PD corona prediction model. Main challenge of this approach would be the conversion of the measured potential distribution on the surface of the test object, which can be performed using an electrostatic voltmeter with a contact-less probe, to the charge distribution. The geometry-dependent distributed stray capacitance of the test object may vary in different point of views.

- **PD prediction**

A theoretical corona discharge model of the water droplet on the surface for partial discharge prediction needs to be developed in order to understand the physical discharge mechanism on the surface. Secondary electron emission from the insulating surface and surface discharges have to be modeled accurately. At the time being, Songoro [Son15] as a member of TP-A5 in frame of the SFB-TRR75 has developed a software package, which can dynamically simulate the E-field around an oscillating water droplet, considering the coupled Navier-Stokes and Electro-Quasi-Static equations. The further idea would be the coupling of Convection-Drift-Diffusion of plasma equations to the existing software package. So the corona discharge on the surface can be estimated when a high amount of charge carriers is present in an initially electrically neutral gas volume over the insulator surface. Considering three types of charged particles (electrons, positive ions and negative ions), the physical discharge process can be modeled as a motion of charges due to the E-field, as a drift due to gradients of concentrations, or as a diffusion for each kind of charge carriers together with Poisson's equation for the electric potential, which are all coupled through E-field dependent coefficients. Some similar approaches on typical needle-plate electrodes in air [Kum09, Bab04, Che03, Bec14, Low92, Mor97] or in oil [Jad12a, Sim03] are reported in the literature. The main challenge of this type of plasma simulation is the optimization of artificial diffusion stabilization techniques and corresponding mesh density distribution [Jad12b]. Coupling the existing software package of TP-A5 with above mentioned plasma equations can result in a good approach, getting better physical understanding of corona discharge initiated from water droplets on polymeric insulating surfaces. The main problem of this part would, however, be the periodic change in the water droplet shapes as well as the electrode-less insulating surface.

As a final massage it can be pointed out that in spite of the benefits of polymeric insulators rather traditional glass and porcelain insulators, they are still in practice a relative new technology. The behavior of water droplets on the surface of polymeric insulators has been shown to be a key parameter to facilitate understandings of long-term and aging behavior of this type of insulators.

Bibliography

[Ada11] K. Adamiak and J. M. Floryan. 'Dynamics of water droplet distortion and breakup in a uniform electric field'. *IEEE Transactions on Industrial App.*, Vol. 47(6):pp. 2374–2383, 2011.

[Ami07] M. Amin, M. Akbar and S. Amin. 'Hydrophobicity of silicone rubber used for outdoor insulation (an overview)'. *Journal of reviews on advanced materials science*, Vol. 16:pp. 10–26, 2007.

[Bab04] N. Babaeva and J. Lee. 'Dust-grain charging in developing air plasma'. *IEEE Transactions on Plasma Science*, Vol. 32(2):pp. 823–828, 2004.

[Bae93] R. Baersch, H. Gremmel, D. König and J. Pilling. 'Verminderung des Isoliervermögens an Feststoff/Gas-Grenzflächen durch fremdschichtinitiierte Teilentladungen'. *ETG-Fachbericht 49, Isolationskoordination in Hoch- und Mittelspannungsanlagen, VDE-Verlag*, Vol. 49:pp. 133–149, 1993.

[Bay98] J. Baygents, N. Rivette and H. Stone. 'Electrohydrodynamic deformation and interaction of drop pairs'. *Journal of Fluid Mechanics*, Vol. 368:pp. 359–375, 1998.

[Bec14] M. Becerra. 'On the estimation of the charge of positive streamers propagating in air'. *IEEE Transactions on Dielectrics and Electrical Insulation*, Vol. 21(2):pp. 627–634, 2014.

[Ber92] A. Beroual. 'Behavior of charged and uncharged bubbles in dielectric liquids subjected to electric stress'. *Journal of applied Physics*, Vol. 71:pp. 1142–1145, 1992.

[Bey02] J. Beyer. *Space charge and partial discharge phenomena in high voltage DC devices.* Ph.D. Thesis, TU Delft, 2002.

[Bo12] L. Bo and R. S. Gorur. 'Modeling flashover of AC outdoor insulators under contaminated conditions with dry band formation and arcing'. *IEEE Transactions on Power Delivery*, Vol. 19(3):pp. 1037–1043, 2012.

[Bra06] T. Braunsberger, S. Iova, V. Hinrichsen and M. Kurrat. 'Partial discharge processes at sessile water drops on insulating surfaces'. *Int. Conf. on Gas Discharges and their Applications*, 2006.

[Bra07] T. Braunsberger. *Verhalten zyklisch betauter Silikonoberflächen bei elektrischer Beanspruchung.* Ph.D. Thesis, TU Braunschweig, 2007.

[BS71] P. Brazier-Smith, M. Brook, J. Latham, C. Saunders and M. Smith. 'The vibration of electrified water drops'. *Proceeding of the Royal Society of London*, Vol. 332:pp. 523–534, 1971.

[Cer08] R. Cervinka, R. Bärsch, F. Exl, J. Kindersberger and H.-J. Winter. 'Untersuchungen zur Beständigkeit der Hydrophobie von polymeren Isolierstoffoberflächen und ihrer Wiederkehr mit dem dynamischen Tropfenprüfverfahren'. *ETG-Fachbericht 112, Grenzflächen in elektrischen Isoliersystemen, VDE-Verlag*, pp. 55–62, 2008.

[Che77] T. Cheng, D. C. Jolly and D. J. King. 'Surface flashover of water repellent insulators under moist conditions'. *IEEE Transactions on Electrical Insulation*, Vol. 12:pp. 208–213, 1977.

[Che84] K. Cheng and J. Chaddock. 'Deformation and stability of drops and bubbles in an electric field'. *Physics Letters*, Vol. 106A(1,2):pp. 51–53, 1984.

[Che03] J. Chen and J. Davidson. 'Model of the negative DC corona plasma: Comparison to the positive DC corona plasma'. *Plasma Chemistry and Plasma Processing*, Vol. 23(1):pp. 83–102, 2003.

[Chr07] K. L. Chrzan and F. Moro. 'Concentrated discharges and dry bands on polluted outdoor insulators'. *IEEE Transactions on Power Delivery*, Vol. 22(1):pp. 466–471, 2007.

[Cig04] Cigré. 'Material properties for a non-ceramic outdoor insulation; state of the art'. *Cigré WG D1.14 TB255*, 2004.

[Cig10] Cigré. 'Evaluation of dynamic hydrophobicity properties of polymeric materials for non-ceramic outdoor insulation; retention and transfer of hydrophobicity'. *Cigré WG D1.14 TB442*, 2010.

[Cig15] Cigré. 'Feasibility study for a dc tracking and erosion test'. *Cigré WG D1.27 TB611*, 2015.

[Den10] H. Deng, Z. He, J. Ma, Y. Xu, J. Liu and R. Guo. 'Initiation and propagation of discharge in liquid droplets: Effect of droplet sizes'. *IEEE Transactions on Plasma Science*, Vol. 38(12):pp. 3282–3288, 2010.

[Dzi05] A. Dziubek, T. Braunsberger and M. Kurrat. 'Effects of water drop corona at dew layers on silicone rubber'. *Int. Symposium on High Voltage Engineering (ISH)*, 2005.

[EK96] H. El-Kishky and R. S. Gorur. 'Electric field computation on an insulating surface with discrete water droplets'. *IEEE Transactions on Dielectrics and Electrical Insulation*, Vol. 3(3):pp. 450–456, 1996.

[Ele01] G. Elert. 'The physics factbook'. http://hypertextbook.com/facts/2001/IgorVolynets.shtml, 2001.

[Eng48] W. N. English. 'Corona from a water drop'. *Phys. Rev.*, Vol. 74(2):pp. 179–189, 1948.

[Far97] M. Farzaneh, J. Zhang and X. Chen. 'Modeling of the ac arc discharge on ice surfaces'. *IEEE Transactions on Power Delivery*, Vol. 12(1):pp. 325–358, 1997.

[Far09] M. Farzaneh and W. A. Chisholm. *Conductivity Theory and Practice*, (John Wiley & Sons, Inc.2009).

[Fei09] S. Feier−Iova. *The Behavior of Water Droplet on Insulating Surfaces Stressed by Electric Field*. Ph.D. Thesis, TU Darmstadt, 2009.

[FI09] S. Feier-Iova and V. Hinrichsen. 'Partial discharge inception voltage of water drops on insulating surfaces stressed by electrical field'. *IEEE Electrical Insulation Conf.(EIC)*, pp. 21–25, 2009.

[Fro95a] U. Fromm. 'Interpretation of partial discharges at dc voltages'. *IEEE Transactions on Dielectrics and Electrical Insulation*, Vol. 2(5):pp. 761–770, 1995.

[Fro95b] U. Fromm. *Partial discharge and breakdown testing at high DC voltage*. Ph.D. Thesis, TU Delft, 1995.

[Fro00] A. Frohn and N. Roth. *Dynamics of droplets*, (Springer; Berlin2000).

[Fuj10] O. Fujii, K. Honsali, Y. Mizuno and K. Naito. 'Vibration of a water droplet on a polymeric insulating material subjected to AC voltage stress'. *IEEE Transactions on Dielectrics and Electrical Insulation*, Vol. 17(2):pp. 566–571, 2010.

[Gao08] H. Gao, Z. Jia, Y. Mao, Z. Guan and L. Wang. 'Effect of hydrophobicity on electric field distribution and discharges along various wetted hydrophobic surfaces'. *IEEE Transactions on Dielectrics and Electrical Insulation*, Vol. 15(2):pp. 435–443, 2008.

[Gho95] P. Ghosh and N. Chatterjee. 'Polluted insulator flashover model for ac voltage'. *IEEE Transactions on Dielectrics and Electrical Insulation*, Vol. 2(1):pp. 723–729, 1995.

[Gor92] R. Gorur, G. Karady, A. Jagota, M. Shah and A. Yates. 'Aging in silicone rubber used for outdoor insulation'. *IEEE Transactions on Power Delivery*, Vol. 7:pp. 525–538, 1992.

[Gua90] Z. Guan and R. Zhang. 'Calculation of ac and dc flashover voltage of polluted insulators'. *IEEE Transactions on Electrical Insulation*, Vol. 25(4):pp. 723–729, 1990.

[Gua05] Z. Guan, L. Wang, B. Yang, X. Liang and Z. Li. 'Electric field analysis of water drop corona'. *IEEE Transactions on Power Delivery*, Vol. 20(2):pp. 964–969, 2005.

[Hac99] R. Hackam. 'Outdoor HV composite polymer insulators'. *IEEE Transactions on Dielectrics and Electrical Insulation*, Vol. 6(5):pp. 557–585, 1999.

[Hig02] Y. Higashiyama, T. Yamada and T. Sugiomoto. 'Effect of resonance of a water droplet located on a hydrophobic sheet on ac flashover'. *Industry Applications Conference*, pp. 2198–2203, 2002.

[Hig07] Y. Higashiyama and M. Kosano. 'Relation between extension of a filamentary channel from a water droplet placed on a hydrophobic sheet under AC field and flashover via the droplet'. *IEEE Industrial App. Conf.*, pp. 2199–2203, 2007.

[Hig12] Y. Higashiyama and T. Shiori. 'Negative corona discharge from a viscous water droplet'. *Proceedings of the Electrostatics Joint Conference*, 2012.

[Hir81] C. W. Hirt and B. D. Nichols. 'Volume of fluid (VOF) method for the dynamics of free boundaries'. *Journal of Computational Physics*, Vol. 39(1):pp. 201–225, 1981.

[Hof95] J. Hofmann. *Elektrische TE- und Ableitstrommessungen mit Impulsspannung an polymeren Isolierstoffoberflächen mit Tropfenbelägen zur Diagnose des Oberflächenzustandes am Beispiel von Elastomeren.* Ph.D. Thesis, TH Zittau, 1995.

[Hoo96] G. Hoogenraad, P. Morshuis and C. Petrarca. 'Classification of partial discharges for DC equipment'. *Annual Rep. IEEE Conf. Electric Insulation and Dielectric Phenomena (CEIDP)*, 1996.

[IEC00] IEC60270. *High-voltage test techniques - Partial discharge measurements*, (IEC2000), 3rd edn.

[IEC03] IEC62073. *Guidance on the measurement of wettability of insulator surfaces*, (IEC/TS2003), 1st edn.

[IEC07] IEC60587. *Electrical insulating materials used under severe ambient conditions Test methods for evaluating resistance to tracking and erosion*, (IEC2007), 3rd edn.

[IEC13] IEC60507. *Artificial pollution tests on high voltage insulators to be used on a.c. systems*, (IEC2013), 3rd edn.

[Ima06] A. M. Imano and A. Beroual. 'Deformation of water droplets on solid surface in electric field'. *Journal of Colloid and Interface Science*, Vol. 298:pp. 869–879, 2006.

[Ima09] A. M. Imano. 'AC discharge current characteristics and LI flashover field intensity of water droplets on insulated solid surface'. *Journal of Electrical Engineering*, Vol. 60(1):pp. 24–28, 2009.

[Jad12a] J. Jadidian, M. Zahn, N. Lavesson, O. Widlund and K. Borg. 'Effects of impulse voltage polarity, peak amplitude and rise-time on streamers initiated from a needle electrode in transformer oil'. *IEEE Transactions on Plasma Science*, Vol. 40(2):pp. 909–918, 2012.

[Jad12b] J. Jadidian, M. Zahn, N. Lavesson, O. Widlund and K. Borg. 'Optimization of artificial diffusion stabilization techniques and corresponding mesh density distribution in drift dominated transport of diluted species'. *Conf. on Electrical Insulation and Dielectric Phenomena*, 2012.

[Jan08] D. Jang, K. Lim and M. Han. 'Analysis of electric field distribution on the surface of polymer post insulator used in electric railway catenary system'. *Conf. on Condition Monitoring and Diagnosis*, pp. 1–4, 2008.

[Jia06] W. Jianwu, W. Xishan, L. Lei and L. Haiyan. 'Study of discharge process and characteristics of discrete water droplets on the RTV hydrophobic surface in the non-uniform electric field'. *Int. Conf. on Power System Technology*, pp. 1–6, 2006.

[Kal02] U. Kaltenborn, P. Meier and Y. Dirix. 'Loss and recovery of hydrophobicity of novel hydrophobic epoxy resins'. *IEEE Conf. Electr. Insul. Dielectr. Phenomena (CEIDP)*, pp. 303–306, 2002.

[Kal05] U. Kaltenborn. *Die Eignung von Diagnoseverfahren zur Beurteilung der Frühphase der Oberflächenalterung von Epoxidharz-Formstoffen bei simultaner elektrischer und klimatischer Beanspruchung.* Ph.D. Thesis, TU Darmstadt, 2005.

[Kam93] A. Kamra, R. Bhalwankar and A. Sathe. 'The onset of inhomogeneous and corona in water drops falling as terminal velocity in horizontal electrical fields'. *Journal of Geophys. Res.*, Vol. D7(98), 1993.

[Kar95] G. Karaday, M. shaw and R. Brown. 'Flashover mechanism of silicone rubber insulators used for outdoor insulation - I'. *IEEE Transactions on Power Delivery*, Vol. 10(4):pp. 1965–1971, 1995.

[Kei03a] S. Keim. *Optische Diagnose an singulären Tropfen auf polymeren Isolierstoffoberflächen im elektrischen Feld*. Ph.D. Thesis, TU Darmstadt, 2003.

[Kei03b] S. Keim, D. König and V. Hinrichsen. 'Experimental investigations on electrohydrodynamic phenomena at single droplets on insulating surfaces'. *IEEE. Conf. Electrical Insulation and Dielectric Phenomena*, pp. 133–136, 2003.

[Kes78] J. Kestin, M. Sokolav and W. A. Wakeham. 'Viscosity of liquid water in the range from −8°C to 150°C'. *Journal of Physical Chemistry*, Vol. 7(3):pp. 941–948, 1978.

[Kna14] J. Knauel, A. Wagner, R. Puffer, J. Seifert, S. Lim, M. Brückner, B. Rusek, S. Steevens, A. Gravelmann and K. Kleinekorte. 'Behaviour of insulators under hybrid electrical ac/dc field stress'. *Cigré Session*, (Report D1-101), 2014.

[Koe93] D. Koenig and Y. N. Rao. *Partial discharges in electrical power apparatus*, (VDE-Verlag1993).

[Kon53] C. Konski and H. Thacher. 'The distortion of aerosol droplets by an electric field'. *Journal of Phys. Chem.*, Vol. 57(9):pp. 955–958, 1953.

[Kri01a] A. Krivda and D. Birtwhistle. 'Breakdown between water drops on wet polymer surfaces'. *IEEE Conf. Electric Insulation and Dielectric Phenomena (CEIDP)*, pp. 572–580, 2001.

[Kri01b] A. Krivda, D. Birtwhistle, S. Coyne and H. Liu. 'Discharge phenomena between water drops on polymer surfaces'. *Int. Symposium on High Voltage Engineering (ISH)*, 2001.

[Kue05] A. Kuechler. *Hochspannungstechnik; Grundlagen, Technologien und Anwendung*, (Springer2005).

[Kum09] S. Kumara, Y. V. Serdyuk and S. M. Gubanski. 'Charging of polymeric surfaces by positive impulse corona'. *IEEE Transactions on Dielectrics and Electrical Insulation*, Vol. 16(3):pp. 726–733, 2009.

[Lai09] M. Lai, C. Lee, C. Liao and Z. Wei. 'Oscillation spectrums and beat phenomenon of a water droplet driven by electrowetting'. *Applied Physics Letters*, Vol. 94(154102):pp. 1–3, 2009.

[Lam01] J. Lambrecht. *Über Verfahren zur Bewertung der Hydrophobieeigenschaften von Silikonelastomer-Formstoffen.* Ph.D. Thesis, TU Dresden, 2001.

[Lan03] D. Langemann. 'A droplet in a stationary field'. *Mathematics and Computers in Simulation*, Vol. 63(6):pp. 529–539, 2003.

[Lan04a] D. Langemann. 'The free transmission problem for a water droplet'. *Proceedings of the 4th Int. Conf. on Large-Scale Scientific Computing*, pp. 387–395, 2004.

[Lan04b] D. Langemann and M. Krüger. '3D model of a droplet in an electric field'. *Mathematics and Computers in Simulation*, Vol. 66(6):pp. 539–549, 2004.

[Lan05] D. Langemann. 'Modeling a droplet moving in an electric field'. *Mathematics and Computers in Simulation*, Vol. 68(2):pp. 157–169, 2005.

[Lan06] D. Langemann. 'Analytical and numerical techniques for simulating a 3D rainwater droplet in a strong electric field'. *Scientific Computing in Electrical Engineering, Mathematics in Industry*, Vol. 9:pp. 51–56, 2006.

[Liu05] H. Liu, G. Cash, D. Birtwhstle and G. George. 'Characterization of a severely degraded silicone elastomer HV insulator - an aid to development of lifetime assessment techniques'. *IEEE Transactions on Dielectrics and Electrical Insulation*, Vol. 12(3):pp. 478–486, 2005.

[Lop01] I. J. S. Lopes, S. H. Jayaram and E. A. Cherney. 'A study of partial discharges from water droplets on a siliconee rubber insulating surface'. *IEEE Transactions on Dielectrics and Electrical Insulation*, Vol. 8(2):pp. 262–268, 2001.

[Low92] J. J. Lowke. 'Theory of electrical breakdown in air-the role of metastable oxygen molecules'. *Journal of Physics, D: Appl. Phys.*, Vol. 25:pp. 202–210, 1992.

[Mac31] W. Macky. 'Some investigations on the deformation and breaking of water drops in strong electrical field'. *Proceeding of the Royal Society of London*, Vol. A133, 1931.

[Mar09] B. Marungsri, W. Onchantuek, A. Oonsivilai and T. Kulworawanichpong. 'Analysis of electric field and potential distributions along surface of silicone rubber insulators under various contamination conditions using finite element method'. *World Academy of Science, Engineering and Technology 53*, Vol. 3(5):pp. 1353–1363, 2009.

[Mbo08] E. Mboungou, C. Mavon, J. Friedt, C. Bergeon and M. Fromm. 'Impact of water content on the electrical behavior of epoxy insulators'. *IEEE Transactions on Dielectrics and Electrical Insulation*, Vol. 15(2):pp. 311–318, 2008.

[Miz01] Y. Mizuno, M. Nagata, K. Naito, K. Kondo, S. Ito and Y. Koshino. 'Water droplet behavior and discharge activity on silicone rubber surface energized by ac voltage'. *Annual Report Conference on Electrical Insulation and Dielectric Phenomena*, pp. 624–627, 2001.

[Mor97] R. Morrow and J. Lowke. 'Streamers propagating in air'. *Journal of Applied Physics*, Vol. 30:pp. 614–627, 1997.

[Mor05] P. Morshuis and J. Smit. 'Partial discharges at dc voltage: Their mechanism, detection and analysis'. *IEEE Transactions on Dielectrics and Electrical Insulation*, Vol. 12(2):pp. 328–340, 2005.

[Mue85] B. Mueller. *Untersuchungen zum Oberflächenverhalten von stabförmigen Isolatoren aus epoxidharz-Formstoff bei simultaner Beanspruchung durch Feuchte und hohe Wechselspannung.* Ph.D. Thesis, TU Darmstadt, 1985.

[Nal26] J. Nalon. 'The breaking of water drops by electrical field'. *Proceeding of the Royal Irish Academic*, (37), 1926.

[Niu10] S. Niu, X. Jia, J. Sang, X. Liu, C. Lu and Y. Lu. 'Distributions of raindrop sizes and fall velocities in a semiarid plateau climate: Convective versus stratiform rains'. *Journal of Applied Meteorology and Climatology*, Vol. 49:pp. 632–645, 2010.

[Nix67] J. R. Nix. 'The normal modes of oscillation of a uniformly charged drop about its saddle-point shape'. *Annals of Physics*, Vol. 41:pp. 52–107, 1967.

[Nob04] X. Noblin, A. Buguin and F. Borchard-Wyart. 'Vibrated sessile drops: Transition between pinned and mobile contact line oscillations'. *The European Physical J.*, Vol. 14:pp. 395–404, 2004.

[Off] M. Office. 'National meteorological library and archive; fact sheet no. 3 water in the atmosphere'. www.metoffice.gov.uk.

[Oko53] C. T. Okonski and H. C. Thacher. 'The distortion of aerosol by an electric field'. *Journal of Phys. Chem.*, Vol. 57:pp. 955–958, 1953.

[Phi99a] A. J. Philips, D. Childs and H. Schneider. 'Water drop corona effects on full-scale 500 kV non-ceramic insulators'. *IEEE Transactions on Power Delivery*, Vol. 14:pp. 258–265, 1999.

[Phi99b] A. J. Phillips, D. J. Childs and H. M. Schneider. 'Aging of non-ceramic insulators due to corona from water drops'. *IEEE Transactions on Power Delivery*, Vol. 14(3):pp. 1089–1999, 1999.

[Phi08] A. J. Phillips, J. Kuffel, A. Baker, J. Burnham, A. Carreira, E. Cherney, W. Chisholm, M. Farzaneh, R. Gemignani, A. Gillespie, T. Grisham, R. Hill, T. Saha, B. Vancia and J. Yu. 'Electric fields on AC composite transmission line insulators, IEEE taskforce on electric fields and composite insulators'. *IEEE Transactions on Power Delivery*, Vol. 23(2):pp. 823–830, 2008.

[Pin05] B. Pinnangudi, R. Gorur and A. Kroese. 'Quantification of corona discharges on nonceramic insulators'. *IEEE Transactions on Dielectrics and Electrical Insulation*, Vol. 12(3):pp. 513–523, 2005.

[Ray79] J. Rayleigh. 'On the capillary phenomena of jets'. *Proceeding of the Royal Society of London*, Vol. 29(196-199):pp. 71–97, 1879.

[Rey99] J. Reynders, I. Jandrell and S. Reynders. 'Surface ageing mechanisms and their relationship to service performance of siliconee rubber insulation'. *Int. Symposium on High Voltage Engineering (ISH)*, Vol. 4:pp. 54–58, 1999.

[Riz81] F. Rizk. 'Mathematical model for pollution flashover'. *Electra*, (78):pp. 71–103, 1981.

[Riz97] F. Rizk and A. rezazada. 'Modeling of altitude effects on ac flashover of high voltage insulators'. *IEEE Transactions on Power Delivery*, Vol. 12(2):pp. 810–822, 1997.

[Row06] S. Rowland and F. Lin. 'Stability of alternating current discharges between water drops on insulation surfaces'. *Journal of Appl. Phys.*, Vol. 39:pp. 3067–3076, 2006.

[Sam70] S. B. Sample and B. Raghupathy. 'Quiescent distortion and resonant oscillations of liquid drop in an electric field'. *Int. Journal of Engineering Science*, Vol. 8:pp. 97–109, 1970.

[San14] B. Sander, J. Lundquist, I. Gutman, C. Neumann, B. Rusek and K. Weck. 'Conversion of ac multi-circuit lines to ac-dc hybrid lines with respect to the environmental impact'. *Cigré Session*, (Report B2-105), 2014.

[Sar11] B. Sarang, P. Basappa, V. Lakdawala and G. Shivaraj. 'Electric field computation of water droplets on a model insulator'. *IEEE Electrical Insulation Conf.(EIC)*, pp. 377–381, 2011.

[Sar13] R. Sarathi, R. Karpagam, A. Singh and T. Tanaka. 'Understanding discharges initiated by water droplet on epoxy nanocomposites under DC voltages adopting UHF technique'. *IEEJ Trans. on Electr. and Electronic Eng.*, Vol. 8:pp. 427–431, 2013.

[SAS] SAS. 'Ribbons of blue handbook'. *booklet, Radiometer Analytical,*.

[Sch90] T. Schütte and S. Hörnfeldt. 'Dynamics of electrically stressed water drops on insulating surfaces'. *IEEE Int. Symposium of Electrical Insulation*, pp. 202–207, 1990.

[Sha11] J. Sharp, D. Farmer and J. Kelly. 'Contact angle dependence of the resonant frequency of sessile water droplets'. *Langmuir J.*, Vol. 27(15):pp. 9367–9371, 2011.

[She88] J. D. Sherwood. 'Break-up of fluid droplets in electric and magnetic fields'. *Journal of Fluid Mechanics*, Vol. 188:pp. 133–146, 1988.

[Shu05] W. Shu, J. Guo and G. Wu. 'Study on characteristic of partial discharge under DC conditio'. *Annual Rep. IEEE Conf. Electric Insulation and Dielectric Phenomena (CEIDP)*, 2005.

[Sil09] E. D. Silva and S. M. Rowland. 'The dependency of water droplet behaviour and leakage current pattern on electrode configuration'. *Annual Rep. IEEE Conf. Electric Insulation and Dielectric Phenomena (CEIDP)*, pp. 242–245, 2009.

[Sim03] W. Sima, C. Jiang, P. Lewin, Q. Yang and T. Yuan. 'Modeling of the partial discharge process in a liquid dielectric: effect of applied voltage, gap distance and electrode type'. *Energies Journal*, Vol. 6:pp. 934–952, 2003.

[SOC] SOCOREX. 'ACURA manual 825, digital reading pipettes'. www.socorex.com.

[Son10] Sonderforschungsbereich Transregio 75. 'Tropfendynamische Prozesse unter extremen Umgebungsbedingung, 2010 Jahresbericht'. http://sfbtrr75.de, December 2010.

[Son11a] Sonderforschungsbereich Transregio 75. 'Tropfendynamische Prozesse unter extremen Umgebungsbedingung, 2011 Jahresbericht'. http://sfbtrr75.de, December 2011.

[Son11b] H. Songoro, E. Gjonaj and T. Weiland. 'Numerical simulation of water droplets in presence of strong electric fields'. *ICEAA Conf.*, pp. 504–507, 2011.

[Son12a] Sonderforschungsbereich Transregio 75. 'Tropfendynamische Prozesse unter extremen Umgebungsbedingung, 2012 Jahresbericht'. http://sfbtrr75.de, December 2012.

[Son12b] H. Songoro, E. Gjonaj and T. Weiland. 'Computational modeling of water droplet deformation in strong electric fields'. *ICEAA Conf.*, pp. 333–336, 2012.

[Son13a] Sonderforschungsbereich Transregio 75. 'Tropfendynamische Prozesse unter extremen Umgebungsbedingung, 2013 Jahresbericht'. http://sfbtrr75.de, December 2013.

[Son13b] Sonderforschungsbereich Transregio 75. 'Tropfendynamische Prozesse unter extremen Umgebungsbedingung, Antrag auf Finanzierung der zweiten Förderperiode des SFB/Transregio 75'. http://sfbtrr75.de, Juni 2013.

[Son13c] H. Songoro, M. Nazemi, E. Gjonaj, V. Hinrichsen and T. Weiland. 'Water droplet oscillation on the hydrophobic surface of polymeric insulators under ac electric field stress'. *Int. Symposium on High Voltage Engineering (ISH)*, pp. 176–181, 2013.

[Son14] Sonderforschungsbereich Transregio 75. 'Tropfendynamische Prozesse unter extremen Umgebungsbedingung, 2014 Jahresbericht'. http://sfbtrr75.de, December 2014.

[Son15] H. Songoro. *Electrohydrodynamic Modeling of Droplet Vibrations under the Influence of Electric Fields*. Ph.D. Thesis, TU Darmstadt, 2015.

[Spi12] J. Spiegel, P. Zieger, N. Bukowiecki, E. Hammer, E. Weingartner and W. Eugster. 'Evaluating the capabilities and uncertainties of droplet measurements for the fog droplet spectrometer (fm-100)'. *Journal of Atmospheric Measurement*, Vol. 5:pp. 2237–2260, 2012.

[Sug01] T. Sugimoto, A. K and Y. Higashiyama. 'Negative corona discharge at a tip of water cone deformed under dc field'. *Journal of Electrostatics*, Vol. 53:pp. 25–38, 2001.

[Sun99] R. Sundararajan, S. Sundhur and T. Asokan. 'Electrohydrodynamics of water droplets on polymer surfaces'. *IEEE. 34th IAS Annual Meeting, Industrial App. Conf.*, Vol. 3:pp. 1817–1824, 1999.

[Sup08] G. Supeene, C. R. Koch and S. Bhattacharjee. 'Deformation of a droplet in an electric field: Nonlinear transient response'. *Journal of Colloid and Interface Science*, Vol. 318:pp. 463–476, 2008.

[Sut90] S. Sutar, C. Switzer and J. Codling. 'Ribbons of blue handbook'. *published by SciTech Discovery Centre*, 1990.

[Tav04] C. Tavakoli. *Dynamic modeling of ac arc development on ice surfaces*. Ph.D. Thesis, Université du Quebéc à Chicoutimi, 2004.

[Tay64] G. Taylor. 'Disintegration of the water drops in an electric field'. *Proceeding of the Royal Society of London*, Vol. A280, 1964.

[Wei14] B. Weigand, C. Tropea and A. Birkefeld. 'The collaborative research center SFB-TRR 75: Droplet dynamics under extreme boundary conditions'. *26th Annual Conference on Liquid Atomization and Spray Systems, ILASS*, 2014.

[Wen08] S. Wenrong, L. Junhao, Y. Peng and L. Yanming. 'Digital detection, grouping and classification of partial discharge signals at DC voltage'. *IEEE Transactions on Dielectrics and Electrical Insulation*, Vol. 15(6):pp. 1663–1674, 2008.

[Wes81] R. West and M. Astle. *CRC Handbook of Chemistry and Physics; Characteristics of Particles and Particle Dispersoids*, (New York1981), 62nd edn.

[Wil25] C. Wilson and G. Taylor. 'he bursting of sopat bubbles in a uniform electric field'. *Proceeding of Camb. Phil. Soc.*, (22), 1925.

[Wil99] D. L. Williams, A. Haddad, A. R. Rowlands, H. M. Young and R. T. Waters. 'Formation and characterization of dry bands in clean fog on polluted insulators'. *IEEE Transactions on Dielectrics and Electrical Insulation*, Vol. 6(5):pp. 724–731, 1999.

[Xu96] G. Xu, P. McGrath and C. Burns. 'Surface degradation of polymer insulators under accelerated climatic aging in weather-ometer'. *IEEE Int. Symposium on Electrical Insulation*, pp. 291–295, 1996.

[Yam03] T. Yamada, T. Sugimoto, Y. Higashiyama, M. Takeishi and T. Aoki. 'Resonance phenomena of a single water droplet located on a hydrophobic sheet under AC electric field'. *IEEE Transactions on Industrial App.*, Vol. 39(1):pp. 59–65, 2003.

[You05] T. Young. 'An essay on the cohesion of fluids'. *Phys. Rev. Lett.*, Vol. 95:pp. 65–87, 1805.

[Yua13] Y. Yuan and T. Lee. 'Contact angle and wetting properties'. *Springer Series in Surface Sciences*, Vol. 51:pp. 1–27, 2013.

[Zha09] X. Zhang and S. M. Rowland. 'Behavior of low current discharges between water drops'. *IEEE Conf. Electric Insulation and Dielectric Phenomena (CEIDP)*, pp. 437–440, 2009.

[Zhu03] Y. Zhu, S.Yamashita, N. Anami, M. Otsubo, C. Honda and Y. Hashimoto. 'Corona discharge phenomenon and behavior of water droplets on the surface of polymer in the ac electric field'. *Proceedings of the 7th International Conference on Properties and Applications of Dielectric Materials*, (P3-31):pp. 638–641, 2003.

[Zhu05] Y. Zhu, M. Otsubo, C. Honda, Y. Hashimoto and A. Ohno. 'Mechanism for change in leakage current waveform on a wet silicone rubber surface; a study using a dynamic 3-D model'. *IEEE Transactions on Dielectrics and Electrical Insulation*, Vol. 12(3):pp. 556–565, 2005.

[Zhu06] Y. Zhu, K. Haj, M. Otsubo, C. Honda and N. Hayashi. 'Electrohydrodynamic behaviour of water droplet on an electrically stressed hydrophobic surface'. *Journal of Applied Physics*, Vol. 39:pp. 1970–1975, 2006.

[Zix03] C. Zixia, L. Xidong, Z. Yuanxiang, W. Shaowu and G. Zhicheng. 'Study of water droplet discharge by electric field computation and highspeed video'. *Proceedings of the 7th Int. Conf. on Properties and Applications of Dielectric Materials*, pp. 820–823, 2003.

Standards and Technical Brochures

[Cig02] Cigré WG 15.04, Electra No. 201: Development of a test technique to assess a polymers long term ability to suppress leakage currents under high voltage and low conductivity salt fog conditions. 2002

[Cig04] Cigré WG D1.14, TB255: Material properties for a non-ceramic outdoor insulation-state of the art. 2004

[Cig10] Cigré WG D1.14, TB442: Evaluation of dynamic hydrophobicity properties of polymeric materials for non-ceramic outdoor insulation; retention and transfer of hydrophobicity. 2010-12

[Cig13] Cigré WG C4.303, TB555: Artificial pollution test for polymer insulators, results of round robin test. 2013-10

[Cig15] Cigré WG D1.27, TB611: Feasibility study for a dc tracking and erosion test. 2015-05

[IEC00] IEC 60270 Ed.3.0: High-voltage test techniques - Partial discharge measurements. 2000-12

[IEC03] IEC TS 62073 Ed.1.0: Guidance on the measurement of wettability of insulator surfaces. 2003-06

[IEC07] IEC 60587 Ed.3.0: Electrical insulating materials used under severe ambient conditions Test methods for evaluating resistance to tracking and erosion. 2007-05

[IEC12] IEC 62217 Ed.2.0: Polymeric HV insulators for indoor and outdoor use - General definitions, test methods and acceptance criteria. 2012-09

[IEC13] IEC 60507 Ed.3.0: Artificial pollution tests on high voltage insulators to be used on a.c. systems. 2013-12

Own Publications

[Naz13a] M. H. Nazemi and V. Hinrichsen, "Experimental Investigations on Water Droplet Oscillation and Partial Discharge Inception Voltage on Polymeric Insulating Surfaces under the Influence of AC Electric Field Stress", *IEEE Transactions on Dielectrics and Electrical Insulation*, Vol. 20, No. 2, pp. 443-453, April 2013.

[Naz13b] M. H. Nazemi and V. Hinrichsen, "Partial discharge investigation and electric field analysis of different oscillation modes of water droplet on the surface of polymeric insulator under tangential AC electric field stress", *11th IEEE international conference on solid dielectrics, ICSD 2013*, June 30th-July 4th 2013, pp. 194-197, Bologna, Italy.

[Naz13c] M. H. Nazemi and V. Hinrichsen, "Partial Discharge of Water Droplets on Polymeric Insulating Surfaces", *12th International Electrical Insulation Conference, INSUCON 2013*, 29th-31st May 2013, pp. 243-248, Birmingham, UK.

[Naz13d] M. H. Nazemi, V. Hinrichsen and E. Gjonaj "Investigations on Partial Discharges of Polymeric Insulators in the Presence of Oscillating Water Droplets on the Surface", *4. ETG-Fachtagung Grenzflächen in elektrischen Isoliersystemen*, 12th-13th November 2013, Dresden, Germany.

[Son13a] H. Songoro, M. H. Nazemi, V. Hinrichsen, E. Gjonaj and T.Weiland "Water droplet oscillation on the hydrophobic surface of polymeric insulators under AC electric field stress", *18th International Symposium on High Voltage Engineering, ISH 2013*, 25th-30th August 2013, Seoul, South Korea.

[Naz15a] M. H. Nazemi and V. Hinrichsen, "Partial Discharge Inception Electric Field Strength of Water Droplets on Polymeric Insulating Surfaces", *IEEE Transactions on Dielectrics and Electrical Insulation*, Vol. 22, No. 2, pp. 1088-1096, April 2015.

[Naz15b] M. H. Nazemi and V. Hinrichsen, "Experimental Investigations on Partial Discharge Characteristics of Water Droplets on Polymeric Insulating Surfaces at AC, DC and Combined AC-DC Voltages", *IEEE Transactions on Dielectric and Electrical Insulation*, Vol. 22, No. 4, pp. 2261-2270, August 2015.

Coordinated student research projects and diploma thesis

1. Amir Pouya Azad, “Frequenz-Analyse der Einsatzspannung leitfähiger und nicht leitfähiger Wassertropfen auf der Oberfläche von Isolierstoffen im elektrischen Feld (AC)”; *Diplomarbeit (2012)*

2. Somashekhar Konappalli, “Investigation of partial discharge of multi water droplets on inclined surface of polymeric insulators”; *Master Thesis (2013)*

3. Sebastian Straßer, “Untersuchung des Verhaltens von geladenen und nichtgeladenen Wassertropfen im elektrischen Feld unter Wechsel.- und Gleichspannung”; *Bachelorarbeit (2013)*

4. Soumya Chatterjee, “Investigations on the influence of viscosity, conductivity and permittivity of water droplet on the PD inception voltage of polymeric insulators in the presence of water droplets”; *Master Thesis (2014)*

5. Afsaneh Mohammadi, “Partial discharge of water droplets on the surface of polymeric insulators under DC electric field stress”; *Master Thesis (2014)*

Curriculum Vitae

Mohammad Hossein Nazemi

Born on September 21th, 1979 in DARAB, IRAN

from 09.2015	Development Engineer R&D Power Products Medium Voltage (PPMV-EA), ABB AG Ratingen, Germany
09.2010 - 09.2015	Scientific Researcher High Voltage Laboratories, Technische Universität Darmstadt Darmstadt, Germany
09.2008 - 08.2010	Ph.D candidate Faculty of Electrical and Computer Engineering, University of Tehran Tehran, Iran
06.2003 - 09.2008	Senior Electrical Engineer MOSHANIR Power Consultant Engineering Tehran, Iran
09.2001 - 12.2003	M.Sc. Student Faculty of Electrical Power Engineering, Amirkabir University of Technology, Tehran, Iran
09.1998 - 08.2001	B.Sc. Student Faculty of Electrical Power Engineering, Power and Water University of Technology, Tehran, Iran

Erklärung laut §9 PromO

Ich versichere hiermit, dass ich die vorliegende Dissertation allein und nur unter Verwendung der angegebenen Literatur verfasst habe. Die Arbeit hat bisher noch nicht zu Prüfungszwecken gedient.

Darmstadt, den 15. September 2015

Mohammad Hossein Nazemi